

University of Kentucky

UKnowledge

---

Theses and Dissertations--Molecular and Cellular Biochemistry

Molecular and Cellular Biochemistry

---

2021

## Therapeutic Targeting of Leukemia Stem Cells to Prevent T-Cell Acute Lymphoblastic Leukemia Relapse

Meghan G. Haney

University of Kentucky, meghan.green@uky.edu

Author ORCID Identifier:

 <https://orcid.org/0000-0002-6088-8553>

Digital Object Identifier: <https://doi.org/10.13023/etd.2021.133>

[Right click to open a feedback form in a new tab to let us know how this document benefits you.](#)

### Recommended Citation

Haney, Meghan G., "Therapeutic Targeting of Leukemia Stem Cells to Prevent T-Cell Acute Lymphoblastic Leukemia Relapse" (2021). *Theses and Dissertations--Molecular and Cellular Biochemistry*. 52.  
[https://uknowledge.uky.edu/biochem\\_etds/52](https://uknowledge.uky.edu/biochem_etds/52)

This Doctoral Dissertation is brought to you for free and open access by the Molecular and Cellular Biochemistry at UKnowledge. It has been accepted for inclusion in Theses and Dissertations--Molecular and Cellular Biochemistry by an authorized administrator of UKnowledge. For more information, please contact [UKnowledge@lsv.uky.edu](mailto:UKnowledge@lsv.uky.edu).

## **STUDENT AGREEMENT:**

I represent that my thesis or dissertation and abstract are my original work. Proper attribution has been given to all outside sources. I understand that I am solely responsible for obtaining any needed copyright permissions. I have obtained needed written permission statement(s) from the owner(s) of each third-party copyrighted matter to be included in my work, allowing electronic distribution (if such use is not permitted by the fair use doctrine) which will be submitted to UKnowledge as Additional File.

I hereby grant to The University of Kentucky and its agents the irrevocable, non-exclusive, and royalty-free license to archive and make accessible my work in whole or in part in all forms of media, now or hereafter known. I agree that the document mentioned above may be made available immediately for worldwide access unless an embargo applies.

I retain all other ownership rights to the copyright of my work. I also retain the right to use in future works (such as articles or books) all or part of my work. I understand that I am free to register the copyright to my work.

## **REVIEW, APPROVAL AND ACCEPTANCE**

The document mentioned above has been reviewed and accepted by the student's advisor, on behalf of the advisory committee, and by the Director of Graduate Studies (DGS), on behalf of the program; we verify that this is the final, approved version of the student's thesis including all changes required by the advisory committee. The undersigned agree to abide by the statements above.

Meghan G. Haney, Student

Dr. Jessica S. Blackburn, Major Professor

Dr. Trevor Creamer, Director of Graduate Studies

THE THERAPEUTIC TARGETING OF LEUKEMIA STEM CELLS TO  
PREVENT T-CELL ACUTE LYMPHOBLASTIC LEUKEMIA RELAPSE

---

DISSERTATION

---

A dissertation submitted in partial fulfillment of the  
requirements for the degree of Doctor of Philosophy in the  
College of Medicine  
at the University of Kentucky

By

Meghan Green Haney

Lexington, Kentucky

Co- Directors: Dr. Jessica Blackburn, Assistant Professor of Biochemistry

and Dr. Douglas Andres, Professor of Biochemistry

Lexington, Kentucky

2021

Copyright © Meghan Green Haney 2021  
<https://orcid.org/0000-0002-6088-8553>

## ABSTRACT OF DISSERTATION

### THERAPEUTIC TARGETING OF LEUKEMIA STEM CELLS TO PREVENT T-CELL ACUTE LYMPHOBLASTIC LEUKEMIA RELAPSE

The survival rate of T-cell Acute Lymphoblastic Leukemia (T-ALL) relapse is a dismal 10% of affected adults and 30% of children, largely due to the relapsed disease being more aggressive and treatment resistant than the initial disease. Relapse is thought to occur because conventional chemotherapies are unable to reliably eliminate a unique cell type known as leukemia stem (or propagating) cells (LSCs). LSCs are the only cells within the leukemia with the ability to self-renew and remake or replenish the ALL from a single cell. Currently, the pathways governing self-renewal in LSCs are largely unknown, precluding our ability to successfully and selectively target this important cell type with anti-cancer drugs. More research is needed to identify targetable pathways and develop new technologies for studying LSCs.

Here, I determined that the oncogenic phosphatase of regenerating liver 3 (PRL-3) plays a role in leukemia progression, migration, and self-renewal of LSCs in T-ALL *in vivo* in a zebrafish Myc-induced T-ALL model, while inhibition of PRL-3 reduced LSC numbers *in vivo* and *in vitro*. RNA sequencing and GSEA of patient T-ALL samples revealed that PRL-3's role in self-renewal is at least partly due to activation of Wnt pathway signaling, a known driver of LSC function in T-ALL. While the Wnt pathway seems an ideal target for LSCs, Wnt signaling is critical for many normal and developmental processes. Clinical trials for Wnt inhibitors have shown undesirable toxicity and these drugs are not practical for use in children with T-ALL due to developmental concerns. Thus, a major gap in knowledge concerning leukemia stem cells in T-ALL is the identification of regulators of Wnt signaling, like PRL-3, that are uniquely expressed by leukemia cells and easily targeted with small molecules. To expand my research beyond PRL-3, I have developed a novel zebrafish T-ALL model where Wnt expressing cells fluorescently labeled. These animals can be used as a model for studying LSC function and identifying novel drugs that can target Wnt-expressing T-ALL cells *in vivo*.

I have also developed novel translational technologies that may be used to predict LSC driven relapse in T-ALL. I have optimized a zebrafish larval xenograft model for transplant and rapid drug screening of human T-ALL cell lines and patient samples to gain insight into tumor progression and resistance to chemotherapy. I have also developed a novel pipeline for using cell-free circulating tumor DNA (ctDNA) as a biomarker of disease relapse in patients with ALL, enabling tracking of disease course, assessment of minimal residual disease, and as a potential predictor of patient relapse.

Taken together, my research has established PRL-3 as a potential therapeutic target in T-ALL, and provided new insight into the role of a PRL-3/Wnt signaling axis in regulating LSC self-renewal. Additionally, the new models and techniques that I have developed are useful tools in analyzing LSC function, targeting self-renewal, and predicting ALL relapse.

KEYWORDS: T-ALL, PRL-3, Wnt, Xenograft, cell-free DNA, Zebrafish

Meghan Green Haney

---

*(Name of Student)*

03/22/2021

---

Date

Therapeutic Targeting of Leukemia Stem Cells to  
Prevent T-Cell Acute Lymphoblastic Leukemia Relapse

By  
Meghan Green Haney

Dr. Jessica S. Blackburn  
Co-Director of Dissertation

---

Dr. Douglas Andres  
Co-Director of Dissertation

---

Dr. Trevor Creamer  
Director of Graduate Studies

---

03/22/2021

---

Date

## ACKNOWLEDGMENTS

The work presented in this dissertation, while an individual work, would not have been possible without the support, guidance, and direction of a community of people. First off, I would like to begin by thanking my mentor, Dr. Jessica Blackburn, for your unwavering support and expertise throughout my graduate training. You have been an exemplary role model of a strong female in science, who I hope to emulate someday, and have taught me more than I can put into words. I am especially grateful for you allowing me the freedom to pursue my research interests, even if they were not your own, and for giving me the space to fail from time-to-time and learn from my mistakes. I have grown an immense amount during my time in your lab and have accomplished many lofty goals I had set out for myself thanks to your mentorship, guidance, and support.

This dissertation also would not have been possible without my committee members: Dr. Doug Andres, Dr. Mark Evers, Dr. Tianyan Gao, and Dr. Mark Wurth. Thank you for the continued support and guidance that you provided me throughout my graduate training. I also would like to thank my outside examiner, Dr. Vincent Cassone, for his willingness to serve on my dissertation committee, supporting the conclusion of my work at UK.

To the past and current members of the Blackburn lab, I could not have done this without you. Min Wei and Caroline Smith, you have not only been the best colleagues, but the best of friends to have in lab. Working alongside you both has been so much fun and I will always cherish all of the laughs we had working late nights and weekends together, making the time fly by. I cannot begin to thank you enough for always being willing to listen, provide advice, and for always being there to lean on throughout graduate

school. I could not have done all of the zebrafish experiments outlined in this dissertation without the help of Kristin Miller, who I not only got to mentor in lab, but got to call a friend. Yelena Chernyavskaya and Shilpa Sampathi, I have learned so much from you both and you have been amazing role models as female scientists. Henry Moore, Stephen Dockins, Anna Cox, and Mary Wimsett, I appreciate your help on multiple projects and also your friendship over the past few years. You all made my time in the lab so much fun! To all the members of the Blackburn lab, Shaw Powell, Sergei Revskoy, Alyse Ptacek, and many other undergraduates and high school students, thank you for all of your help and for making the lab a great place to come to work every day!

To the University of Kentucky MD/PhD program, thank you for taking a chance on me and believing in my potential as a physician scientist. To the Directors, Dr. Wally Whiteheart, Dr. Brandon Miller, and Dr. Richard King, thank you for all of the time you have put into my training and our program, your dedication to training students does not go unnoticed. Therese Stearns, thank you for all you do for this program and for the constant support, guidance, and friendship you have provided me throughout my training. Finally, to the friends I have made in the program, you have been a great group of colleagues to learn from and go through this journey with. Especially Laura Krueger, you have been the best friend and biggest support system throughout my training and I most definitely could not have done it without you. I appreciate that you and Therese are always there to lend an ear and have helped me through so many situations, both professional and personal throughout my training.

I also would like to acknowledge the Markey Cancer Center for supporting my training on a T32 grant over the last 3 years. Erin Oakley, Dr. Kathy O'Connor, and Dr.

Vivek Ragnekar, you have provided me with the resources and support to make all of the work in this dissertation possible and I cannot thank you enough.

Finally, I would like to acknowledge all of my friends and family for being there with me every step of the way throughout this journey. To my parents, sister, and in-laws, I cannot imagine doing this without all of your support and thank you for always believing in me, even when I doubted myself. Mom and dad, thank you for inspiring me to be a strong-willed and determined woman and for always pushing me to achieve my goals and to never take no for an answer. To my husband Jay, thank you for your unwavering support and for all of the sacrifices that you have made, both professionally and personally, to support me in achieving my goals. I know it has not always been easy, but I appreciate you more than you know. Finally, to my daughter Olivia, you sat with me while I wrote my entire dissertation! You have brought a bright light into a challenging time in my life this year and I am beyond thankful for you. I would not be earning my PhD without the support, guidance, and encouragement of everyone who has been a part of my journey.

# TABLE OF CONTENTS

<b>ACKNOWLEDGMENTS .....</b>	<b>iii</b>
<b>LIST OF TABLES.....</b>	<b>ix</b>
<b>LIST OF FIGURES.....</b>	<b>x</b>
<b>PART 1: Introduction.....</b>	<b>1</b>
<b>CHAPTER 1. T-Cell Acute Lymphoblastic Leukemia.....</b>	<b>2</b>
1.1 <i>Clinical Features of T-cell Acute Lymphoblastic Leukemia (T-ALL) .....</i>	3
1.2 <i>Treatment of T-ALL.....</i>	6
1.3 <i>Patients with T-ALL Relapse have a Poor Overall Prognosis .....</i>	8
1.4 <i>Targeted Therapies Remain a Challenge in T-ALL Treatment.....</i>	10
<b>CHAPTER 2. Leukemia Stem Cells.....</b>	<b>13</b>
2.1 <i>Cancer Stem Cells Drive Cancer Progression and Relapse .....</i>	14
2.2 <i>Leukemia Stem Cells Self-Renew and are Treatment Resistant .....</i>	17
2.3 <i>Targeting Cancer Stem Cells .....</i>	19
2.4 <i>LSCs in ALL are Responsible for Disease Relapse.....</i>	23
2.5 <i>Targeting LSCs in T-ALL.....</i>	25
<b>PART 2. The Role of the Protein Tyrosine Phosphatase PRL-3 in T-ALL Self-Renewal.....</b>	<b>28</b>
<b>CHAPTER 3. PRL-3 Accelerates ALL Progression and Increases LSC Frequency.....</b>	<b>29</b>
3.1 <i>Introduction.....</i>	30
3.1.1 <b>PRL-3 Identified as a Driver of Self-Renewal in T-ALL.....</b>	30
3.1.2 <b>PRL-3 is a Dual-Specificity Protein Tyrosine Phosphatase.....</b>	31
3.1.3 <b>PRL-3 Acts as an Oncogenic Driver in Solid Tumors .....</b>	34
3.1.4 <b>Hypothesis and Specific Aims .....</b>	36
3.2 <i>Results.....</i>	36
3.2.1 <b>PRL-3 is Upregulated in Human T-ALL Samples .....</b>	36
3.2.2 <b>PRL-3 Accelerates T-ALL Progression in a Zebrafish Model .....</b>	37
3.2.3 <b>PRL-3 Promotes T-ALL Cell Migration in a Zebrafish Model.....</b>	42
3.2.4 <b>Over-Expression of PRL-3 Increases LSC Frequency in a Zebrafish Model .....</b>	43
3.2.5 <b>Inhibition of PRL-3 Decreases LSC Frequency <i>In Vivo</i>.....</b>	48
3.2.6 <b>Knock-down of PRL-3 Decreases LSC Frequency <i>In Vitro</i> .....</b>	50
3.3 <i>Discussion.....</i>	51
3.3.1 <b>Future Directions.....</b>	53
3.4 <i>Methods .....</i>	54
3.4.1 <b>Zebrafish Husbandry .....</b>	54

3.4.2	Zebrafish T-ALL Models .....	54
3.4.3	Limiting Dilution Transplantation .....	55
3.4.4	Apoptosis Assay .....	57
3.4.5	Proliferation Assay .....	57
3.4.6	T-ALL Cell Culture .....	57
3.4.7	Generation of T-ALL Knock-Down Cells by Lentivirus Infection .....	58
3.4.8	Colony Formation Assay .....	58
3.4.9	Statistical Analysis .....	58
<b>CHAPTER 4.</b>	<b>PRL-3 Modulates Beta-Catenin Signaling in T-ALL LSCs .....</b>	<b>60</b>
4.1	<i>Introduction</i> .....	61
4.1.1	Beta-Catenin/Wnt Signaling Maintains LSC Self-Renewal .....	61
4.1.2	Hypothesis and Specific Aims .....	63
4.2	<i>Results</i> .....	64
4.2.1	$\beta$ -Catenin is Highly Expressed in PRL-3 Over-Expressing T-ALL .....	64
4.2.2	PRL-3 Modulates Beta-Catenin Signaling <i>in Vitro</i> .....	68
4.2.3	PRL-3 Modulates Beta-Catenin Signaling <i>in Vivo</i> .....	73
4.3	<i>Discussion</i> .....	75
4.3.1	Future Directions .....	76
4.4	<i>Methods</i> .....	76
4.4.1	Gene Set Enrichment Analysis (GSEA) .....	76
4.4.2	RNAseq .....	77
4.4.3	RT-PCR .....	77
4.4.4	Western Blot .....	78
4.4.5	Cell Culture .....	78
4.4.6	TopFlash Assay .....	79
4.4.7	TCF/LEF Zebrafish Experiments .....	80
4.4.8	Statistical Analysis .....	80
<b>PART 3.</b>	<b>Novel Technology/Techniques to Detect and Prevent T-ALL Patient Relapse and Improve Outcomes .....</b>	<b>81</b>
<b>CHAPTER 5.</b>	<b>Development of a Fluorescently Tagged Leukemia Stem Cell Model in Zebrafish .....</b>	<b>82</b>
5.1	<i>Introduction</i> .....	83
5.1.1	Hypothesis .....	84
5.2	<i>Results</i> .....	84
5.3	<i>Discussion</i> .....	86
5.3.1	Future Directions .....	87
5.4	<i>Methods</i> .....	88
5.4.1	Generation of Model in Sheer TCF/LEF Zebrafish .....	88
5.4.2	Generation of TCF/LEF CG1 Transgenic Line .....	88
5.4.3	Flow Cytometry .....	89
5.4.4	Microscopy .....	89
<b>CHAPTER 6.</b>	<b>Zebrafish as a Xenograft Model .....</b>	<b>90</b>

6.1	<i>Introduction</i> .....	91
6.2	<i>Results</i> .....	93
6.2.1	<b>Optimization of Xenograft Injection Site and Cell Number</b> .....	93
6.2.2	<b>Temperature Affects Zebrafish Survival and Metabolism</b> .....	98
6.2.3	<b>Temperature Affects Xenografted Cell Survival and Metabolism</b> .....	100
6.2.4	<b>Primary Patient Samples Can Be Xenografted into Larval Zebrafish</b> .....	103
6.2.5	<b>Zebrafish Xenograft Model Shows Inconsistencies in Drug Screening of Cell Lines</b> .	107
6.3	<i>Discussion</i> .....	114
6.4	<i>Methods</i> .....	116
6.4.1	<b>IRB/Collection of Patient Samples</b> .....	116
6.4.2	<b>Cell Line Experiments</b> .....	116
6.4.3	<b>Xenograft Experiments</b> .....	117
6.4.4	<b>Zebrafish Immunofluorescence and Imaging Experiments</b> .....	119
6.4.5	<b>Thawing of Patient Samples</b> .....	120
6.4.6	<b>Drug Screening</b> .....	120
6.4.7	<b>Metabolism Experiments</b> .....	121
6.4.8	<b>Seahorse Experiments</b> .....	123
6.4.9	<b>Statistical Analysis</b> .....	124
<b>CHAPTER 7.</b>	<b>Circulating Tumor DNA as a Biomarker in Acute Lymphoblastic Leukemia</b> .....	<b>125</b>
7.1	<i>Introduction</i> .....	126
7.1.1	<b>Cell Free DNA Serves as a Biomarker in Cancer</b> .....	128
7.1.2	<b>Cancer-Specific Methylation Signatures are Present in Hematologic Malignancies</b> .....	129
7.1.3	<b>Hypothesis</b> .....	130
7.2	<i>Results</i> .....	131
7.2.1	<b>Clonality Tracking in ctDNA using MinION Sequencing</b> .....	131
7.2.2	<b>ctDNA Methylation as a Biomarker in ALL</b> .....	136
7.3	<i>Discussion</i> .....	139
7.3.1	<b>Future Directions</b> .....	140
7.4	<i>Methods</i> .....	142
7.4.1	<b>Collection of Patient Samples</b> .....	142
7.4.2	<b>Isolation of genomic DNA from Patient Samples</b> .....	142
7.4.3	<b>Isolation of Cell-Free DNA from Plasma and CSF</b> .....	143
7.4.4	<b>Clonality PCR</b> .....	144
7.4.5	<b>Nanopore Library Preparation and Minion Sequencing</b> .....	144
7.4.6	<b>Methylation Sequencing</b> .....	145
7.4.7	<b>Statistical Analysis</b> .....	145
<b>CHAPTER 8.</b>	<b>Final Conclusions</b> .....	<b>146</b>
<b>REFERENCES</b>	.....	<b>149</b>
<b>VITA</b>	.....	<b>170</b>

## LIST OF TABLES

TABLE 2.1 STRATEGIES FOR THERAPEUTIC TARGETING OF LEUKEMIA STEM CELLS .....	27
TABLE 3.2 REALTIME RT-PCR PRIMER SEQUENCES .....	55
TABLE 4.1 REALTIME RT-PCR PRIMER SEQUENCES .....	78

## LIST OF FIGURES

FIGURE 2.1 CANCER STEM CELLS DRIVE PATIENT RELAPSE.....	20
FIGURE 3.1 PRL-3 PROTEIN STRUCTURE.....	33
FIGURE 3.2 MICROARRAY DATA REVEALS PRL-3 EXPRESSION INCREASED IN T-ALL.....	37
FIGURE 3.3 PRL-3 OVER-EXPRESSION ACCELERATES T-ALL PROGRESSION. ....	38
FIGURE 3.4 CHARACTERIZATION OF MYC AND PRL-3 OVER-EXPRESSING T-ALLS.....	39
FIGURE 3.5 MUTATION OF THE PRL-3 PHOSPHORYLATION DOMAIN AFFECTS T-ALL PROGRESSION .....	41
FIGURE 3.6 CHARACTERIZATION OF PRL-3 MUTANT T-ALLS .....	42
FIGURE 3.7 PRL-3 PROMOTES T-ALL MIGRATION IN A ZEBRAFISH MODEL .....	43
FIGURE 3.8 LSC FREQUENCY INCREASES WITH PRL-3 OVER-EXPRESSION .....	44
FIGURE 3.9 PRL-3 OVER-EXPRESSION DOES NOT AFFECT APOPTOSIS OR PROLIFERATION.....	45
FIGURE 3.10 OVER-EXPRESSION OF PRL-3 MUTANTS DOES NOT SIGNIFICANTLY CHANGE LSC FREQUENCY .....	47
FIGURE 3.11 PRL-3 MUTANT OVER-EXPRESSION DOES NOT AFFECT PROLIFERATION OR APOPTOSIS .....	48
FIGURE 3.12 CHEMICAL INHIBITION OF PRL-3 DECREASES LSC FREQUENCY .....	49
FIGURE 3.13 KNOCK-DOWN OF PRL-3 DECREASES HUMAN LEUKEMIA CELL STEMNESS.....	51
FIGURE 4.1 CONSTITUTIVELY ACTIVE B-CATENIN OVER-EXPRESSION INCREASES LSC FREQUENCY IN VIVO.....	62
FIGURE 4.2 XAV939 TREATMENT OF HIGH SELF-RENEWAL T-ALL DECREASES LSC FREQUENCY .....	63
FIGURE 4.3 GSEA ANALYSIS REVEALS PATHWAYS ENRICHED IN PRL-3 HIGH PATIENT T-ALL SAMPLES.....	65
FIGURE 4.4 BETA-CATENIN IS HIGHLY EXPRESSED IN PRL-3 OVER-EXPRESSING ZEBRAFISH T-ALL SAMPLES .....	66
FIGURE 4.5 PRL-3 OVER-EXPRESSION INDUCES Z-MYCA EXPRESSION IN VIVO.....	67
FIGURE 4.6 RNASEQ ANALYSIS OF MYC AND PRL-3 OVER-EXPRESSION FISH TUMORS .....	68
FIGURE 4.7 TOPFLASH ASSAY REVEALS PRL-3 MODULATES WNT/BETA-CATENIN SIGNALING IN VITRO .....	70
FIGURE 4.8 PRL-3 OVER-EXPRESSION INDUCES C-MYC EXPRESSION UPON WNT STIMULATION .....	71
FIGURE 4.9 PRL-3 OVER-EXPRESSION INCREASES WNT TARGET GENE EXPRESSION IN VITRO .....	72
FIGURE 4.10 INHIBITION OF PRL-3 MODULATES BETA-CATENIN PHOSPHORYLATION.....	73
FIGURE 4.10 PRL-3 CHEMICAL INHIBITION DECREASES BETA-CATENIN SIGNALING IN VIVO .....	75
FIGURE 5.1 SCHEMATIC OF LSC REPORTER MODEL GENERATION .....	85
FIGURE 5.2 BETA-CATENIN EXPRESSING LEUKEMIA CELLS LOCATED IN THYMUS .....	85
FIGURE 5.3 BETA-CATENIN EXPRESSING LSCs CAN BE SORTED BY FLOW CYTOMETRY .....	86
FIGURE 6.1 RECIPIENT SURVIVAL POST-XENOGRAFT VARIES BY INJECTION SITE.....	94
FIGURE 6.2 ZEBRAFISH METABOLITES VARY BETWEEN BODY AND YOLK INJECTION SITES .....	96
FIGURE 6.3 OPTIMIZATION OF CELL NUMBER FOR INJECTION .....	97
FIGURE 6.4 OPTIMIZATION OF TEMPERATURE FOR XENOGRAFT MAINTENANCE .....	99
FIGURE 6.5 TEMPERATURE AFFECTS ZEBRAFISH METABOLISM.....	100
FIGURE 6.6 EFFECT OF TEMPERATURE ON CANCER CELL LINES.....	101
FIGURE 6.7 TEMPERATURE AFFECTS MAMMALIAN CELL METABOLISM .....	103
FIGURE 6.8 INJECTION SITE AND REPRESENTATIVE IMAGES OF SCREENING XENOGRAFTED FISH .....	104
FIGURE 6.9 XENOGRAFT DRUG SCREEN AND IMAGING WORKFLOW .....	105
FIGURE 6.10 DRUG TREATMENT CAN REDUCE XENOGRAFTED TUMOR AREA IN VIVO .....	106
FIGURE 6.11 BRDU STAINING OF DII STAINED CELL LINES.....	108
FIGURE 6.12 XENOGRAFTED MAMMALIAN CELL GROWTH IS AFFECTED BY INJECTION SITE AND TEMPERATURE.....	109
FIGURE 6.13 TEMPERATURE AFFECTS RESPONSE OF MAMMALIAN CELL LINES TO DRUG TREATMENT .....	111
FIGURE 6.14 DRUG TREATMENT PRODUCES INCONSISTENT RESULTS WITH VARIATIONS IN XENOGRAFT SITE OR TEMPERATURE .....	113
FIGURE 7.1 WORKFLOW FOR MINION SEQUENCING OF IGH VARIABLE REGIONS .....	132
FIGURE 7.2 MINION LIBRARY RUN STATISTICS.....	133

FIGURE 7.3 MINION CLONALITY TRACKING .....	135
FIGURE 7.4 LEUKEMIA SAMPLES CLUSTER INDEPENDENTLY FROM HEALTHY BASED ON METHYLATION PROFILE .....	136
FIGURE 7.5 METHYLATION SEQUENCING RESULTS .....	138
FIGURE 7.6 GENOMIC LOCATION OF DIFFERENTIALLY METHYLATED REGIONS .....	139

PART 1: INTRODUCTION

## CHAPTER 1. T-CELL ACUTE LYMPHOBLASTIC LEUKEMIA

## **1.1 Clinical Features of T-cell Acute Lymphoblastic Leukemia (T-ALL)**

In the United States, there are approximately 16,000 cases of pediatric cancer diagnosed per year, which equates to 43 children diagnosed with cancer each day (data from Alex's Lemonade Stand Foundation). T-cell acute lymphoblastic leukemia (T-ALL) is an aggressive subset of the most common pediatric malignancy, acute lymphoblastic leukemia (ALL). ALL makes up about 1/3 of pediatric malignancies and is characterized by an abnormal proliferation of leukocytes. T-ALL is characterized by an abnormal proliferation of thymocytes and makes up 15-25% of all pediatric leukemias <sup>1,2</sup>. A great deal of progress has been made towards improving outcomes in leukemia patients, yet outcomes for T-ALL are far inferior to those for B-cell acute lymphoblastic leukemia (B-ALL) <sup>3</sup>. T-ALL is also plagued by a high relapse rate, nearing 20% of patients, which is characterized by an aggressive and often treatment-resistant form of disease from which only 10% of adults and 30% of children will recover <sup>4</sup>.

Clinically, T-ALL occurs most commonly in adolescent children, with a median age of onset of 9 years, and has a three-fold higher incidence in males than in females <sup>5</sup>. T-ALL can present acutely or symptoms can come on over a duration of months. Patients often present with constitutional symptoms, including fever, weight loss, and fatigue. Additional symptoms include joint and bone pain, adenopathy, recurrent infection, mucosal bleeding, paleness, and hepatosplenomegaly. T-ALL also commonly has central nervous system (CNS) involvement which can present as headache, visual impairment, and nausea.

When ALL is suspected, clinicians will order a complete blood count (CBC) which will show an elevated white blood cell (WBC) count, consistent with a leukemia diagnosis. However, a bone marrow biopsy is required for a true ALL diagnosis, showing >25%

leukemic blasts, or immature white blood cells. An anterior mediastinal mass is also seen in by radiography in 2/3 of T-ALL patients and represents an enlargement of the thymus. CNS involvement can be seen by magnetic resonance imaging (MRI). Finally, immunophenotyping must be done to distinguish T-ALL from other acute leukemias and genetic testing is run for risk-stratification.

Assays to measure the genetic subgroups and immunophenotypes of T-ALL are still somewhat controversial in terms of prognostic implications, and most differentiation stage subgroups are still not formally included in the classification of T-ALL <sup>6</sup>. Current standards for ALL diagnosis and characterization integrate cell morphology, immunophenotype, and genetics/cytogenetics based on the guidelines established by the World Health Organization (WHO) classification of solid tumors and leukemias/lymphomas. There are five recognized immunophenotype subgroups of T-ALL, characterized by the 2008 update to the WHO classification, that can delineate when the block in differentiation occurred and what stage of maturation the leukemic blasts are in <sup>7</sup>. The first stage of differentiation is pro-T which is cytoplasmic CD3+ (cCD3+), CD7+, CD2-, CD1a-, and CD34+/- . Next is pre-T which is cCD3+, CD7+, and CD5/CD2+, CD1a-, and CD34+/- . Precursor T-ALL makes up about 15% of childhood T-ALL with a variable clinical onset and a 5-year event-free survival of about 75% <sup>8</sup>. Cortical T is cCD3+, CD7+, CD2+, Cd1a+, and CD34-. Finally, mature or medullary T is cCD3+, CD7+, CD2+, CD1a-, CD34- and surface CD3+ (sCD3+) <sup>9</sup>. Cases of pro- and pre- T-ALL tend to have a worse outcome than cortical or mature T-ALL as the cells are less differentiated and often more aggressive. A new subgroup recently characterized in the 2016 WHO classification update is early-T precursor ALL (ETP-ALL) which is CD1a-, CD8-, weakly CD5+ and shows expression of

at least one myeloid and/or stem cell marker <sup>6</sup>. This type of T-ALL was originally thought of as being more aggressive, however with more aggressive treatment the prognosis is now the same as other types of T-ALL <sup>6,10</sup>.

Cytogenetics also play a major role in characterizing and stratifying T-ALL based on prognosis. One important cytogenetic abnormality associated with good prognosis in T-ALL is t(10;14)(q24;q11) <sup>7</sup>. The most frequent abnormalities in T-ALL involve 14q11 breakpoints such as t(10;14)(q24;q11), t(11;14)(p13;q11), or others. The presence of t(8;14) with breakpoints at q24;q11 in T-ALL is associated with a lymphomatous, aggressive presentation <sup>11,12</sup>. However, despite some cytogenetic characterization in T-ALL, this information rarely correlates with risk stratification or differences in treatment regimens.

Finally, since the onset of next generation sequencing, T-ALL can be further characterized based on gene mutations and aberrant gene expression, yet this has still not translated to changes in clinical practice. In T-ALL, aberrations in the T-cell receptor (TCR) gene, NOTCH1, MYC, LMO2, FBW7, BCL11B, JAK1, PTPN2, IL7R, and PHF6 are the most common <sup>7</sup>. NOTCH1 is the most commonly mutated gene in pediatric T-ALL with >60% of pediatric T-ALL patients containing an activating mutation in NOTCH1 <sup>13,14</sup>. Chromosomal rearrangements can also lead to in-frame fusion genes encoding chimeric proteins such as PICALM-MLLT10, NUP214-ABL1, EML-ABL1, SET-NUP214, and MLL gene rearrangements with oncogenic properties <sup>7</sup>. However, the prognostic features of these mutations and gene rearrangements have not been well characterized as there is such a wide variety of mutations and rearrangements from patient to patient, unlike other adult cancers which have more concordance in mutations between patients.

## 1.2 Treatment of T-ALL

Because T-ALL has a higher rate of treatment resistance and tends to have earlier and more frequent relapse than B-ALL, it is often treated with similar, but more aggressive treatment regimens than B-ALL<sup>3</sup>. Treatment for T-ALL consists of three phases spanning multiple years: induction, consolidation, and maintenance phases. In each of these phases, patients are treated with different cocktails of chemotherapies. Prior to treatment, patients are stratified into low, intermediate, or high-risk sub-groups which determines their course of treatment as well. However, one unique feature of T-ALL compared to B-ALL is that age and presenting white blood cell (WBC) count are not necessarily independently prognostic in T-ALL patients, so more research is needed to better risk stratify T-ALL patients prior to treatment<sup>2</sup>. Furthermore, although there are standard of care therapies for treating T-ALL, many patients are enrolled in clinical trials, most of which are run by the Children's Oncology Group, to compare new treatment regimens to each other or study the effect of newer therapies for T-ALL treatment.

The induction phase of treatment for T-ALL typically lasts 4-6 weeks and is the initial phase of treatment in patients, with the goal being to induce remission by the end of induction therapy. This phase consists of treatment with a cocktail of chemotherapies, including: vincristine, glucocorticoids, L-asparaginase, an anthracycline (often danorubicin) and sometimes cyclophosphamide<sup>15</sup>. Patients who fail to achieve remission and still have detectable residual disease by bone marrow biopsy at the end of induction therapy may have to undergo re-induction depending on their risk stratification and prognostic factors.

The consolidation phase of treatment lasts 6-8 months and is made up of intensive combination chemotherapy treatment. Chemotherapies used during consolidation therapy are often a cocktail of the same drugs that are used during induction phase, as well as Ara-C, etoposide, methotrexate, and 6-mercaptopurine. This phase tends to be very taxing on patients, and they often require multiple hospitalizations, fluid resuscitation, blood transfusions, and management of opportunistic infections.

The maintenance phase is the final phase of treatment, lasts 18-24 months, and is characterized by lower intensity, anti-metabolite-based chemotherapy. Chemotherapy during this phase is often given orally and treatment with methotrexate and 6-mercaptopurine are common. This phase is often better tolerated by patients, and they can start returning to their normal life at this time.

Because involvement of the central nervous system (CNS) is not uncommon in T-ALL, patients will receive intrathecal chemotherapy of methotrexate, cytarabine, or hydrocortisone as a prophylactic treatment. This is routinely given in 6 or more doses over the course of treatment for prophylaxis and usually occurs within the first 2-4 months of treatment. If CNS involvement is detected, patients will then be subjected to further intrathecal chemotherapy treatment and cranial radiation.

Another treatment option in ALL that is sometimes, but not frequently, utilized in high-risk T-ALL patients is hematopoietic stem cell transplantation. Cytogenetics is the most common risk factor in predicting which patients should go on to have a stem cell transplant, and this treatment is not often curative. Patients who undergo stem cell transplantation still have a very high rate of disease relapse and often maintain a poor prognosis after transplant. While treatment with chemotherapy and stem cell transplant

have significantly improved patient survival, they do not come without significant toxicities and sequelae that patients have to endure, making research necessary to develop more targeted therapies with less long-term side effects.

There are very few targeted therapies available for T-ALL patients, and this field is lacking far behind other diseases. However, one class of targeted therapies that are used in T-ALL treatment is imatinib or dasatinib, which are tyrosine kinase receptor inhibitors that are used in conjunction with other more traditional chemotherapies in patients with Philadelphia chromosome positive T-ALL. Development of other targeted therapies is still a work in progress and clinical or pre-clinical trials are undergoing utilizing inhibitors of many common cancer signaling pathways as therapeutic targets including: Notch inhibitors, PI3K/AKT/mTOR inhibitors, JAK/STAT inhibitors, MAPK inhibitors, In addition, cell cycle inhibitors and proteasome inhibitors are in clinical trials for T-ALL treatment. Finally, epigenetic agents and immunotherapies are under development for T-ALL, including monoclonal antibody and BiTE/CAR immunotherapies <sup>2</sup>.

### **1.3 Patients with T-ALL Relapse have a Poor Overall Prognosis**

The cure rate for T-ALL has drastically improved in recent years, with 5-year event-free and overall survival rates over 70% and 80%, respectively <sup>5,16</sup>. However, relapse is relatively common in T-ALL, with approximately 25% of children diagnosed with T-ALL experiencing disease relapse. Both extramedullary relapse and induction failure are more common in T-ALL than in B-ALL, and the prognosis of relapse is very poor, with only a 30-50% survival rate <sup>16,17</sup>.

Currently, strong predictors for disease relapse are lacking, yet some factors are known to put patients at a higher risk of disease relapse. Relapse typically occurs within 2 years of initial diagnosis and most often occurs during the maintenance phase of treatment<sup>2</sup>. Relapse can be characterized by clonal evolution and selection of resistant genetic variants, with the dominant clone at relapse often being a minor clone at diagnosis<sup>2,16</sup>.

At the present time, the best indicator of a high risk of relapse is having a high minimal residual disease (MRD) at the end of induction therapy and end of consolidation therapy<sup>2,16</sup>. MRD is defined as the persistence of leukemic cells after therapy, which are often tracked by molecular methods or flow cytometry throughout the course of treatment. More sensitive methods using quantitative polymerase chain reaction (qPCR) to assess for fusion transcripts or T-cell receptor (TCR) rearrangements is starting to become the dominant method for MRD tracking<sup>5,18,19</sup>.

Additionally, the presence of certain mutations have been associated with relapse as well. For example, cytosolic 5'-nucleotidase II (NT5C2) mutations are found in 20% of T-ALL relapses and transcription factor Dp family member 3 (TFDP3) mutations are highly associated with chemoresistance<sup>20,21</sup>. Relapsed clones are also enriched for additional chemoresistance genes such as mutS homolog 6 (MSH6) or mutations in the mitogen-activated protein kinase (MAPK) gene leading to resistance to glucocorticoid treatment<sup>2</sup>.

Treatment for T-ALL relapse involves re-induction chemotherapy, where patients cycle back and re-start induction therapy until they are able to achieve remission without detectable MRD at the end of induction. The re-induction remission rate for relapsed T-ALL is only 30-40%. Other treatments are being studied for use in T-ALL relapse such as bortezomib, which is a proteasome inhibitor that shows some promise. Eventually, most

relapsed patients undergo stem cell transplantation, which can have undesirable side effects and risks to the patient <sup>2</sup>.

#### **1.4 Targeted Therapies Remain a Challenge in T-ALL Treatment**

Despite the significant amount of progress that has been made in improving treatment regimens and outcomes for patients with T-ALL, there are still many challenges that remain. First, treatment with intensive chemotherapy over the course of multiple years does not come without significant toxicities and side effects. Patients end up severely immunocompromised and hospitalized with opportunistic infections. Each chemotherapy drug also has associated toxicities, such as nephrotoxicity, ototoxicity, cardiotoxicity, along with common side effects such as loss of hair, nausea, and fatigue.

Treatment with chemotherapy or radiation can also increase the likelihood of patients developing secondary cancers from their treatment regimens. For example, alkylating agents (cyclophosphamide) and anthracyclines (doxorubicin) which are part of standard of care treatment for T-ALL have been linked to an increased risk of developing acute myeloid leukemia (AML) secondary to treatment. Radiation, depending on the site of treatment, can lead to secondary cancers of the skin, breast, thyroid gland, bones, spine, or brain <sup>22</sup>.

CNS prophylaxis or treatment of CNS disease with intrathecal chemotherapy or cranial radiation can induce debilitating toxicities and disabilities in patients. Many chemotherapies are neurotoxic and can induce side effects such as headaches, dizziness, fatigue, blurred vision or loss of balance. Long-term effects of intrathecal chemotherapy include but are not limited to: seizures, impaired executive function, cognitive deficits,

brain abnormalities, and leukoencephalopathy<sup>23,24</sup>. Cranial irradiation has many of the same toxicities as intrathecal chemotherapy, however these toxicities are more commonly observed and tend to be more severe than with chemotherapy. One additional side effect seen with cranial irradiation is brain tissue necrosis, which is devastating to patients<sup>25</sup>. Physicians are consciously limiting the amount of cranial irradiation done in patients with ALL, especially as a prophylactic measure, due to the long term cognitive effects and toxicities that are detrimental to patient quality of life.

The shift towards using more targeted therapies would significantly reduce toxicities and long-term sequelae seen in patients after treatment. Unfortunately, the use of target therapies and immunotherapies in T-ALL is lagging significantly behind other leukemias. This is due to both a lack of knowledge of specific oncogenic targets as well as major challenges in utilizing T-cell based immunotherapies in T-ALL<sup>26</sup>. While chimeric antigen receptor (CAR) T-cells have completely revolutionized the treatment regimens in B-ALL, engineering CAR T-cells from leukemic cells has many barriers, including T-cell fratricide by T-cell targeted clones and risk of severe immunodeficiency secondary to elimination of normal T-cells<sup>3,26</sup>. Recent studies using monoclonal antibody immunotherapy, such as antibodies targeting IL-7R $\alpha$ , have shown promise in pre-clinical trials in the treatment of T-ALL<sup>27</sup>. The development of targeted therapies towards oncogenic mutations common in T-ALL, such as NOTCH and PI3K/AKT/mTOR pathways, and immunotherapies utilizing monoclonal antibodies are underway, they have yet to show major success in clinical trials in T-ALL<sup>3</sup>.

In total, the major clinical concern regarding T-ALL is the disproportionately high rate of relapse in this disease compared to other acute leukemias. Not only is the relapse

rate higher, but the prognosis of relapsed patients is worse for T-ALL than in any other type of acute leukemia. More research is needed to better understand the causes of T-ALL relapse and identify better treatment regimens to improve the outcome of patients with relapsed T-ALL.

## CHAPTER 2. LEUKEMIA STEM CELLS

## 2.1 Cancer Stem Cells Drive Cancer Progression and Relapse

The idea of cancer stem cells (CSCs) is not a novel concept, despite the recent resurgence in research interest in cancer stem cells. The concept first came about in 1937 when it was demonstrated that a single cell from a mouse tumor could form a new tumor in a recipient mouse<sup>28</sup>. In the decades following, further transplantation studies validated that solid tumors were able to re-form in mouse recipients from a very small population of initial tumor cells, ranging from  $10^3$  to  $10^7$  cells<sup>29-31</sup>. In the late 1960s and 1970s, stem-like cells were first reported in hematologic malignancies<sup>31-35</sup>. However, the discovery of oncogenes and tumor suppressor genes in the 1970s shifted the focus of cancer research away from cancer stem cells for decades to follow<sup>32</sup>.

In 1994, a resurgence of cancer stem cell research began when John Dick's group identified a sub-population of tumor-initiating cells in acute myeloid leukemia (AML) upon transplantation into immune-compromised mice<sup>36</sup>. CSCs behave much like normal tissue stem cells and it is thought that they may arise from normal adult stem cells or precursor cells. CSCs have been identified in a wide variety of both hematologic malignancies and solid tumors, including but not limited to, leukemia, breast cancer, colon cancer, liver cancer, pancreatic cancer, lung cancer, prostate cancer, melanoma, and brain cancer<sup>37-39</sup>.

Current research in the field suggests that cancer stem cells make up a small minority of a bulk tumor and these cells are long-lasting, chemotherapy and radiation resistant, and are capable of undergoing self-renewal and differentiation, both reproducing themselves and repopulating the tumor, causing relapse in patients or tumor re-growth upon transplantation into mice<sup>39</sup>. The bulk of the tumor is then made up of non-CSCs that are

fully-differentiated and only capable of transient, rapid proliferation and do not contribute to long-term growth and maintenance of the tumor <sup>32</sup>. However, some groups have identified tumors in which CSCs are both abundant and rapidly proliferating <sup>40</sup>. It is likely that different tumors types and even individual tumors of the same type have significant variations in CSC frequency and properties.

Self-renewal, a defining characteristic of CSCs, is a process by which stem cells, including CSCs, undergo division to repopulate the undifferentiated stem cell population <sup>41</sup>. Adding layers of complexity to the CSC phenotype, the cancer stem cell/self-renewing state may not be hard-wired in specific cells, and instead be a state that any tumor cell could transition in and out of, a concept known as CSC plasticity. Yet many people believe it is an intrinsic property of CSCs that can be regulated by either intrinsic or extrinsic signals from the CSC niche <sup>40,41</sup>. Some cancer types, such as colorectal cancer, seem to have more plasticity in their cancer stem cells compared to more hierarchical, unidirectional organization of CSCs found in other cancers such as glioblastoma and AML <sup>40</sup>. Cancers with CSC plasticity will present their own unique challenges for targeting CSCs therapeutically, as targeting a transient state is very difficult.

Another defining feature of CSCs is resistance to standard cytotoxic chemotherapy regimens. Treatment resistance in CSCs is due to a combination of mechanisms, including: upregulation of drug efflux pumps, ability to adopt a quiescent state, cell plasticity, increased DNA-repair capacity, anti-apoptotic protein expression and protection against reactive oxygen species <sup>32,40,42</sup>. Current cancer treatment eliminates rapidly dividing cells and therefore favors the selection of dormant, quiescent clones that then have the potential to become dominant after treatment <sup>43</sup>. This adaptation of a dormant state can be via gene

expression changes or epigenetic changes from selection pressure induced by cancer treatment <sup>40</sup>.

Studying CSCs and their properties has also proved challenging. Oftentimes, CSCs are selected for or enriched for by cell surface markers, however this introduces bias and often misses critical CSC biology <sup>39,44</sup>. Identifying CSC-specific cell surface markers is a major area of research focus currently and is required to be able to isolate, study, and target CSCs in the future. The gold standard of CSC experimentation remains limiting dilution transplantation assessing self-renewal potential with regeneration of a tumor resembling the original tumor that the cancer stem cell was derived from <sup>39</sup>. Another method for studying CSCs is by lineage-tracing, which may be a more appropriate method for better understanding CSC fate because it allows for following specific cells and tracking their behavior over time <sup>40</sup>. However, the lack of pre-clinical models available for studying and tracking CSCs *in vivo* and in primary tumors is a major limitation in CSC research and development of new models is imperative <sup>32,45</sup>.

Despite all the different theories and unknowns surrounding cancer stem cells, cancer relapse has been demonstrated to be enriched in cancer stem cells, likely due to selection pressures towards resistant cells during cancer treatment, and targeting these CSCs in relapse is going to be critical to improving outcomes in relapsed patients <sup>46-49</sup>. Local recurrence of disease is inevitable in patients treated with only cytotoxic chemotherapy and radiation treatment due to the presence of cancer stem cells that are inherently resistant to these types of therapies <sup>32</sup>.

## 2.2 Leukemia Stem Cells Self-Renew and are Treatment Resistant

The first evidence of leukemia stem cell clonal origin in acute myeloid leukemia (AML) was in 1974 and since then, AML has served as a model disease for both leukemia and cancer stem cell research<sup>50</sup>. In 1992, evidence of LSCs in long-term co-culture models was published and in 1994, a small sub-population of AML-initiating cells was identified and characterized after transplantation into immune compromised mice<sup>36,51</sup>. These leukemia-initiating cells were found to be CD34<sup>+</sup>/CD38<sup>-</sup> with a LSC frequency of one in one-million cells was a LSC<sup>36</sup>. Expanded clonal populations of pre-leukemic HSCs have been identified in AML patient samples and in myeloid leukemias, LSCs and pre-leukemic LSCs, for the most part, arise directly from mutations in HSCs or hematopoietic progenitor cells<sup>52-55</sup>. Clinically, LSCs are treatment resistant and responsible for relapse in patients, with residual LSCs evading chemotherapy, undergoing clonal expansion, and causing patient relapse<sup>56-58</sup>.

The CD34<sup>+</sup>/CD38<sup>-</sup> phenotype was the first LSC immunophenotype identified and widely accepted<sup>36,59,60</sup>. Since then, AML LSCs have been identified in both CD34<sup>+</sup> and CD34<sup>-</sup> cell populations and there is a lack of consensus in the field on consistent markers for LSCs in leukemias<sup>61-64</sup>. Some believe that non-CD34<sup>+</sup>/CD38<sup>-</sup> LSCs arise from more mature myeloid cells compared to CD34<sup>+</sup>/CD38<sup>-</sup> LSCs which are thought to arise from hematopoietic stem cells (HSCs)<sup>65</sup>. More than 15 different cell surface markers have been identified as LSC markers in chronic myelogenous leukemia (CML) and AML<sup>65</sup>. Due the wide variety and lack of consensus in LSC-specific cell-surface markers, engraftment into immune compromised mice remains the gold-standard of identifying LSCs in patient AML samples<sup>65</sup>. However, many CML samples fail to engraft into xenograft models, making

studying CML LSCs more complicated and these cells may have compromised self-renewal potential<sup>51,65</sup>. The advent of single cell analysis and cell barcoding will likely help to identify newer, more consistent, and more specific LSC markers in the future that can be capitalized on as therapeutic targets.

Despite the high degree of plasticity and reversibility observed in many different solid tumor CSCs, LSCs in AML were found to follow a hierarchical pattern<sup>60</sup>. Additionally, functional hierarchies and heterogeneity may even be present within LSC populations from a single patient. LSCs are non-cycling cells and are located in the endosteal bone marrow region<sup>66</sup>. They are further characterized by their resistance to treatment, and even demonstrate resistance against targeted therapies, such as imatinib in CML<sup>67</sup>. LSC quiescence and self-renewal, much like CSC self-renewal in general, has been attributed to signaling through growth factors, microRNAs and other regulatory pathways<sup>65</sup>. LSCs can also be reversibly quiescent and can be driven into cell cycling, which can be taken advantage of as a therapeutic strategy<sup>66,68,69</sup>.

A large number of signaling pathways have been implicated in the maintenance and leukemia-initiating properties of LSCs. Many of the same pathways critical to CSC maintenance and self-renewal are important in LSC self-renewal and maintenance. Wnt, NOTCH, Hedgehog, and bone morphogenic protein signaling are commonly de-regulated in LSCs<sup>70,71</sup>. Other pathways such as PI3K/AKT/mTOR and JAK/STAT are also important in LSC maintenance. Finally, signaling from the bone marrow niche of LSCs in myeloid malignancies via CXCR4, HIF, SCF and VEGF is essential to LSC maintenance as well<sup>72</sup>.

Epigenetics also plays a role in LSCs, with the first evidence of altered epigenomes in LSCs arising in 2011<sup>73</sup>. LSCs in AML display an epigenetic and mRNA signature that is similar to HSCs or hematopoietic progenitor cells, yet are still distinct from this population<sup>62,74-76</sup>. Methylation patterns and regulation of epigenetic markers are often unique in LSCs<sup>75,77,78</sup>.

Finally, metabolism has recently become an emerging area of focus in LSC research and is critical to LSC survival. In 2013 it was published that LSCs are dependent on oxidative phosphorylation and inhibition of this process can specifically target LSCs<sup>79</sup>. Recent studies have looked at sorting for the presence of reactive oxygen species (ROS) as a marker of LSCs<sup>80</sup>. Yet even this is inconsistent, as CML LSCs show high levels of ROS and AML LSCs show low ROS levels compared to bulk tumor cells<sup>79,81-83</sup>.

### **2.3 Targeting Cancer Stem Cells**

Current chemotherapies target rapidly proliferating cells, which do not impact slow-dividing, often quiescent, cancer stem cells. Furthermore, bias is introduced in pre-clinical testing for cancer therapeutics as the end-point of these studies is often shrinking of the bulk tumor, selecting for drugs that likely target bulk tumor cells and not complete elimination of cancer stem cells (**Figure 2.1**). Research is being done on treatments that target CSCs specifically via a variety of mechanisms. It is likely that combination treatment targeting both CSCs and the bulk tumor will be necessary to both eliminate CSCs and bulk tumor cells.

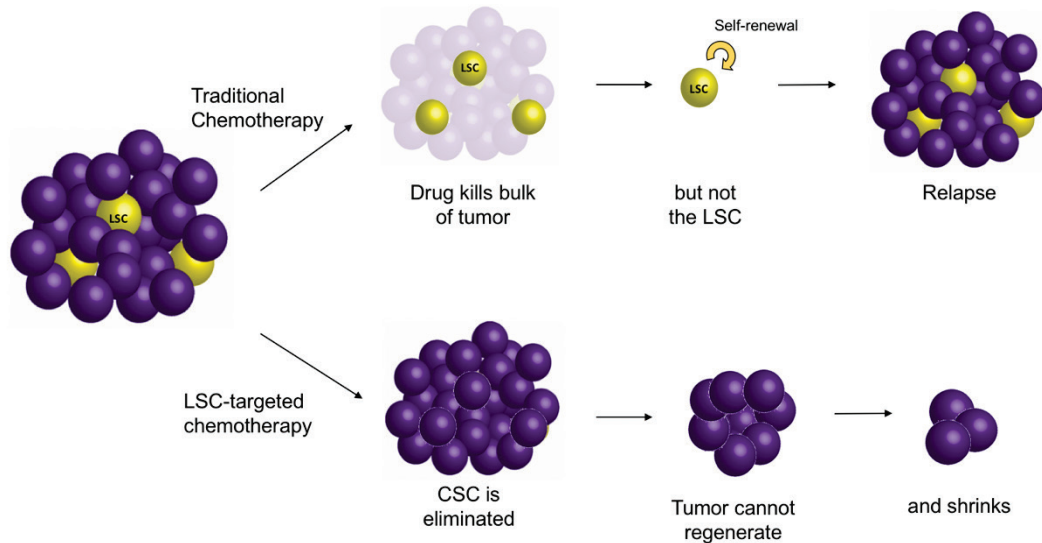


**Figure 2.1 Cancer Stem Cells Drive Patient Relapse**

Cancer or leukemia stem cells (yellow) make up a small minority of bulk cancer tumors. These cancer stem cells are chemotherapy and radiation therapy resistant, can undergo self-renewal and differentiation, and re-populate a tumor, causing cancer relapse in patients. With LSC or CSC targeted therapies, CSCs would be eliminated or forced to terminally differentiate, and when combined with traditional chemotherapy and radiation therapy, would both shrink the tumor and prevent tumor regeneration, eliminating relapse potential.

One current limitation is that a lack of correlation remains between the proportion of CSCs in a patient's tumor and prediction of clinical outcomes, preventing translational applications of cancer stem cell research and therapies<sup>39</sup>. Additionally, there is a large degree of patient-to-patient variability in CSCs and the CSC frequency between patients is highly inconsistent<sup>45</sup>. Yet despite the challenges, recent efforts have devised a variety of strategies to specifically target LSCs or CSCs, some of which have had more success than others. There are two main strategies for targeting CSCs: forcing differentiation to increase susceptibility to chemotherapy, or preventing activation or differentiation of quiescent cells, preventing them from ever forming cancer relapse<sup>39,45,84</sup>. Both of these strategies are

being tested in combination with an array of different types of therapy aimed at preventing or better treating patient relapse *in vivo*.

The most obvious way to target CSCs is to target signaling pathways that are critical in maintaining CSCs or that are involved in CSC self-renewal. Research is ongoing on the potential of targeting cell-cycle checkpoints and DNA-damage repair pathways in CSCs<sup>45</sup>. Drugs aimed at developmental pathways have been developed and many are in clinical trials, including Wnt pathway inhibitors, which are described in detail in Chapter 4. Antibodies against Notch signaling components, such as delta like ligand 4 (DLL4) decreased tumor cell proliferation and CSC function in a colon cancer mouse model and eliminated tumor initiating cells in neuroendocrine cancer<sup>85,86</sup>. Signal transducer and activator of transcription 3 (STAT3) inhibitors are also in clinical trials and seem promising for targeting LSCs in AML<sup>84,87</sup>.

Another way to target CSCs is by identifying and targeting unique cell-surface markers, making identification of CSC-specific markers imperative. A monoclonal antibody against the interleukin-3 receptor alpha chain (CD123) decreases LSCs in a mouse model of AML<sup>88</sup>. Targeting of the receptor for interleukin-8 (CXCR1) on the cell surface of breast cancer cells in combination with traditional chemotherapy eliminated breast cancer bulk tumor and cancer stem cells in a xenograft mouse model<sup>89,90</sup>. Antibody-drug conjugates directed against CD33<sup>+</sup> leukemic stem cells showed success in clinical trials in AML, but ultimately displayed too high of a degree of toxicities<sup>91</sup>.

Epigenetic manipulation of CSCs is an additional strategy being studied as a CSC therapeutic. Clinical trials are ongoing using epigenetic regulators of CSCs in AML and solid tumors. The most popular epigenetic targets currently are: bromodomain and

extraterminal domain (BET) proteins, histone deacetylases (HDACs), lysine-specific histone demethylase 1A (LSD1), and isocitrate dehydrogenases (IDH1/IDH2)<sup>40</sup>. The most promising of these epigenetic regulators seem to be HDAC inhibitors, which are FDA-approved in multiple malignancies.

Finally, targeting interactions with the CSC niche holds promise. The cancer stem cell niche is made up of the extracellular matrix and a variety of cell types, including fibroblasts, neutrophils, macrophages, and stromal cells. Targeting of each of these cell types are currently being studied as therapeutic options<sup>92-94</sup>. Additionally, targeting of the extracellular matrix components and interactions with cancer stem cells, such as disruption of matrix metalloproteinases (MMPs), integrins, collagenase, and hyaluronidase have shown potential<sup>95-97</sup>.

A major success story and proof of principle for CSC-targeted therapy is in acute promyelocytic leukemia (APML). In this disease, leukemic cells are blocked in an undifferentiated state, acting similar to undifferentiated LSCs<sup>98</sup>. The use of all-trans retinoic acid (ATRA) and arsenic trioxide, which has been used in the treatment of APL clinically for decades, induces terminal differentiation of APML stem-like cells, leading to eradication of this disease<sup>99-102</sup>. When combined with traditional chemotherapy, these leukemic cells are forced to terminally differentiate and are eliminated by traditional chemotherapy, improving outcomes even further<sup>103,104</sup>. These studies provide proof of principle for therapies that strive to induce differentiation of CSCs in clinical practice.

Overall, there are a wide variety of strategies that are being studied as CSC therapeutics, many of which hold promise in pre-clinical or clinical trials. Yet with these successes, there are challenges that remain in targeting CSCs, including: CSC plasticity,

potential damage to normal stem cell populations, a lack of CSC-specific markers, and a lack of experimental models to perform high-throughput drug screens for efficacy against CSCs *in vivo*. Despite these challenges, therapeutic targeting of CSCs holds promise and the first successes in CSC based therapies are starting to emerge.

#### **2.4 LSCs in ALL are Responsible for Disease Relapse**

In ALL, LSCs are not as well characterized as they are in myeloid leukemias. Leukemia stem cells have been identified in B-ALL with a wide variety of cell-surface markers. CD34<sup>+</sup>/CD38<sup>-</sup> cells are enriched for LSCs in B-ALL as they are in myeloid leukemias<sup>105</sup>. This is likely due to the fact that B-ALL is derived from the bone marrow progenitor cells similar to AML. Yet additional cell populations have been identified as enriched for LSCs in B-ALL, including: CD34<sup>+</sup>/CD19<sup>-</sup>, CD34<sup>+</sup>/CD19<sup>+</sup>, CD34<sup>+</sup>/CD38<sup>+</sup>/CD19<sup>+</sup>, CD34<sup>+</sup>/CD38<sup>-</sup>/CD19<sup>+</sup>, and CD34<sup>-</sup>/CD19<sup>+</sup><sup>106-111</sup>. Despite a lack of consensus markers of LSCs in B-ALL, there is a consensus that there are leukemia-initiating cells present in B-ALL that are capable of self-renewal, differentiation, and tumor formation *in vivo*.

In T-ALL, disease origin is unique, as leukemic T-cells are not derived from the bone marrow as in other leukemias, but from immature T-cells located in the thymus driven by T-cell receptor (TCR) rearrangements<sup>112</sup>. There is a great deal of evidence that LSCs exist in T-ALL, derived from immature thymocytes, that are capable of de novo tumor formation, self-renewal, and quiescence. LSCs in T-ALL that form leukemias upon transplantation have been identified in zebrafish models, mouse models, and patient samples<sup>106,113-128</sup>. In T-ALL patients, LSCs are present throughout the course of initial

disease and relapse and were found to persist even after treatment with dexamethasone in high-risk T-ALL <sup>117</sup>.

In normal T-cell differentiation, early thymocytes can acquire stemness features, self-renew, and can repopulate the full T-cell repertoire <sup>112,129,130</sup>. This happens via Notch signaling, leading to activation of TCF7 and GATA3 which then leads to activation of BCL11B and LEF1 <sup>131</sup>. These changes cause transcriptional silencing of TAL1 and LMO2, leading to a loss of stem and progenitor cell potential. In addition, RAG1, RAG2, and PTCRA are upregulated and function in TCR recombination <sup>112</sup>. Dysregulation of these proteins, such as Notch, TAL1, and LMO2 are drivers of T-ALL disease formation and promote a more immature, stem-like phenotype.

As in B-ALL, there is a lack of consensus on stem cell-specific cell surface markers in T-ALL. CD34<sup>+</sup>/CD4<sup>-</sup>, CD34<sup>+</sup>/CD7<sup>-</sup>, and CD34<sup>+</sup>/CD7<sup>+</sup> cell populations have all been shown to have leukemia-initiating capacity and engraftment capabilities <sup>113,115</sup>. CD7<sup>+</sup>/CD1a<sup>-</sup> cells are also enriched in LSCs and demonstrate glucocorticoid resistance <sup>117</sup>. CKit<sup>mid</sup>/CD3<sup>+</sup> cells with Myc over-expression act as LSCs in a Pten null mouse model of T-ALL and can be targeted by inhibition of PI3K and Myc simultaneously <sup>114,132</sup>. ROS<sup>low</sup> and ROS<sup>low</sup>CD44<sup>+</sup> cell populations are enriched for T-ALL LSCs, implicating a role for metabolism in T-ALL LSCs <sup>119</sup>. Finally, IL7R<sup>+</sup> has been used as a cell-surface marker for isolating LSCs in T-ALL <sup>124</sup>.

Signaling pathways critical in T-ALL have a significant amount of overlap with CSC signaling pathways in general. Even though T-ALL LSCs are not derived from the bone marrow, it appears that a HSC-like transcriptional signature is induced in T-ALL LSCs <sup>112</sup>. Notch signaling is essential for normal T-cell precursor development via Hes1

and Myc expression, and Notch inhibition abolished leukemia-initiating potential in a mouse T-ALL model <sup>14,116</sup>. In a zebrafish T-ALL model, AKT/mTORC1 activation was identified as a driver of LSC self-renewal <sup>128</sup>. Another protein enriched in LSCs in T-ALL is CXCR4, which modulates interaction with the microenvironment <sup>126,127</sup>. Beta-catenin and HIF1 $\alpha$  are also crucial to LSC self-renewal and maintenance in a mouse T-ALL model <sup>133</sup>. Further research will help to clarify signaling pathways important in T-ALL LSCs and characterize cross-talk between those pathways that have already been identified.

## **2.5 Targeting LSCs in T-ALL**

A wide range of strategies have been suggested for targeting LSCs in T-ALL, yet none have become clinical realities. These strategies for targeted T-ALL LSC therapy are outlined in (**Table 2.1**) below. The most studied and most common strategy remains chemical inhibition of LSC signaling pathways, such as Notch, IGF, PI3K/AKT/mTOR, or Wnt/beta-catenin signaling <sup>40,116,119,128,133,134</sup>. These strategies have shown promise, with targeting of Notch and Wnt/beta-catenin signaling demonstrating inhibition of LSCs in T-ALL mouse models <sup>116,133</sup>. Antibody therapies, cell-surface targeted therapies and cell cycle regulators are additional strategies for targeting LSCs<sup>135–143</sup>. More recently, data has emerged demonstrating epigenetic regulators and niche modulators may target LSCs in T-ALL as well <sup>126,127,144–150</sup>. Two major challenges with all of these methods is that there is overlap between normal stem cell and LSC signaling pathways, leading to depletion of normal stem cell populations with LSC-targeted therapies and LSC plasticity <sup>151</sup>.

The most promising strategy to eliminate LSCs with the least amount of side effects and without depletion of normal stem cell populations would be targeting of LSC-specific

cell-surface markers; however these markers have yet to be discovered. Identification of cell surface markers that are widely expressed on T-ALL LSCs and specific to LSCs is critical to the development of improved LSC-targeted therapies. The advent of LSC-targeted therapies in T-ALL treatment, eliminating LSCs, would decrease patient relapse and dramatically improve T-ALL survival. Therefore, there is a major need in the field to define mechanisms of self-renewal in order to identify molecular targets for therapeutic targeting of T-ALL LSCs.

Overall, the work in this dissertation examines leukemia stem cell biology and function and also looks at biomarkers or predictors of patient relapse and poor prognosis in ALL. **Part 2** outlines a novel role for the oncogenic phosphatase of regenerating liver-3 (PRL-3) in leukemia stem cell self-renewal (**Chapter 3**), at least in part, through the Wnt/ $\beta$ -catenin signaling pathway (**Chapter 4**). While **Part 3** outlines novel technologies and techniques used to detect and prevent ALL patient relapse and improve patient outcomes. **Chapter 5** describes a novel LSC reporter zebrafish line that can be used to study LSC behavior and response to drug treatment *in vivo*. **Chapter 6** focuses on utilization of zebrafish as a xenograft model for patient-derived cancer cells to predict patient response to drug treatment and the effect that different temperature and injection sites have on cancer cell behavior and metabolism. Finally, **Chapter 7** outlines the use of cell-free DNA as a potential biomarker of residual disease in ALL. The work detailed in this dissertation both identifies a possible novel therapeutic target in T-ALL LSCs and describes new techniques developed for study of LSCs and disease relapse in a zebrafish model and in ALL patients.

**TABLE 2.1 STRATEGIES FOR THERAPEUTIC TARGETING OF LEUKEMIA STEM CELLS**

<b>Strategy</b>	<b>Examples</b>	<b>Mechanism</b>	<b>Challenges</b>	<b>References</b>
Chemical inhibition of stem-cell signaling pathways	Notch, IGF, PI3K/AKT/mTOR, Wnt/beta-catenin pathway inhibition	Inhibition of critical stem-cell pathways to block self-renewal or promote differentiation	Toxicities against normal stem cells, lack of signaling pathways specific to cancer stem cells, LSC plasticity causes changes in signaling pathways	40, 116, 119, 128, 133-134
Antibody therapies	Anti-LMO2 intracellular antibody, antibodies against cell surface markers	Antibody-dependent cell cytotoxicity or disruption of protein complex formation	Lack of specific targets, depletion of normal stem cells	135-137
Targeting cell surface proteins	CAR-T cells or antibodies against CD5, CD1a, or CD7	Target proteins expressed specifically on the surface of LSCs leading to LSC elimination	Lack of LSC-specific cell-surface markers in T-ALL,	138-141
Cell cycle regulation	CDK7 inhibitors	Modulate cell-cycle critical to LSC self-renewal and differentiation	Quiescence impairs sensitivity to cell-cycle directed therapies	142-143
Epigenetic regulators	bromodomain inhibitors (BET4, JQ1), EZH2 inhibitors, HDAC inhibitors	Epigenetic modulation of expression of genes involved in self-renewal or differentiation	Acquired resistance, toxicities, identification of epigenetic modulators	144-150
Niche modulators	CXCR4/CXCL12 inhibition	Disrupt interaction with stromal cells	Disruption of normal stem-cell niche interactions	126-127

PART 2. THE ROLE OF THE PROTEIN TYROSINE PHOSPHATASE PRL-3 IN T-ALL SELF-RENEWAL

CHAPTER 3. PRL-3 ACCELERATES ALL PROGRESSION AND INCREASES LSC  
FREQUENCY

*Partially taken from: Protein tyrosine phosphatase 4A3 (PTP4A3/PRL-3) drives migration and progression of T-cell acute lymphoblastic leukemia in vitro and in vivo. Min Wei, Meghan Haney, Dylan Rivas, Jessica Blackburn. Oncogenesis, 2020.*

## 3.1 Introduction

### 3.1.1 PRL-3 Identified as a Driver of Self-Renewal in T-ALL

Preliminary data from an unbiased serial limiting dilution transplantation screen for drivers of self-renewal in a Myc-induced zebrafish T-ALL models suggested that PRL-3 may play a role in leukemogenesis. Serial limiting dilution transplantation was done with tumors isolated from single leukemia clones to identify drivers of self-renewal in T-ALL. While most of the tumors maintained approximately the same LSC frequency with each passage, a subset (6 of 47) clonal leukemias developed an increase in LSC frequency with each serial transplantation<sup>128</sup>. Microarray-based comparative genomic hybridization (aCGH) was done comparing low-self renewal tumors, or tumors with a low LSC frequency, with high self-renewal tumors with a high LSC frequency. aCGH showed 16 recurrent amplifications at the genomic level in the tumors that evolved high self-renewal, one of which was PRL-3. PRL-3 expression was elevated in 13 of 36 leukemia clones that had high self-renewal at the initial limiting dilution transplantation and in 90% of clones that evolved high self-renewal over time with serial passaging (Blackburn and Langenau, unpublished).

Based on this preliminary data indicating that PRL-3 plays a role in T-ALL, our lab began interrogating the role of PRL-3 in leukemia. We found that over-expression of PRL-3 in leukemia cell lines increases migration capabilities and this phenotype is reversed by PRL-3 knock-down with shRNAs, without any effect on cell proliferation or apoptosis. This migration effect is due to activation of the Src kinase pathway signaling cascade. Overall, this publication demonstrated a clear role for PRL-3 in T-ALL migration and progression *in vitro* via Src kinase pathway signaling<sup>152</sup>.

### 3.1.2 PRL-3 is a Dual-Specificity Protein Tyrosine Phosphatase

Protein tyrosine phosphatase 4A3 (PTP4A3) or phosphatase of regenerating liver-3 (PRL-3) is a cysteine-based dual-specificity protein tyrosine phosphatase. PTPs remove phosphate groups that are attached to tyrosine residues on their substrates. This class of phosphatases is made up of four different sub-families, characterized based on their catalytic domains and amino acid sequences. The first class of PTPs is the largest class and is known as the type-I cysteine-based PTPs. This class can then be further divided into the classical PTPs and the dual specificity PTPs (DUSPs). The phosphatase of regenerating liver (PRL) family is a subset of the DUSP family. The DUSP family, which PRL-3 belongs to, is made up of 7 different subfamilies: Slingshots, PRLs, CDC14s, PTENs, Myotubularins, MKPs, and atypical DUSPs. The defining feature of DUSPs is that they are able to dephosphorylate both tyrosine and serine/threonine residues within one substrate<sup>153</sup>.

PRL-3 is a member of the PRL family of DUSPs. PRL-1 was the first protein identified in the PRL family in 1991 and was identified as one of the genes upregulated early in regenerating livers after partial hepatectomy<sup>154</sup>. PRL-2 and PRL-3, the other two PRL family members, were later identified based on sequence homology in mice to PRL-1<sup>155</sup>. PRL-1 and PRL-2 are most similar in amino acid sequence, with PRL-3 being the most unique, yet still having 79% and 76% homology to PRL-1 and PRL-2 respectively<sup>156,157</sup>. The PRL proteins have a small molecular weight, at 22 kDa, and sequence alignment of PRL-1, 2, and 3 reveals a conserved catalytic PTP motif (also known as a P loop), a tryptophan-proline-phenylalanine-aspartate-aspartate (WPFDD) loop, a polybasic region and a cysteine-aliphatic amino acid- (any amino acid) (CAAX) prenylation motif (**Figure**

**3.1)** <sup>156,158</sup>. Mutation of C104S in the P-loop region, and D72A in the WPFDD loop region yields a phosphatase dead mutant form of PRL-3. C104S mutation has been shown to lead to a loss of PRL-3 phosphatase activity *in vivo* and a loss of metastasis in a mouse xenograft model <sup>159,160</sup>. Mutation of D72A has been reported to further decrease PRL enzymatic activity <sup>161,162</sup>.

The prenylation motif is unique to the PRL family of phosphatases and allows for anchoring of the protein into the cell membrane <sup>158</sup>. The CAAX prenylation motif in PRL-3 plays a role in subcellular localization, and PRL-3 has been demonstrated to shuttle between the cell membrane and nucleus during different phases of the cell cycle <sup>162-165</sup>. Mutation of C170S in this prenylation motif disrupts the ability of PRL-3 to interact with negatively charged phospholipids in the membrane, inhibiting PRL-3 localization in the membrane <sup>166,167</sup>. Deletion of the C-terminal prenylation motif of PRL-3 promotes nuclear accumulation yet the functional significance of this has not been well characterized <sup>162</sup>. In addition to the prenylation motif, PRL-3 has a predicted nuclear localization sequence and may traffic predominately to the nucleus when the prenylation motif is disturbed and may play a role in functional regulation of PRL-3 <sup>162</sup>.

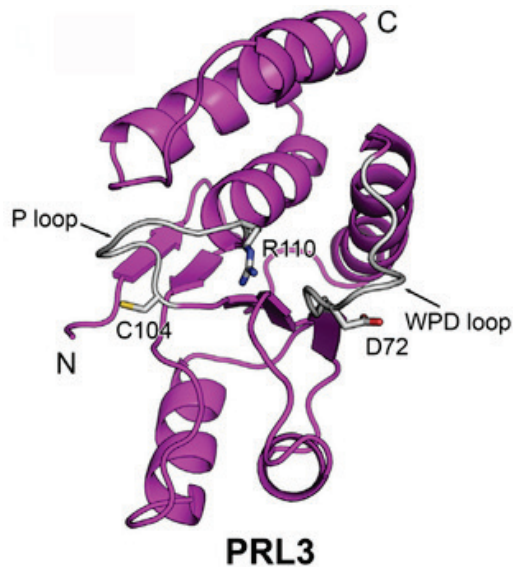


**Figure 3.1 PRL-3 Protein Structure**

The cysteine residue in the P-loop (C104) acts as a nucleophile during phosphorylation and is critical for PRL-3 phosphatase activity. The aspartate residue in the WPFDD loop (D72A) acts as a proton donor and promotes formation and hydrolysis of the enzyme intermediate and is also critical for PRL-3 phosphatase activity. The CAAX motif at the C-terminus is unique to the PRL family of PTPs and facilitates membrane binding (Adapted from Wei et al 2018<sup>158</sup>).

In addition to acting as a phosphatase, PRL-3 has been demonstrated to have a non-phosphatase dependent function as well. PRL-3 binds the a family of magnesium transporters, the cyclin M (CNNM) family, increasing intracellular magnesium concentrations<sup>160</sup>. This increase can contribute to tumorigenesis and cancer progression both *in vitro* and *in vivo*<sup>168</sup>. Interestingly, the phosphorylation binding site of PRL-3 is required for its role in binding to the magnesium transporter, even though it is not via a phosphorylation-dependent mechanism<sup>160</sup>. These studies demonstrated a role for PRL-3 in cancer that is not dependent on its function as a phosphatase, leading to the hypothesis

by some that PRL-3 may actually function as more of a pseudophosphatase than a true phosphatase.

The normal cellular functions of PRLs have not yet been identified; however, expression of the PRLs has been shown to follow a magnesium-dependent circadian pattern and may play a role in circadian control of behavior and metabolism<sup>169</sup>. Recently, animal knockout models of PRLs have shed some insight into their physiologic roles, but the knockout phenotypes are likely masked by the redundancy of PRL-1, 2, and 3. Two groups have created PRL-3 conditional knock-out mice with very different results. One group showed no phenotype in PRL-3 knock-out mice, while the other group showed sex-dependent decreases in body weight and BMI, suggesting PRL-3 may be involved in metabolism in a sex-dependent manner<sup>170,171</sup>. PRL-3 mRNA expression can be detected primarily in the heart, skeletal muscle, vasculature and brain<sup>155</sup>. Further research needs to be done to identify the physiologic and oncogenic roles of PRL-3 and other PRLs.

### **3.1.3 PRL-3 Acts as an Oncogenic Driver in Solid Tumors**

The mammalian protein tyrosine phosphatase (PTP) family has been implicated in many different diseases, such as cancer, immunodeficiencies, and diabetes<sup>172</sup>. PRL-3 has been known and studied as an oncogenic driver in solid tumors for the last two decades. In 2001, PRL-3 was first identified as an oncogene when it was found to be upregulated in liver metastases compared to primary colorectal cancer tumors or normal colon epithelium. Interestingly, PRL-3 was the only molecule that was consistently elevated amongst all of the metastatic samples in that study<sup>173</sup>. Since then, PRL-3 has been studied extensively as a driver of progression and metastasis in colon cancer and high PRL-3 expression correlates with increased colorectal cancer progression and metastasis<sup>174-178</sup>.

In 2006, PRL-3 was found to be upregulated in breast cancer and was correlated with a decrease in disease free survival and an increase in distant metastases<sup>179,180</sup>. Since then, PRL-3 elevation has been reported in many other solid tumors. In gastric cancer, PRL-3 expression in primary tumors correlates with later occurrence of metastases and it is elevated in primary gastric cancer samples compared to normal tissue<sup>181,182</sup>. Additionally, PRL-3 is elevated in ovarian cancer and higher PRL-3 expression is correlated with later stage primary tumors and also with local tumor invasion<sup>183</sup>.

Since the early 2000s, PRL-3 has not only been recognized as a driver of solid tumor progression and metastases, but has also been identified as a possible biomarker or prognostic marker in colorectal cancer, breast cancer, gastric cancer, and other solid tumors<sup>166</sup>. PRL-3 expression is elevated in a wide variety of solid and liquid tumors, including those mentioned above, and prostate cancer, lung cancer, AML, and B-ALL<sup>184-188</sup>. In B-ALL, PRL-3 was found to regulate cell migration and adhesion through Src pathway signaling<sup>188</sup>. Furthermore, PRL-3 is associated with poor prognosis in both solid tumors and hematologic malignancies. Finally, more recently PRL-3 has been implicated in angiogenesis and tumor initiation<sup>171,178,189</sup>.

Based on previous studies, the oncogenic role of PRL-3 occurs via a wide variety of mechanisms and signaling pathways. PRL-3 has been implicated in many major signaling pathways, including p53, PTEN/PI3K/Akt, Src/ERK1/2, Rho family GTPases and adhesion proteins including integrin, E-cadherin, and MMPs<sup>157,190</sup>. While PRL-3 has been implicated in many different signaling pathways, there are challenges with studying and targeting PRL-3. Few studies have identified direct binding partners of PRL-3 as it has a very shallow binding pocket and is thought to have transient interactions with substrates.

This makes it both challenging to study PRL-3 direct substrates and challenging to directly target PRL-3. One strategy to target PRL-3 is with small molecule inhibitors. Theinopyridone and derivatives of theinopyridone have been identified as possible small molecule inhibitors of PRL-3 *in vitro* and *in vivo* <sup>191,192</sup>. Additionally, monoclonal antibodies against PRL-3, such as PRL3-zumab, which has shown promise in mouse studies against liver cancer <sup>193</sup>. The oncogenic role for PRL-3 has been well-characterized in solid tumors, yet there is a lack of knowledge about the role of PRL-3 in leukemias, and more specifically in T-ALL.

#### **3.1.4 Hypothesis and Specific Aims**

While the role that PRL-3 plays in T-ALL migration and progression *in vitro* has been clearly established, the role of PRL-3 *in vivo* in leukemia progression and migration has not yet been demonstrated. Additionally, PRL-3 was initially identified as a possible driver of self-renewal of LSCs in a Myc-induced zebrafish T-ALL model, yet its' function in LSCs has yet to be elucidated. Given this preliminary data, *I hypothesized that PRL-3 plays an important role in leukemia progression, migration and LSC self-renewal in vivo in T-ALL. To test this hypothesis, the following specific aims were developed: 1) To determine the role of PRL-3 in leukemia migration and progression in vivo, and; 2) To characterize the function of PRL-3 on LSC self-renewal.*

### **3.2 Results**

#### **3.2.1 PRL-3 is Upregulated in Human T-ALL Samples**

Our lab has previously shown that protein levels of PRL-3 are significantly elevated in human T-ALL cell lines and primary patient T-ALL samples compared to healthy

peripheral blood mononuclear cells (PBMCs) <sup>152</sup>. Additionally, microarray data from publicly available T-ALL patient bone marrow samples (GSE13159) shows significantly increased expression of PRL-3 mRNA compared to healthy control bone marrow (**Figure 3.2**). This data set included microarray gene enrichment data from over 200 samples <sup>194,195</sup>.

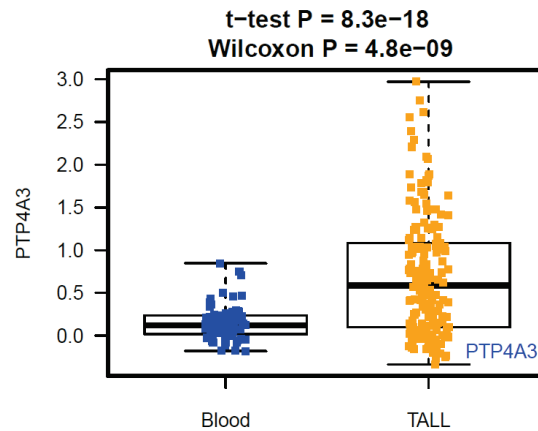


**Figure 3.2 Microarray Data Reveals PRL-3 Expression Increased in T-ALL**  
 Microarray gene enrichment data of GSE13159 comparing samples from healthy donors (n=72) to T-ALL patients (n=174). PRL-3 expression is increased in T-ALL compared to healthy controls (p=8.3x10<sup>-18</sup>).

### 3.2.2 PRL-3 Accelerates T-ALL Progression in a Zebrafish Model

The elevated expression of PRL-3 in T-ALL patient samples and its role in promoting migration in T-ALL cell lines suggests it may play an oncogenic role in T-ALL. I wanted to know if PRL-3 expression had any *in vivo* effects on T-ALL progression or self-renewal. I used a zebrafish Myc-induced T-ALL model to assess the role of PRL-3 in T-ALL onset and progression <sup>196-198</sup>. Zebrafish *prl-3* has 88% homology to human PRL-3 with conservation of critical domains <sup>199</sup>. One-cell stage zebrafish embryos were injected with plasmids containing *rag2:Myc* with *rag2:mCherry*, and with or without *rag2:prl-3*. The *rag2* promoter drives gene expression in lymphocytes. T-ALL developed in zebrafish from the thymus and expanded into local tissues before entering the circulation. Fish were

monitored for leukemia growth by quantifying the percent mCherry-positive cells within the body of the animal; >70% mCherry-positive was considered leukemic. Zebrafish T-ALL that expressed *prl-3* consistently expanded from the thymus into surrounding tissues earlier than T-ALLs expressing *Myc* alone (**Figure 3.3A**) and there was a significant difference in the leukemia progression, measured by time to full leukemia onset between the groups (**Figure 3.3B**).

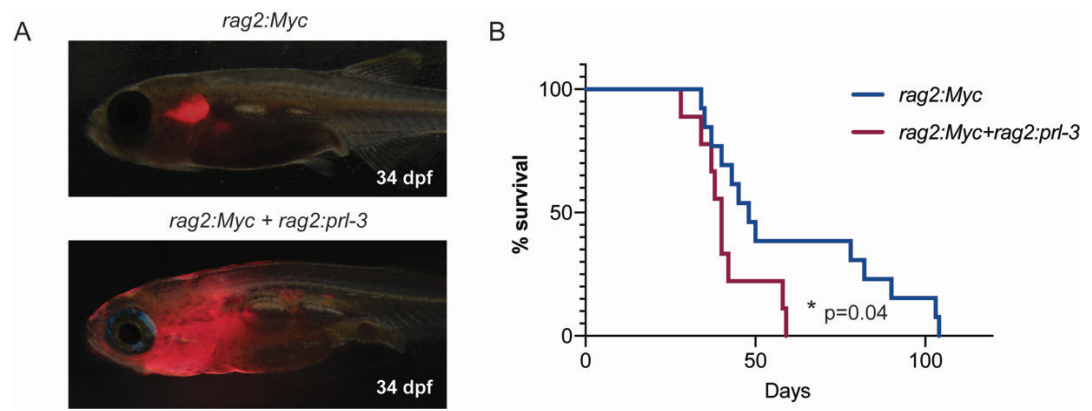


**Figure 3.3 PRL-3 over-expression accelerates T-ALL progression.**

(A) Representative images of transient transgenic zebrafish expressing *rag2:Myc+rag2:mCherry* (n=13) or *rag2:Myc+rag2:mCherry+rag2:prl-3* (n=9) at 34 days post-fertilization (dpf). (B) Kaplan-Meier analysis of time (days) versus percent survival (>70% of the animal is mCherry-positive) for *Myc* control tumors compared to PRL-3 over-expressing tumors. \*p=0.0412. (Figure adapted from Wei et al, 2020<sup>152</sup>).

The lymphoblasts were morphologically similar between groups (**Figure 3.4A**), and there was no significant difference in *Myc* expression between *Myc* and *Myc+prl-3* T-ALL samples (**Figure 3.4B**). Gene expression analyses indicated that both the *rag2:Myc* and *rag2:Myc+rag2:prl-3* leukemias expressed the lymphocyte specific genes *rag1* and *rag2* and the T-cell genes *lck* and *trb*, but not B-cell related genes *igD* or *igM*, indicating all leukemias generated were of T-cell origin. I verified that the *rag2:Myc+rag2:prl-3*

leukemias expressed >10-fold higher levels of PRL-3 than the *Myc* control group (**Figure 3.4C**). Interestingly, endogenous *prl-3* expression was also significantly higher in the *rag2:myc* T-ALLs than normal blood, suggesting that PRL-3 may be an important collaborating oncogene in T-ALL development.

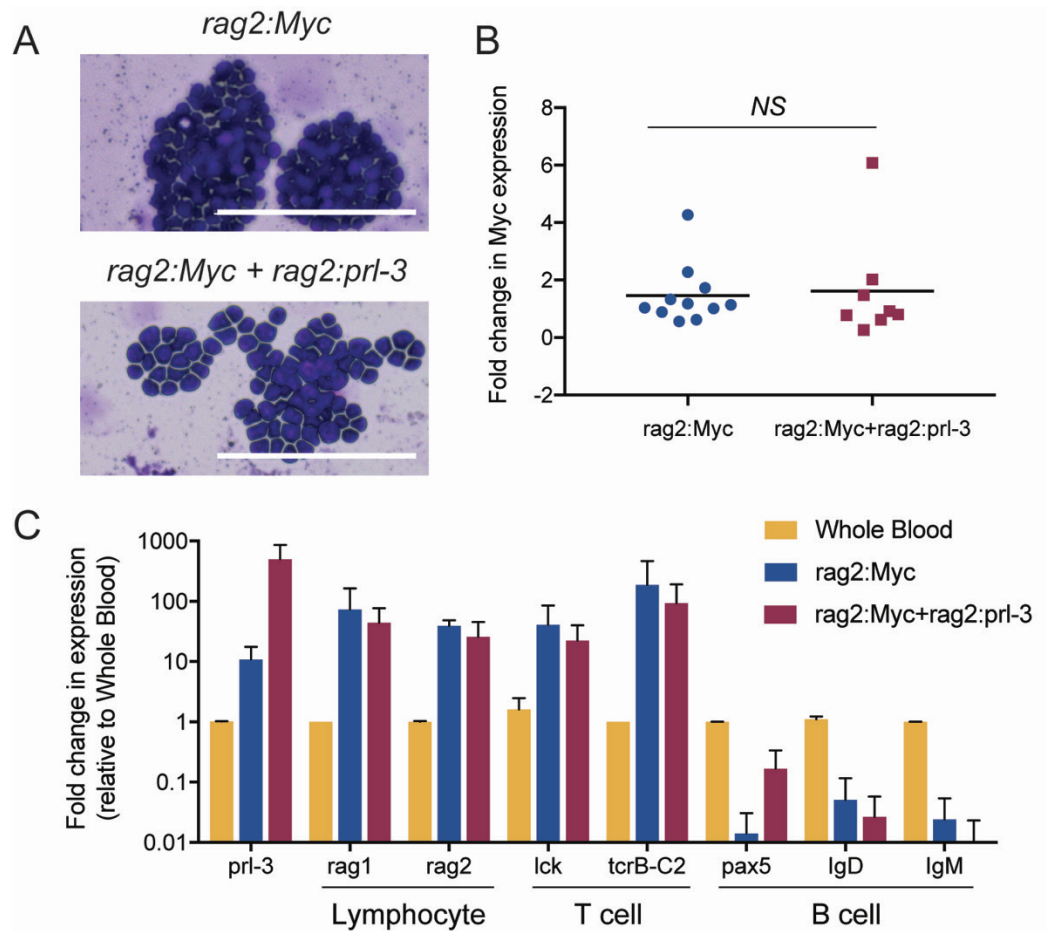


**Figure 3.4 Characterization of Myc and PRL-3 Over-Expressing T-ALLs**

(A) Representative images of May-Grunwald Giemsa staining of blood samples from fish from each leukemia type. Scale bar=100μm. (B) Realtime RT-PCR analysis of *Myc* expression between *rag2:Myc+rag2:mCherry* (n=11) and *rag2:Myc+rag2:mCherry+rag2:prl-3* (n=8). Each point represents one fish sample. NS=not significant. (C) Real-time RT-PCR analysis of lymphocyte, T-cell, and B-cell specific genes. Bars are the average expression of >8 samples per group. *Rag2* RT-PCR is the average of three samples per group. Whole blood is the average of two samples. (Adapted from Wei et al, 2020<sup>152</sup>)

PRL-3 over-expression leads to an increase in T-ALL progression *in vivo*; however the mechanism by which PRL-3 is working to do this is unclear. As mentioned above, PRL-3 has a conserved phosphatase domain and a prenylation domain. In order to see if PRL-3 phosphatase activity or prenylation were crucial to the role of PRL-3 in T-ALL progression, I studied the effects of PRL-3 mutant over-expression on T-ALL onset. One-cell stage zebrafish embryos were injected with plasmids containing *rag2:Myc* with *rag2:mCherry*, and with or without *rag2:prl-3 DM* (C104S and D72A mutations) or *rag2:prl-3 C170S*. PRL-3 DM is the phosphatase impaired mutant, and PRL-3 C170S is the prenylation impaired mutant, so PRL-3 is unable to localize to the membrane. As in previous studies, T-ALL developed in zebrafish from the thymus and expanded into local tissues before entering the circulation. Fish were monitored for leukemia growth by quantifying the percent mCherry-positive cells within the body of the animal; >70% mCherry-positive was considered leukemic. Zebrafish T-ALL that expressed PRL-3 C170S did not show any differences in progression from PRL-3 WT expressing T-ALL. PRL-3 DM expressing T-ALL progressed significantly slower than PRL-3 WT and tracked more closely with the pattern of progression of Myc-only control fish, measured by time to full leukemia onset between groups (**Figure 3.5**). The lack of difference in T-ALL progression with the C170S mutant compared to the PRL-3 WT leukemias suggests that the role of PRL-3 in T-ALL progression is not dependent on prenylation of PRL-3. The significantly slowed progression in PRL-3 DM mutant leukemias compared to PRL-3 WT, almost to the level of Myc-only control leukemias, suggests that the phosphatase domain and/or activity of PRL-3 may be critical to its' function as a driver of T-ALL progression.

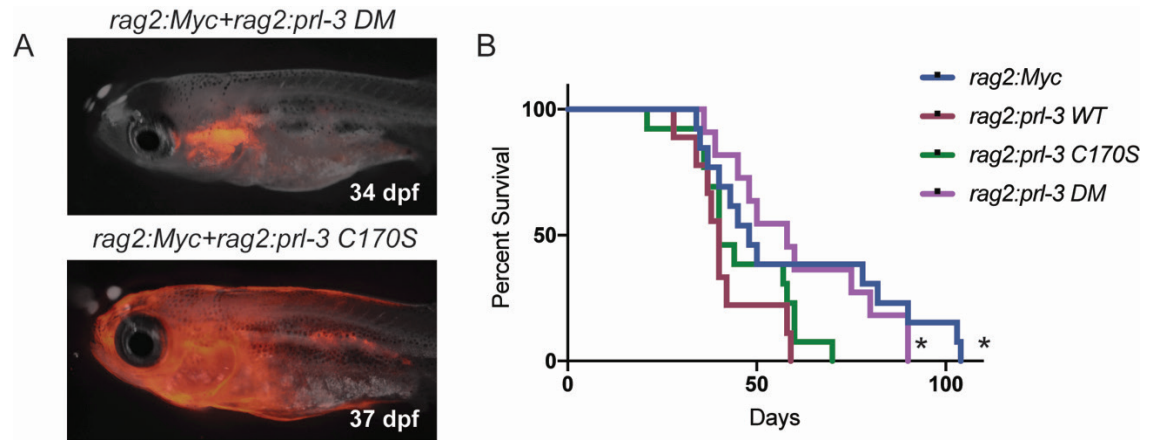


**Figure 3.5 Mutation of the PRL-3 Phosphorylation Domain Affects T-ALL Progression** (A) Representative images of transient transgenic zebrafish expressing *rag2:Myc+rag2:mCherry+rag2:prl-3 DM* (n=11) or *rag2:Myc+rag2:mCherry+rag2:prl-3 C170S* (n=13) at 34 or 37 dpf, respectively. (B) Kaplan-Meier analysis of time (days) versus percent survival (>70% of the animal is mCherry-positive) for Myc control tumors compared to PRL-3 WT and mutant tumors. \*p=0.0412 comparing PRL-3 WT to Myc control. \*p=0.011 comparing PRL-3 WT to PRL-3 DM leukemias.

Characterization of PRL-3 mutant leukemias revealed that again, there was no significant difference in *mMyc* expression between Myc control, PRL-3 WT, or either of the PRL-3 mutant leukemia samples (**Figure 3.6A**). Gene expression analysis by RT-PCR demonstrated that all of the leukemias expressed a lymphocyte marker, *rag1*, and T-cell genes *lck* and *trb*. While none of the leukemias expressed B-cell related genes *IgD* or *IgM*, indicating that all of the PRL-3 mutant leukemias were also of T-cell origin. Additionally, the PRL-3 mutant leukemias were verified to express PRL-3 levels similar to that of the PRL-3 WT T-ALLs (**Figure 3.6B**).

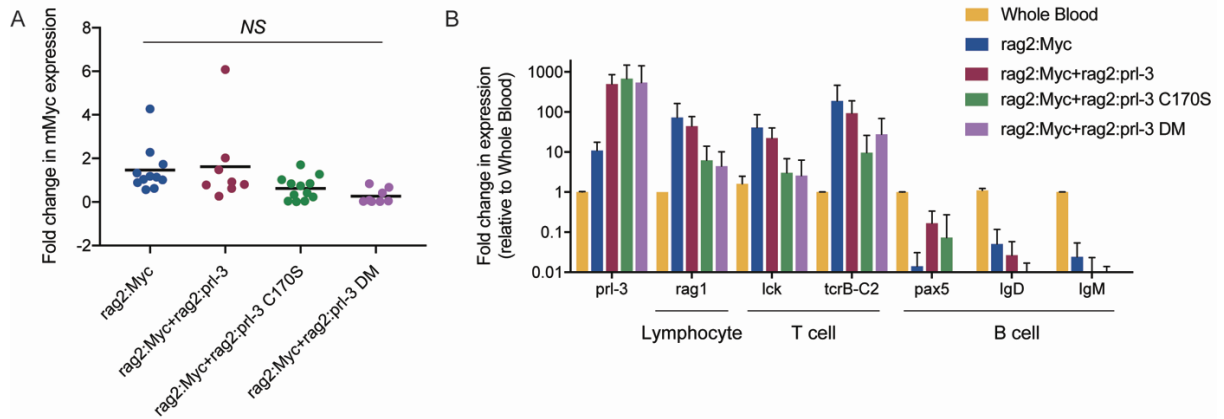


**Figure 3.6 Characterization of PRL-3 Mutant T-ALLs**

(A) Realtime RT-PCR analysis of *Myc* expression between *rag2:Myc*+*rag2:mCherry* (n=11), *rag2:Myc*+*rag2:mCherry*+*rag2:prl-3* (n=8), *rag2:Myc*+*rag2:mCherry*+*rag2:prl-3 C170S* (n=12), and *rag2:Myc*+*rag2:mCherry*+*rag2:prl-3 DM* (n=8). Each point represents one fish sample. NS=not significant. (B) Real-time RT-PCR analysis of lymphocyte, T-cell, and B-cell specific genes. Bars are the average expression of >8 samples per group. Whole blood is the average of two samples.

### 3.2.3 PRL-3 Promotes T-ALL Cell Migration in a Zebrafish Model

Because the T-ALL cells were fluorescently labeled and can be monitored in living animals, I was also able to determine the time at which leukemia cells begin to circulate by visualizing cells within the vasculature in the tail fin (**Figure 3.7A**). While more than half of animals with T-ALL in the *Myc*-expressing group never developed circulating disease by >100d, more than 80% of the *Myc+prl-3* expressing T-ALLs were circulating at a median time point of 42d,  $p=0.047$  (**Figure 3.7B**).

Taken together, these data suggest that PRL-3 can play an important role in T-ALL onset and progression *in vivo*, likely by enhancing migration into local tissues and contributing to the ability of the cells to enter circulation.

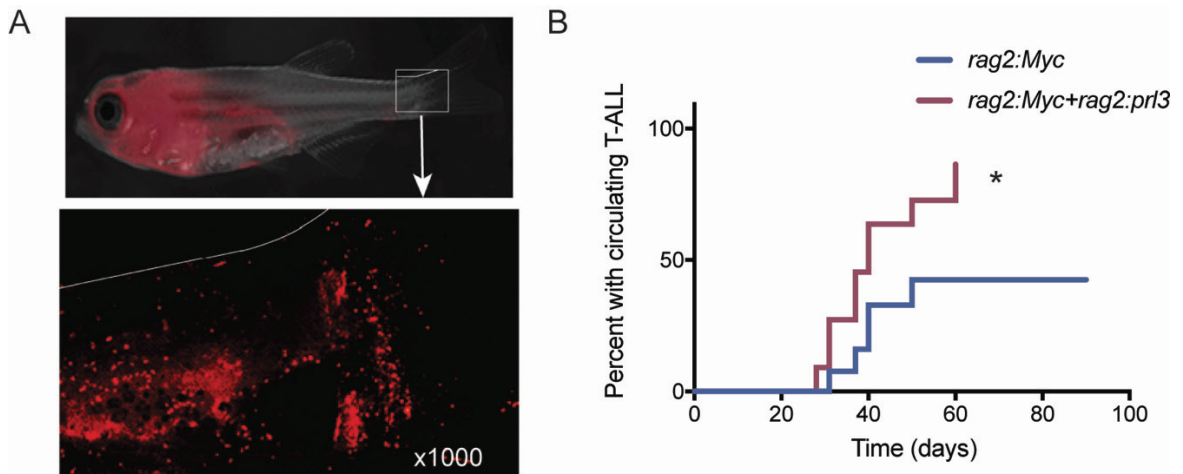


**Figure 3.7 PRL-3 Promotes T-ALL Migration in a Zebrafish Model**  
 (C) Representative *rag2:Myc+rag2:mCherry+rag2:prl-3* animal, showing circulating mCherry<sup>+</sup> leukemia cells within the tail fin. (D) Kaplan-Meier analysis of time (days) for each T-ALL to be visualized in circulation, \*  $p=0.047$ . (Figure adapted from Wei et al, 2020<sup>152</sup>).

### 3.2.4 Over-Expression of PRL-3 Increases LSC Frequency in a Zebrafish Model

The PRL family has been shown to be involved in stem cell self-renewal, division, and cell cycle in various types of stem cells<sup>200–202</sup>. More specifically, PRL-3 has been identified to play a role in inducing a sub-population of ovarian cancer stem cells via a phosphatase-independent mechanism<sup>202</sup>. However, a functional role for PRL-3 in leukemia stem cells has not yet been demonstrated.

As described above, zebrafish were injected with *rag2:Myc* with or without *rag2:PRL-3*, leading to formation of Myc-induced zebrafish T-ALL tumors with or without PRL-3 overexpression. These primary tumors were then harvested when the fish developed >70% leukemic burden, and limiting dilution transplantation was performed to determine the LSC frequency of each tumor. Each limiting dilution transplantation used 36 recipient



diamidino-2-phenylindole (DAPI) to determine the percent of apoptotic cells in each tumor. The same was done with 5'-ethynyl-2'-deoxyuridine (EdU) uptake using ClickIT EdU conjugated to Alexa Fluor 488 and DAPI to determine the percent of actively proliferating cells in each tumor. Three secondary tumors were harvested and stained for each primary tumor and analyzed by flow cytometry. The data demonstrated that there was no overall difference in apoptosis or proliferation between the tumors from the two groups, indicating that the differences in tumor formation upon limiting dilution transplantation can be attributed to differences in LSC frequency (**Figure 3.9**).

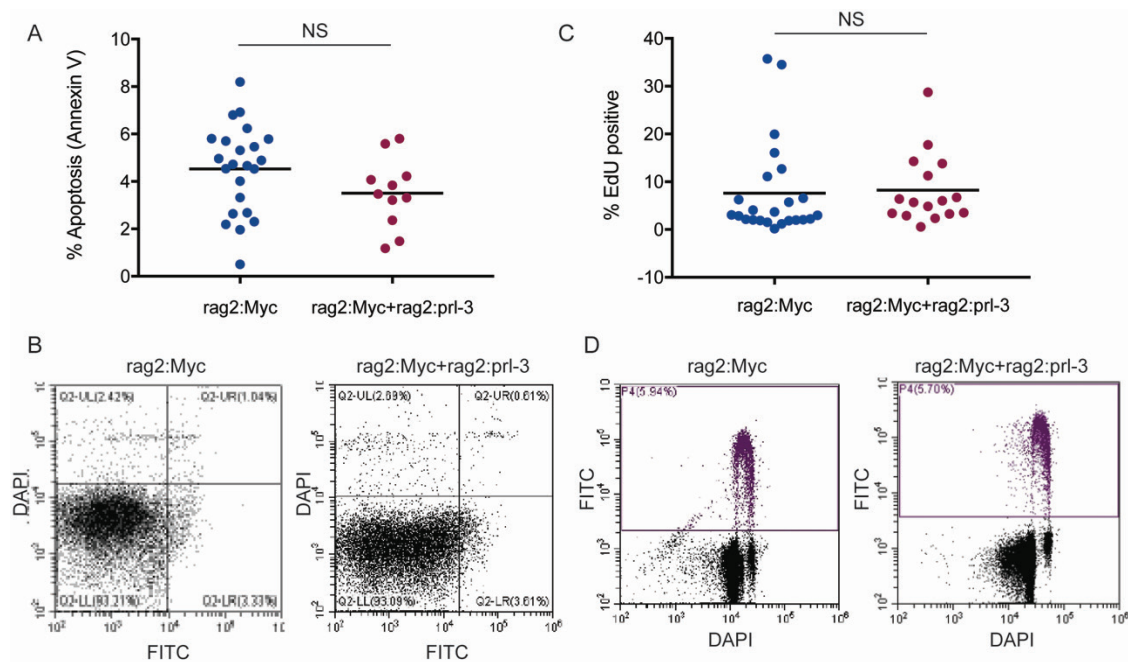


**Figure 3.9 PRL-3 Over-Expression Does Not Affect Apoptosis or Proliferation**  
 (A) Percent apoptosis of *rag2:Myc+rag2:mCherry* and *rag2:Myc+rag2:mCherry+rag2:prl-3* tumors by Annexin V-FITC staining. (B) Representative flow cytometry analysis for a *rag2:Myc+rag2:mCherry* and a *rag2:Myc+rag2:mCherry+rag2:prl-3* tumor. (C) Percent proliferation (EdU positive cells) of *rag2:Myc+rag2:mCherry* and *rag2:Myc+rag2:mCherry+rag2:prl-3* tumors by EdU Alexa Fluor 488 uptake. (D) Representative flow cytometry analysis for a *rag2:Myc+rag2:mCherry* and a *rag2:Myc+rag2:mCherry+rag2:prl-3* tumor. NS = not significant.

Since it is debated in the field whether PRL-3 works as a phosphatase or via non-phosphatase dependent activity, I next studied the effect of over-expression of PRL-3 mutants on LSC frequency. As described above, the PRL-3 double mutant (DM) contains a C104S and D72A mutation, abolishing phosphatase activity of PRL-3. The C170S mutant PRL-3 interrupts the prenylation motif. I over-expressed both PRL-3 mutant forms in our Myc-induced T-ALL and performed limiting dilution transplantation of the primary tumors into 36 recipient zebrafish per primary tumor to determine the LSC frequency to gain insight into how PRL-3 was working to increase LSC frequency *in vivo*. Over-expression of PRL-3 DM did not change the LSC frequency, suggesting that the role of PRL-3 in LSC self-renewal is likely not dependent on its' phosphatase activity, opposite from what was found with the role of PRL-3 in T-ALL progression (**Figure 3.10**). Over-expression of PRL-3 C170S showed an increase in LSC frequency that was significantly higher than the Myc alone control group. Additionally, while not significant, the overall trend of over-expression of the PRL-3 C170S mutant showed an increase in LSC frequency with mutation of the prenylation motif of PRL-3 compared to PRL-3 WT over-expression (**Figure 3.10**). This suggests that a change in PRL-3 subcellular localization, possibly with increased trafficking to the nucleus, may contribute to the role of PRL-3 in LSC self-renewal. However, there was a great deal of variation in LSC frequency between primary tumors in this group, so in order to draw any true conclusions about the loss of prenylation contributing to the role of PRL-3 in LSC self-renewal further studies need to be conducted.



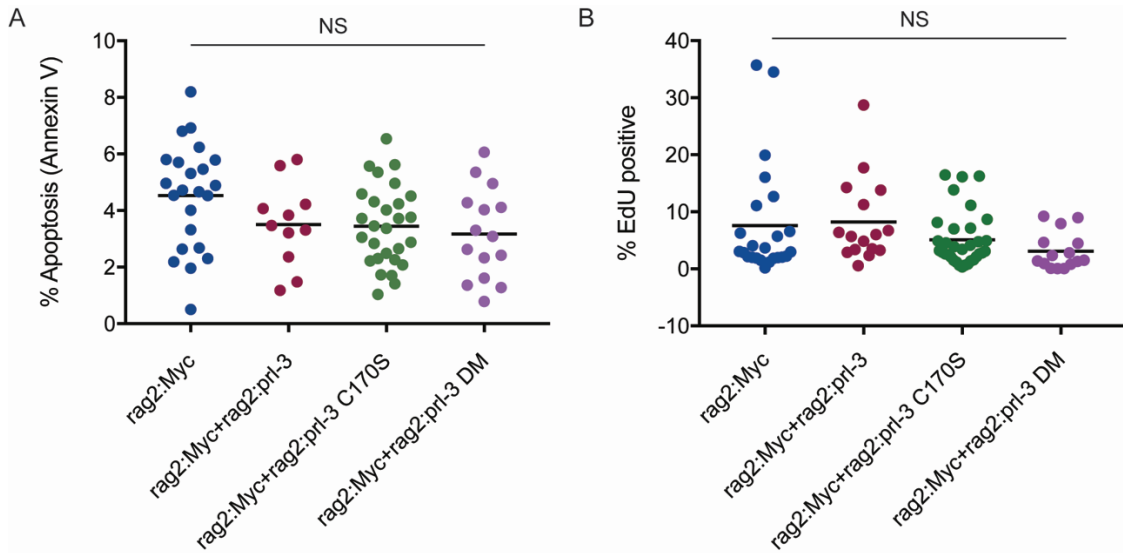


**Figure 3.11 PRL-3 Mutant Over-Expression Does Not Affect Proliferation or Apoptosis**  
 (A) Percent apoptosis of *rag2:Myc+rag2:mCherry* or *rag2:Myc+rag2:mCherry+rag2:prl-3* WT, C170S, or DM mutant tumors by Annexin V-FITC staining. (B) Percent proliferation (EdU positive cells) of *rag2:Myc+rag2:mCherry* and *rag2:Myc+rag2:mCherry+rag2:prl-3* WT, C170S or DM mutant tumors by EdU Alexa Fluor 488 uptake. NS = not significant.

### 3.2.5 Inhibition of PRL-3 Decreases LSC Frequency *In Vivo*

In order for PRL-3 to be a possible drug target for leukemia stem cells, inhibition of PRL-3 must cause a decrease in LSC frequency. Currently, there are no specific PRL-3 chemical inhibitors available; however, there are a few chemical inhibitors that have been shown to block activity of the PRL family of proteins. PRL-3 Inhibitor I (Sigma-Aldrich) is a rhodanine derivative that non-specifically inhibits PRL family activity with minimal activity against other phosphatases<sup>204</sup>. JMS-053 (iminothienopyridinedione 13) is a derivative of theinopyridone that is the most specific PRL-3 inhibitor available, but still non-specifically inhibits the entire PRL family<sup>192</sup>. JMS-053 is the first small-molecule PRL-3 inhibitor to be used *in vivo*, where it inhibited ovarian cancer cell growth, however it has poor stability and it's toxicity profile has yet to be determined.

Treatment of a high-self renewal clonal leukemia from Blackburn et al 2014, with the Sigma PRL-3 inhibitor (PRLi) for 8 hours *ex vivo* before limiting dilution transplantation revealed an 11.9 fold decrease in LSC frequency ( $p < 0.001$ ), providing preliminary evidence that inhibition of PRL-3 may be a suitable drug target to decrease LSC frequency<sup>128</sup>. Treatment of that same tumor with JMS-053, a more specific inhibitor for PRL-3, for 48 hours *ex vivo* before limiting dilution transplantation led to a 7.8 fold reduction in LSC frequency ( $p < 0.01$ ). Finally, treatment with one of the high self-renewal *rag2:Myc+rag2:mCherry* tumors that also expressed high levels of zebrafish *prl-3* (Myc #8) with JMS-053 for 6 hours *ex vivo* before limiting dilution transplantation in media containing drug or DMSO as a vehicle control revealed a 17 fold decrease in LSC frequency ( $p < 0.01$ ) (**Figure 3.12**). Taken together, this data provides preliminary data that inhibition of PRL-3 is a potential target for decreasing LSCs *in vivo*.

Treatment	Tumor	Lower CI (% LSC)	Estimate (% LSC)	Upper CI (% LSC)	Fold Change in LSC Frequency	P-value
DMSO	13.1	1:14	1:6	1:3	11.9	0.000131
PRLi 40 $\mu$ M	13.1	1:166	1:67	1:28		
DMSO	13.1	1:273	1:98	1:35	7.9	0.00906
JMS-053 10 $\mu$ M	13.1	1:2604	1:774	1:230		
DMSO	Myc #8	1:1044	1:291	1:81	17.3	0.00128
JMS-053 10 $\mu$ M	Myc #8	1:35517	1:5034	1:714		

**Figure 3.12 Chemical Inhibition of PRL-3 Decreases LSC Frequency**

Table showing LSC frequency (% LSC) and fold change in LSC frequency of a clonal high self-renewal tumor (13.1) and a heterogenous high self-renewal *rag2:Myc+ rag2:mCherry* tumor (Myc #8) treated with the PRL-3 inhibitors PRLi or JMS-053. LSC frequency, upper and lower confidence intervals (CI), and p-values were determined by extreme limiting dilution analysis (ELDA)<sup>203</sup>.

Although these tumors showed a significant decrease in LSC frequency after chemical inhibition of PRL-3, two other clonal high self-renewal tumors tested did not show the same decrease in LSC frequency. One showed a 3-fold decrease in LSC frequency, yet this decrease was not statistically significant and the other showed no change in LSC frequency (data not shown). This provides evidence that different leukemia clones may respond differently to drug treatment targeting LSCs and there may not be one universal pathway or molecule that can be targeted to eliminate LSCs in patient tumors. Furthermore, additional data is required to demonstrate that pathways downstream of PRL-3 are affected by drug treatment of cells, confirming that the drugs are acting via inhibition of PRL-3, yet these precise pathways remain unknown.

### **3.2.6 Knock-down of PRL-3 Decreases LSC Frequency *In Vitro***

Data to this point has demonstrated that PRL-3 plays a role in T-ALL progression and is an important driver in LSC self-renewal *in vivo* in a Myc-induced zebrafish T-ALL model. Furthermore, chemical inhibition of PRL-3 in high self-renewal leukemias shows a decrease in LSC frequency *in vivo*, signifying PRL-3 may be a potential drug target for LSCs. However, all of this data was collected in a zebrafish model. Despite evidence showing that PRL-3 is elevated in human T-ALL samples, studying LSC biology or function in human leukemia cells, or even mouse models, has many challenges and limitations. Currently, colony formation assays are accepted as a measure of stemness or stem-like potential in human leukemia cells *in vitro*. To measure the effect of PRL-3 on stemness in human leukemia cells, Jurkat cells, a human T-ALL cell line, were used for colony formation assays.

Jurkat cells, which have high endogenous PRL-3 expression, were transfected with short-hairpin RNAs (shRNA) targeting PRL-3 or scrambled (SCR) control shRNA. Cells were checked for knock-down of PRL-3 by western blot analysis four days post-infection with Lentivirus shRNA constructs. PRL-3 knock-down cells were then plated in methylcellulose-containing media and monitored for colony formation for one week before counting colonies. I found that PRL-3 knock-down in Jurkat cells significantly decreased colony formation ( $p < 0.05$ ) compared to SCR control (**Figure 3.13**). This data indicates that PRL-3 is a driver of leukemia cell stemness not only in our zebrafish model, but also *in vitro* in human T-ALL cells.

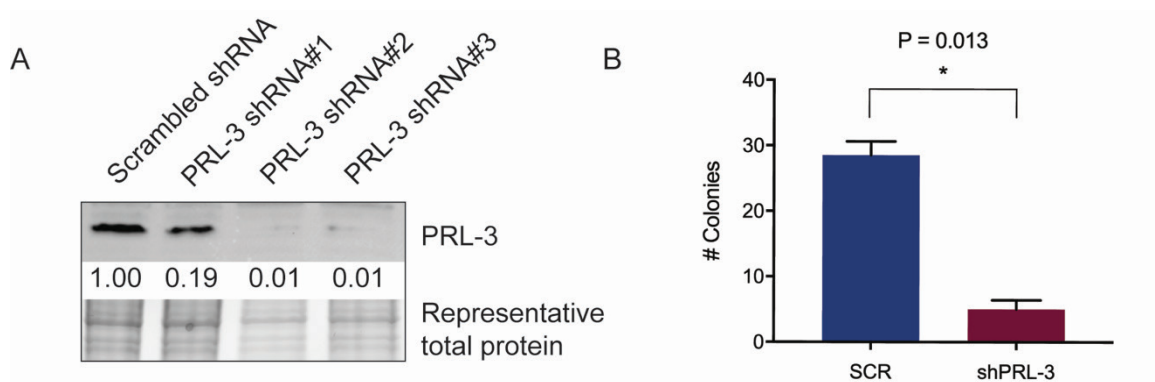


**Figure 3.13 Knock-down of PRL-3 Decreases Human Leukemia Cell Stemness**  
 (A) Representative western blot showing PRL-3 protein expression in Jurkat T-ALL cells 4 days post-infection with lentivirus carrying shRNA. Numbers represent relative expression of PRL-3 protein, normalized to total protein loaded, and compared to scrambled shRNA control. (B) Colony formation of PRL-3 knock-down Jurkat cells (shPRL-3) compared to scrambled control (SCR). Cells were plated in methylcellulose containing media for one week before colonies were counted. \* $p = 0.013$ .

### 3.3 Discussion

While the prognosis for children diagnosed with leukemia has improved drastically, relapse remains a major clinical concern. The relapse rate in T-ALL is even higher than in

other leukemia subtypes and is associated with a far inferior prognosis. This relapse is due to LSCs that are chemotherapy resistant and capable of undergoing self-renewal and rapid proliferation, driving tumor relapse. Gaining insight into signaling pathways important in LSCs and identifying drivers of LSC self-renewal is critical to decreasing relapse rates in patients and identifying ways to target LSCs during cancer treatment.

Our lab previously found that PRL-3 was highly expressed in T-ALL patient samples and cell lines, consistent with studies reporting PRL-3 upregulation in solid tumors and B-ALL<sup>152,188,205</sup>. I also demonstrated that over-expression of PRL-3 resulted in an increase in T-ALL progression and migration *in vivo* in our zebrafish model. In zebrafish, PRL-3 expression enhanced the spread of T-ALL cells from the thymus into surrounding tissues and promoted their rapid entry into circulation. Furthermore, utilizing PRL-3 mutants, our data suggests that this increase in progression is likely due to its function as a phosphatase. Additionally, I established a role for PRL-3 in self-renewal of LSCs in T-ALL. Our data shows both that over-expression of PRL-3 results in an increase in LSC frequency and that chemical inhibition of PRL-3 is able to decrease the LSC frequency *in vivo* in our zebrafish model. Over-expression of PRL-3 mutants suggested that the role of PRL-3 in self-renewal may not be dependent on its activity as a phosphatase, and may in fact be affected by cellular localization of PRL-3. Finally, I have shown that PRL-3 knock-down in a human leukemia cell line leads to a decrease in colony formation, which serves as a measure of stemness *in vitro*.

Overall, our data suggests that PRL-3 functions in T-ALL as both a driver of leukemia progression and migration, and as a driver of LSC self-renewal. However, the role of PRL-3 in both of these processes may be via different mechanisms. Our lab has

previously demonstrated that PRL-3 enhances migration in T-ALL through the Src signaling pathway<sup>152</sup>. While our data clearly shows a functional role for PRL-3 in LSC self-renewal in T-ALL, the mechanism of this has yet to be elucidated. Uncovering drivers of self-renewal in T-ALL and their mechanisms of action is crucial to gaining a better understanding of LSC biology and coming closer to targeted therapies towards LSCs in patient care to prevent relapse.

### **3.3.1 Future Directions**

While a functional role for PRL-3 in T-ALL LSC self-renewal has been established, further work is needed to characterize the role of PRL-3 in this process. Preliminary studies have been done to study whether PRL-3 works in a phosphatase or prenylation-dependent manner to increase LSC frequency, but further studies need to be done to assess the mechanism of action specifically of PRL-3 in LSC biology. Additionally, I am currently expanding our studies that show PRL-3 chemical inhibition can decrease LSC frequency from zebrafish genetic models to patient derived xenograft (PDX) models in mice. Experiments are currently underway with PDX samples that are being expanded in mice, harvested, and treated with PRL-3 chemical inhibition or transient PRL-3 knock-down before performing colony formation assays as a measure of stemness. Our hope is that PRL-3 knock-down or chemical inhibition will decrease stemness and target LSCs in PDX samples, demonstrating direct translational relevance of our findings from our zebrafish studies.

## 3.4 Methods

### 3.4.1 Zebrafish Husbandry

Use and handling of zebrafish was approved by the University of Kentucky's Institutional Animal Care and Use Committee (IACUC), protocol 2015-2225. CG1 strain syngeneic zebrafish were used for these studies<sup>206</sup>. Fish were kept at a temperature of 28°C with a light/dark cycle of 14:10 hours in compliance with IACUC animal care regulations. Eggs were collected into 1X E3 media (14.6g of 5.0mM NaCl, 0.65g of 0.17mM KCl, 2.20g of 0.33mM CaCl, and 4.05g of 0.33mM MgSO<sub>4</sub> per liter of 50X stock) with 200µL/L of methylene blue.

### 3.4.2 Zebrafish T-ALL Models

Microinjections of 15ng/µL *rag2:Myc* + 45ng/µL *rag2:mCherry* or 15ng/µL *rag2:Myc* + 15ng/µL *rag2:prl-3* + 30ng/µL *rag2:mCherry* were used to generate zebrafish T-ALL in CG1 strain zebrafish as previously described, and number of animals used in each group were chosen based on previous experiments<sup>196,197,207</sup>. PRL-3 mutant T-ALL tumors were made by injection of 15ng/µL *rag2:Myc* + 15ng/µL *rag2:prl-3 DM* or *C170S* + 30ng/µL *rag2:mCherry*. Zebrafish were monitored for leukemia onset and progression starting at 21 days post-fertilization (dpf) and every 3 days onwards by analyzing percent of the body expressing mCherry-positive leukemia cells using a Nikon fluorescence-equipped SMZ25 microscope. Circulating mCherry-positive T-ALL was noted by examining the vessels within the tail vasculature. Animals were monitored until 90 dpf or until they had to be sacrificed due to leukemia burden. Animals that died before the end of the monitoring period without leukemia progression outside the thymus were excluded.

Zebrafish leukemias were harvested and cytospin and May-Grunwald Giemsa staining were performed as previously described before imaging on a BioTek Lionheart FX microscope<sup>196,207</sup>. To assess gene expression, RNA was isolated from the leukemia cells using Zymo Research Quick-RNA kit (R1054, Irvine, CA, USA). Total RNA was reverse transcribed (BioRad iSCRIPT, 1708891) and real time PCR performed using iTaq Universal SYBR Green Supermix (Biorad, 1725120) with primer sequences available in Table 3.2. Data were normalized to efla expression and fold change was calculated using the  $2^{-\Delta\Delta Cq}$  method.

**TABLE 3.2 REALTIME RT-PCR PRIMER SEQUENCES**

Gene	Forward Primer	Reverse Primer	Purpose
<i>z-ptp4a3</i>	GGTGTCACGACAGTGGTCAG	TCAATCAAGGCCACAGCCAC	
<i>z-rag1</i>	AGCAATGATGCAAGGCAGAG	TGTGCAGGGGCTGGAATATC	Lymphocytes
<i>z-rag2</i>	AGCTCTCAGATTTCCGGAGTACAC	ACAAGGCTGCCACAATTCAC	Lymphocytes
<i>z-lck</i>	AGAAGATCTCGATGGTTTGTCTGT	CGCAGTTCCCATGTTTACG	T-cell
<i>z-tcr β-c2</i>	ATTCACCTGCACTGTCCGAT	AGCTTCAATCCCTTCGGCTT	T-cell
<i>z-pax5</i>	AAGGCAGTTACTCCACACCC	ACCGTACTCCTGCTGAAACAC	B-cell
<i>z-igD</i>	GACACATTAGCCCATCAGCA	CTGGAGAGCAGCAAAAGGAT	B-cell
<i>z-igM</i>	GAAGCCTCCAATTCTGTTGG	CCGGGCTAAACACATGAAG	B-cell
<i>m-cMyc</i>	AGCGACTCTGAAGAAGAGCAA	GCACCTCTTGAGGACCAGTG	
<i>z-eef1a1</i>	ATGGCACGGTGACAACATGCT	CCACATTACCACGACGGATG	normalizing

### 3.4.3 Limiting Dilution Transplantation

Limiting dilution transplantation of primary zebrafish tumors was performed as previously described<sup>197</sup>. Briefly, primary tumors were harvested by maceration of the

zebrafish, filtered and fluorescent leukemia cells counted using a Countess automated cell counter (Invitrogen). From there, different cell doses ranging from 10 cells/animal to 25,000 cells/animal were transplanted into recipient adult zebrafish in a volume of 5 $\mu$ l per animal into a total of 36 recipient zebrafish per primary tumor. Zebrafish were screened weekly for tumor growth for 90 days post-transplantation. Any zebrafish who died before any tumors developed in that cohort were removed from analysis.

For drug treatment studies, cells were harvested as described above and plated at a density of  $1 \times 10^6$  cells/well in a 6-well dish containing RPMI 1640 (ThermoFisher 11875119) supplemented with 10% heat-inactivated fetal bovine serum (Atlanta Biologicals, S11150H, Lot M17161, Flowery Branch, GA, USA), Penicillin/Streptomycin 1:100 dilution (Gibco 10378-016) and gentamycin (Amresco E737-20ML) at a final concentration of 50  $\mu$ g/mL. Cells were cultured in media containing either DMSO control, PRL-3 inhibitor I (Sigma-Aldrich P0108-5MG) or JMS-053 (a gift from Dave Lazo, UVA) at a final concentration of 40  $\mu$ M or 10  $\mu$ M respectively. Cells were treated at timepoints ranging from 6 hours to 48 hours *ex vivo*, depending on the experiment. After drug treatment, cells were again counted on the Countess automated cell counter (Invitrogen), confirmed that cell viability was >90% by trypan blue staining, and prepared for limiting dilution transplantation as described above. For one experiment, cells were resuspended in RPMI + 10% FBS media containing 10  $\mu$ M JMS-053 or DMSO prior to transplantation and transplanted into recipient animals in drug-containing media.

#### **3.4.4 Apoptosis Assay**

Zebrafish cells were harvested as described above. Apoptosis was quantified by staining cells with Annexin V FITC (Life Technologies V13242) according to the manufacturer's protocol in the presence of DAPI (0.1µg/ml) (ThermoFisher 62248). Cells were analyzed by flow cytometry on the CytoFLEX benchtop flow cytometer (Beckman Coulter).

#### **3.4.5 Proliferation Assay**

Zebrafish cells were harvested as described above. Cell cycle was analyzed by quantifying 5'-ethynyl-2'-deoxyuridine (EdU) uptake using ClickIT EdU Alexa Fluor 488 (Thermo Fisher Scientific, C10635) according to the manufacturer's protocol. DAPI (0.1µg/ml) was also used to stain the DNA. Cells were analyzed by flow cytometry on the CytoFLEX benchtop flow cytometer (Beckman Coulter).

#### **3.4.6 T-ALL Cell Culture**

All of the human T-ALL cell lines used in the study were authenticated by short tandem repeat (STR) DNA profiling and tested for mycoplasma contamination prior to experimentation. Cells were grown in RPMI 1640 (ThermoFisher 11875119) supplemented with 10% heat-inactivated fetal bovine serum (Atlanta Biologicals, S11150H, Lot M17161, Flowery Branch, GA, USA). Cells were cultured at 37°C in a humidified atmosphere with 5% CO<sub>2</sub>.

### **3.4.7 Generation of T-ALL Knock-Down Cells by Lentivirus Infection**

PRL-3 knock-down was performed as previously described<sup>152</sup>. Lentivirus was produced in 293T cells using TransIT-LT1 (Mirus Bio MR2300, Madison, WI, USA), according to the manufacturer's instructions using scrambled or shPRL-3 plasmids. For T-ALL cell infection, 2.5mL virus with 10µg/mL polybrene (Thermo Fisher Scientific TR-1003-G) was added to  $5 \times 10^5$  cells and centrifuged at 2250 rpm for 90 minutes. Virus was washed out with PBS after 24h, and cells were selected in culture media with 5µg/mL puromycin for 48h before experiments. PRL-3 knock-down was confirmed by western blot prior to using cells for experiments.

### **3.4.8 Colony Formation Assay**

After confirmation of PRL-3 knock-down by Western blot, Jurkat cells were plated in triplicate in 24-well plates at a density of 1,000 cells per well. Cells were strained using a 25 µm filter to obtain a single cell suspension prior to plating. Cells were plated in a methylcellulose-based media (Methocult H4100, Stem Cell Technologies, Cat #04100) supplemented with 20% BSA substitute + 5 µg/mL puromycin for selection of knock-down cells. Colonies were counted 14 days after plating.

### **3.4.9 Statistical Analysis**

Results are shown as mean  $\pm$  standard deviation. Statistical analyses were performed using GraphPad Prism 7 (San Diego, CA, USA), combining data from all samples across all replicates. Two-tailed t-tests were performed to compare two groups with similar distribution, and Analysis of Variance with Tukey's multiple comparisons was used to compare more than two groups. Kaplan-Meier analyses were performed using a

Log-rank (Mantel-Cox) test. Analyses of limiting dilution transplantation data and calculation of 95% confidence intervals were performed using Extreme Limiting Dilution Analysis (ELDA) software<sup>203</sup>.

## CHAPTER 4. PRL-3 MODULATES BETA-CATENIN SIGNALING IN T-ALL LSCs

## 4.1 Introduction

### 4.1.1 Beta-Catenin/Wnt Signaling Maintains LSC Self-Renewal

As described in Chapter 2, Wnt/beta-catenin signaling is a critical pathway in the growth, maintenance, and self-renewal of both normal and cancer stem cells <sup>208</sup>. Wnt ligands bind to their receptors, frizzled (FZD) and LRP5/6 complex, on the cell surface. This causes sequestration of the destruction complex by phosphorylated LRP and accumulation of  $\beta$ -catenin.  $\beta$ -catenin then translocates into the nucleus, binding TCF/LEF transcription factors, inducing transcription of target genes. Most Wnt target genes are tissue and developmental stage specific. Without Wnt ligand present,  $\beta$ -catenin is bound to the destruction complex, phosphorylated, ubiquitinated, and targeted for degradation <sup>208</sup>.

The Wnt/ $\beta$ -catenin pathway has recently been implicated in the maintenance of LSCs in T-ALL and other leukemias <sup>133,209–211</sup>. For example, constitutive activation of  $\beta$ -catenin, a downstream effector of Wnt signaling, can induce T-ALL in mouse models <sup>212</sup>, and blockade of Wnt signaling leads to a decrease of LSC frequency in mice <sup>133</sup>. LSCs in T-ALL have elevated expression of  $\beta$ -catenin in human cells and mouse models <sup>114,132,133,212,213</sup>. Finally, XAV939, which is a tankyrase inhibitor that stabilizes the destruction complex, leading to  $\beta$ -catenin degradation, showed promise against T-ALL cell lines *in vitro* and xenograft models <sup>133</sup>.

In a large-scale serial limiting dilution transplantation screen in our Myc-induced zebrafish T-ALL model, Wnt pathway signaling was identified as a potential driver of LSC self-renewal <sup>128</sup>. Bulk RNA sequencing data showed that T-ALL clones with high self-renewal had high expression of Wnt related genes compared to those with low self-renewal. This was validated by over-expression of a constitutively active form of  $\beta$ -catenin (S33Y)

in our zebrafish T-ALL model, which demonstrated that constitutive activation of  $\beta$ -catenin enhances LSC self-renewal  $\sim$ 10-fold, in agreement with what others have found in mouse models (**Figure 4.1**). Additionally, treatment of high self-renewal clones with XAV939 decreased LSC frequency *in vivo* (**Figure 4.2**). Together, these data suggest that the Wnt/ $\beta$ -catenin pathway may be an attractive drug target to differentiate LSCs in ALL.

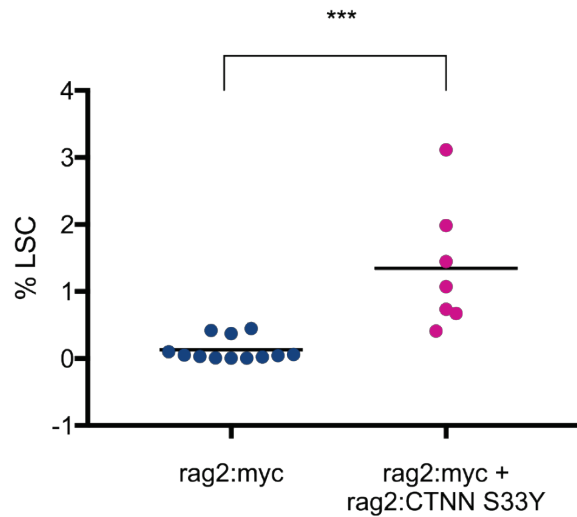


**Figure 4.1 Constitutively Active  $\beta$ -Catenin Over-Expression Increases LSC Frequency In Vivo**

% LSC frequency of *rag2:Myc+rag2:mCherry+rag2:CTNN S33Y* compared to *rag2:Myc+rag2:mCherry* alone. Each data point represents the % LSC by limiting dilution transplantation into 36 recipient animals of each primary zebrafish T-ALL tumor. \*\*\*p=0.0004.

Treatment	Tumor	Lower CI (% LSC)	Estimate (% LSC)	Upper CI (% LSC)	Fold Change in LSC Frequency	P-value
DMSO	13.1	7.35	17.70	39.06	19.7	0.0000107
XAV939 10 $\mu$ M	13.1	0.31	0.90	2.57		
DMSO	14.1	3.08	8.13	20.62	4.1	0.0399
XAV939 10 $\mu$ M	14.1	0.79	2.00	5.03		

**Figure 4.2 XAV939 Treatment of High Self-Renewal T-ALL Decreases LSC Frequency**  
Table showing LSC frequency (% LSC) and fold change in LSC frequency of two clonal high self-renewal tumors (13.1 and 14.1) treated with the Wnt pathway signaling inhibitor XAV939. LSC frequency, upper and lower confidence intervals (CI), and p-values were determined by extreme limiting dilution analysis (ELDA)<sup>203</sup>.

However, Wnt signaling is essential in a variety of tissues and developmental processes, and targeted inhibition of the Wnt pathway remains challenging in all types of cancer, due to intolerable toxicities, with major concerns regarding the use of Wnt inhibitors in pediatric patients<sup>214</sup>. Current strategies for Wnt pathway inhibition include: inhibition of Wnt ligand production, Wnt antagonists, tankyrase inhibitors to stabilize the destruction complex interaction with beta-catenin, and inhibitors of TCF/LEF mediated transcription<sup>134,215</sup>. Targeting regulators of Wnt signaling that are mis-expressed uniquely by T-ALL cells could be an effective strategy to block abnormal Wnt/Beta-catenin activity specifically in LSCs without the associated toxicities.

#### 4.1.2 Hypothesis and Specific Aims

As demonstrated above, PRL-3 plays a role as a driver of self-renewal in T-ALL LSCs *in vivo*, yet the mechanism by which it is working has yet to be elucidated. Recent research suggests that there may be a link between PRL-3 and  $\beta$ -catenin signaling pathways in AML, with PRL-3 over-expressing AML cells showing an increase in active  $\beta$ -catenin

accumulation in the nucleus and transcription of downstream Wnt target genes<sup>216-219</sup>. However, the molecular mechanisms by which PRL-3 modulates Wnt signaling, and a PRL-3/Wnt signaling effect on LSCs *in vivo* are unknown. Our preliminary data also hinted that PRL-3 may be working through Wnt pathway signaling to enhance LSC signaling in leukemias. Given this preliminary data, *I hypothesized that PRL-3 directly intersects with the Wnt signaling cascade to enhance self-renewal of LSCs in T-ALL, and disruption of this PRL3/Wnt signaling axis by inhibition of PRL-3 will block LSC self-renewal. To test this hypothesis, the following specific aims were developed: 1) To define the role of PRL-3 in modulating Wnt pathway signaling in vitro, and; 2) To determine if PRL-3 inhibition can modulate  $\beta$ -catenin signaling in vivo.*

## 4.2 Results

### 4.2.1 $\beta$ -Catenin is Highly Expressed in PRL-3 Over-Expressing T-ALL

As described above, a role for PRL-3 in regulation of  $\beta$ -catenin signaling has been demonstrated in AML<sup>216,217,219</sup>. To explore if PRL-3 played a role in  $\beta$ -catenin signaling in T-ALL, I first confirmed that  $\beta$ -catenin expression was enriched in PRL-3 high T-ALL samples. Patient samples from a publicly available microarray expression analysis study (GSE13159) were analyzed by gene set enrichment analysis and showed that T-ALL samples in the top quartile of PRL-3 expression were enriched for both  $\beta$ -catenin signaling and embryonic stem cell signaling compared to T-ALL samples in the bottom quartile of PRL-3 expression (**Figure 4.3**). This suggests that there is a correlation between PRL-3 expression and  $\beta$ -catenin signaling in human T-ALL.

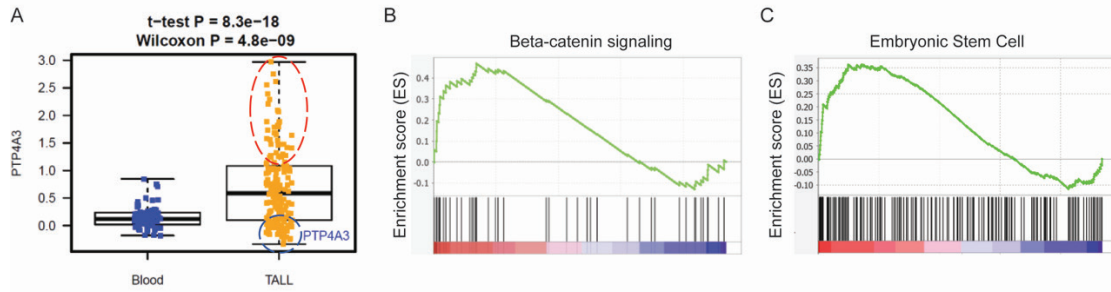


**Figure 4.3 GSEA Analysis Reveals Pathways Enriched in PRL-3 High Patient T-ALL Samples**

(A) Microarray expression analysis of GSE13159 comparing samples from healthy donors (n=72) to T-ALL patients (n=174). Red dotted circle represents top 25% of PRL-3 expressing T-ALL samples. Blue dotted circle represents bottom 25% of PRL-3 expressing T-ALL samples. (B and C) Gene set enrichment analysis (GSEA) of T-ALL patient samples that were in the top (red) or bottom (blue) quartile of PRL-3 expression in GSE13159. High PRL-3 samples were enriched for Beta-catenin signaling (B) and embryonic stem cell signaling (C) pathways.

After confirming that high PRL-3 expression is correlated with  $\beta$ -catenin signaling in human T-ALL, I next examined *rag2:Myc* and *rag2:Myc+prl-3* zebrafish leukemia for an association between PRL-3 and  $\beta$ -catenin signaling. I first performed a western blot comparing *rag2:Myc+rag2:mCherry* control samples to PRL-3 over-expressing, *rag2:Myc+rag2:mCherry+rag2:prl-3*, leukemias and confirmed that PRL-3 protein was indeed over-expressed in the PRL-3 over-expressing leukemias. Further, I found that  $\beta$ -catenin protein expression was only detectable in the PRL-3 over-expressing leukemias and not detectable in the Myc control leukemias (**Figure 4.4**). This suggested that PRL-3 can induce  $\beta$ -catenin expression and signaling in the zebrafish T-ALL model.

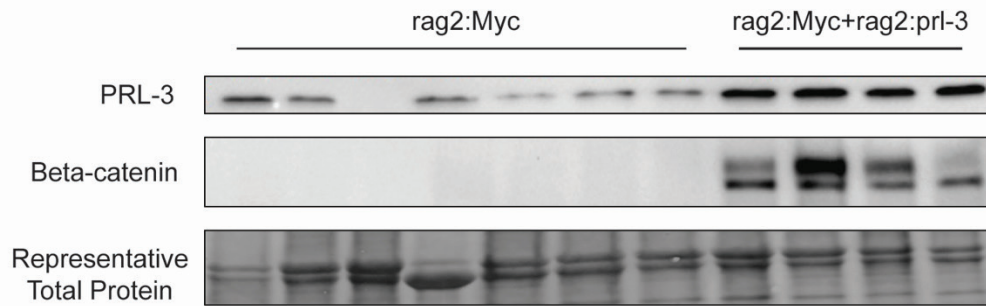


**Figure 4.4 Beta-Catenin is Highly Expressed in PRL-3 Over-Expressing Zebrafish T-ALL Samples**

Western blot showing PRL-3 over-expressing zebrafish leukemias (*rag2:Myc+rag2:prl-3*) have elevated expression of PRL-3 (Genetex antibody, GTX89930) compared to *rag2:Myc* control zebrafish tumors. Only *rag2:Myc+rag2:prl-3* leukemias express  $\beta$ -catenin (Abcam antibody, ab16051) and not *rag2:Myc* control leukemias. Representative band of total protein gel shown for normalization.

To examine the mechanism by which PRL-3 may be working through  $\beta$ -catenin to increase LSC frequency *in vivo*, I used RT-PCR to quantify relative mRNA expression levels of Wnt target genes in our zebrafish leukemia samples. This experiment demonstrated that zebrafish myc a (*z-myca*), which is the zebrafish ortholog to the human oncogene *c-myc*, expression was significantly elevated in two out of three PRL-3 over-expressing leukemias compared to Myc control leukemias (**Figure 4.5**). Interestingly, the PRL-3 over-expressing leukemia with the highest *z-myca* expression was also one that was a significant outlier for the highest LSC frequency, suggesting that PRL-3 may be driving  $\beta$ -catenin induced expression of *z-myca*, increasing LSC frequency in T-ALL. This is important because it has been shown that activation of the *c-Myc* oncogene alone can be enough to activate stem-cell-like programming and increase cancer-initiating cells in human keratinocytes<sup>220</sup>. More importantly, *c-Myc* inhibition targets LSCs in a T-ALL mouse model<sup>221</sup>.

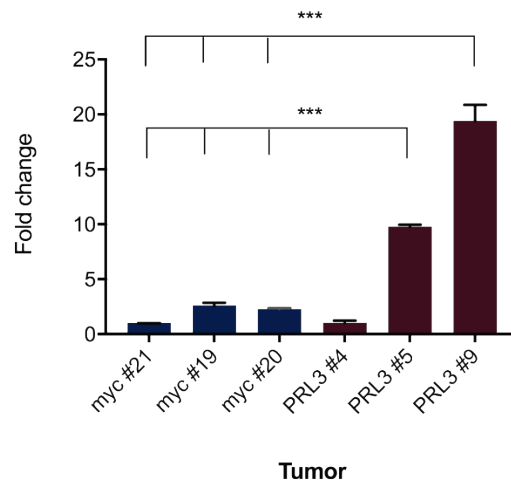


**Figure 4.5 PRL-3 Over-Expression Induces z-myca Expression In Vivo**  
 RT-PCR analysis of *rag2:Myc* zebrafish T-ALL samples (n=3) and *rag2:Myc+rag2:prl-3* samples (n=3) for *z-myca* which is the zebrafish ortholog to the oncogene *c-myc*. \*\*\*p<0.001.

RNA sequencing between Myc control leukemias and PRL-3 over-expressing zebrafish leukemias was done to gain a better understanding of gene expression changes that were causing PRL-3 to have an effect on LSC frequency *in vivo*. Sequencing was done first at the University of Louisville on three Myc control leukemias and 3 PRL-3 over-expressing leukemias. At a later timepoint, two additional Myc control tumors and three PRL-3 over-expressing leukemias were sequenced using a third party company, Genewiz. RNA sequencing demonstrated upregulation of *notch1a* in the PRL-3 over-expression group, which is a central driver of leukemia initiation in human leukemias. It also showed upregulation of Casein kinase 1 epsilon (CSNK1E), which is involved in regulation of Wnt pathway signaling (**Figure 4.6**). *Csnk1ε* is responsible for phosphorylation of disheveled, which leads to activation of Wnt signaling through the β-catenin/TCF/LEF complex<sup>222,223</sup>. Over-expression of *Csnk1ε* can also directly regulate β-catenin phosphorylation and regulation<sup>223</sup>.

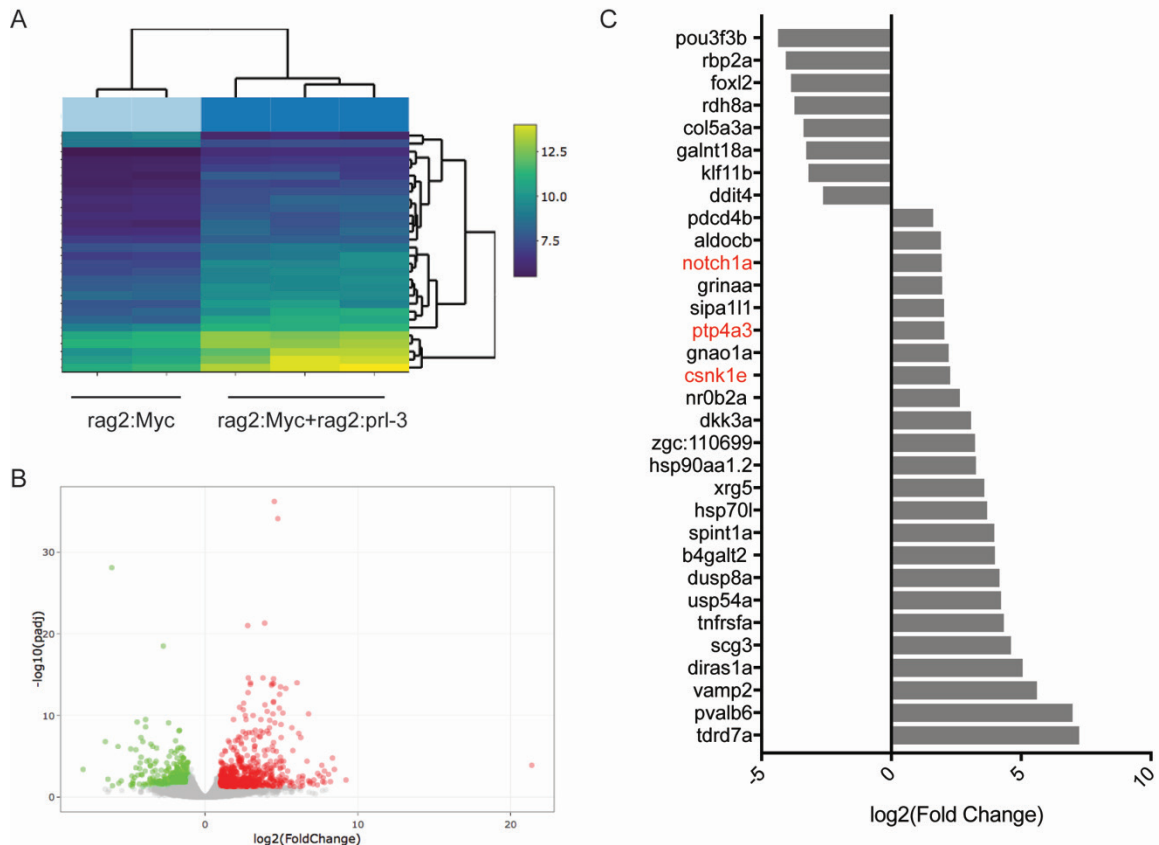


**Figure 4.6 RNAseq Analysis of Myc and PRL-3 Over-Expression Fish Tumors**  
 RNA sequencing of *rag2:Myc+rag2:mCherry* leukemias compared to *rag2:Myc+rag2:mCherry+rag2:prl-3* zebrafish leukemias. (A) Heat map showing PRL-3 over-expressing leukemias cluster independently from Myc control leukemias. (B) Volcano plot showing significantly upregulated or downregulated expressed genes. (C) Waterfall plot showing genes that were up- or down-regulated in both rounds of RNA sequencing in the PRL-3 over-expressing leukemias compared to Myc control leukemias.

#### 4.2.2 PRL-3 Modulates Beta-Catenin Signaling *in Vitro*

To determine if PRL-3 can modulate  $\beta$ -catenin signaling in human cells *in vitro*, the TopFlash beta-catenin/TCF/LEF reporter system was used<sup>224,225</sup>. Briefly, repeats of the TCF and LEF binding sites were coupled with a firefly luciferase reporter to make up the TopFlash plasmid. This plasmid was co-transfected with a Renilla luciferase plasmid that controls for transfection efficiency. A stable human cell line expressing both the TopFlash

and Renilla plasmids, which will be referred to as TopFlash cells from here forward, was used for all TopFlash experiments. TopFlash cells are then transfected with constructs of interest before stimulation with Wnt conditioned media and measurement of the ratio of firefly to Renilla luciferase. Over-expression of *CMV:PRL-3* in TopFlash cells led to an average of a 4.5 fold increase in luminescence compared to *pMax-GFP* control, suggesting that PRL-3 over-expression augments  $\beta$ -catenin signaling (**Figure 4.7A**). Additionally knock-down of PRL-3 with three different shRNA constructs led to a decrease in luminescence, indicating that PRL-3 knock-down decreases  $\beta$ -catenin signaling *in vitro* (**Figure 4.7B**). Furthermore, treatment of TopFlash cells with the PRL inhibitor JMS-053 decreased the luminescence to the levels detected in the unstimulated DMSO treated cells (**Figure 4.7C**). This indicates that chemical inhibition of PRL-3 can almost completely abolish Wnt/ $\beta$ -catenin signaling *in vitro*. Finally, over-expression of *CMV:PRL-3(C170S)* and *CMV:PRL-3(C104S)* mutants induce  $\beta$ -catenin activity in a similar manner as *CMV:PRL-3* wild-type over-expression. While this data may suggest that PRL-3 localization and phosphatase activity do not play a role in PRL-3 activation of  $\beta$ -catenin, there was a significant amount of variation between experiments in these assays, making it difficult to draw any definitive conclusions (**Figure 4.7D**). Taken together, the TopFlash experiments demonstrate that PRL-3 plays a role in modulating  $\beta$ -catenin signaling in human cells *in vitro*.

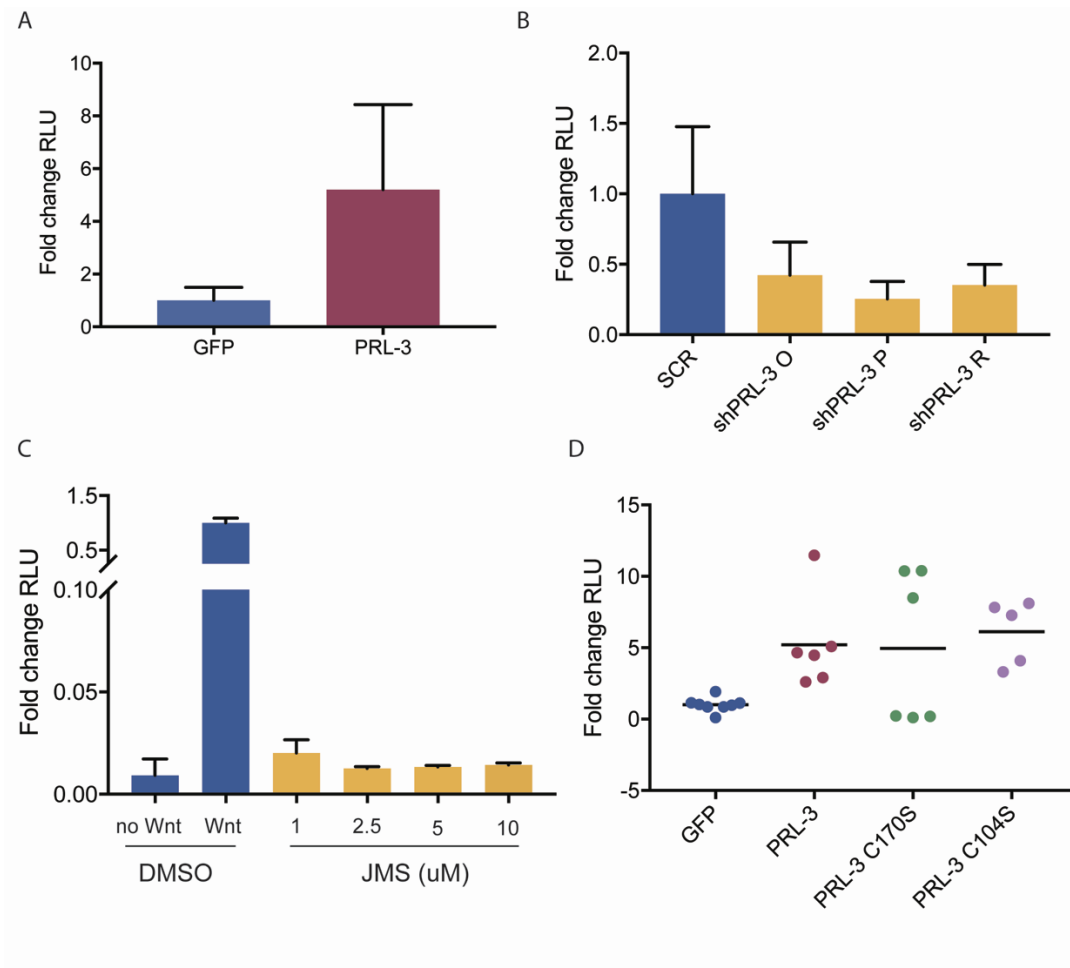


**Figure 4.7 TopFlash Assay Reveals PRL-3 Modulates Wnt/Beta-catenin Signaling In Vitro**  
 TopFlash assay for studying effect on Wnt/beta-catenin signaling (A) Over-expression of wild-type CMV PRL-3 compared to pMax GFP control. Results depicted as fold change in relative light units (RLU). (B) PRL-3 knock-down in TopFlash cells with three different shRNA constructs compared to SCR control. (C) JMS-053 treatment in TopFlash cells at increasing doses from 1 to 10  $\mu$ M compared to DMSO control with and without stimulation with Wnt conditioned media. (D) Over-expression of CMV PRL-3 C104S and C170S mutants compared to wild-type CMV PRL-3 over-expression and pMax GFP.

While I demonstrated that PRL-3 can modulate  $\beta$ -catenin signaling *in vitro* in human cells with the TopFlash assays, it was yet to be determined whether PRL-3 was able to modulate  $\beta$ -catenin target genes in human leukemia cell lines. Jurkat T-ALL stable cell lines over-expressing wild-type PRL-3 or GFP control were stimulated with Wnt

conditioned media for 4 or 6 hours before they were collected and RNA was isolated. RT-PCR for  $\beta$ -catenin target genes revealed that the oncogene *c-MYC* was significantly elevated after Wnt stimulation in the PRL-3 over-expressing T-ALL cells compared to GFP control expressing cells (**Figure 4.8A**). PRL-3 over-expression was also confirmed by RT-PCR and showed significant up-regulation compared to GFP control Jurkat cells (**Figure 4.8B**). This data suggests that PRL-3 can modulate  $\beta$ -catenin to enhance *c-MYC* expression in human leukemia cells, likely contributing to leukemia initiation.

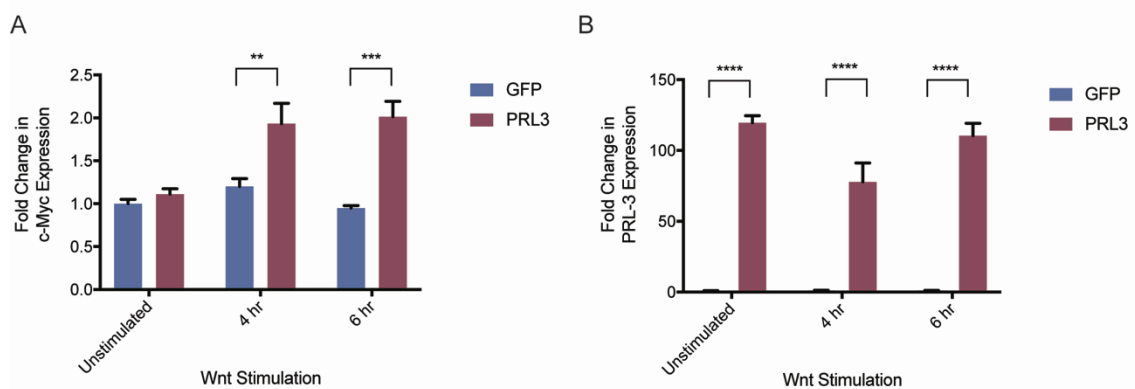


**Figure 4.8 PRL-3 Over-Expression Induces *c-Myc* Expression Upon Wnt Stimulation**  
Jurkat cells stably expressing wild-type PRL-3 or GFP control were stimulated with Wnt conditioned media for 4 or 6 hours. RT-PCR was performed for fold change in (A) *c-myc* and (B) PRL-3 expression in PRL-3 over-expressing T-ALL compared to GFP control. \*\* $p < 0.01$ , \*\*\* $p < 0.001$ , and \*\*\*\* $p < 0.0001$ .

To determine if other target genes downstream of  $\beta$ -catenin signaling were differentially regulated as a result of PRL-3 over-expression in human leukemia cell lines, a RT profiler array was performed. The Wnt signaling targets RT profiler array (Qiagen) was done on Jurkat PRL-3 over-expressing cells compared to Jurkat GFP expressing control cells. Results from this array identified several Wnt target genes that were differentially expressed in Jurkat PRL-3 cells compared to Jurkat GFP cells (**Figure 4.9A**). These differentially expressed genes included LEF1, RUNX2, MMP9, ANGPTL4,

CEBPD, and ID2 (**Figure 4.9B**). This data is encouraging, as lymphoid enhancer binding factor 1 (LEF1), inhibitor of DNA binding 2 (ID2), and RUNX family transcription factor 2 (RUNX2) have both been implicated in leukemogenesis<sup>226–228</sup>. Matrix metalloproteinase 9 (MMP9) and CCAAT enhancer binding protein delta (CEBPD) have also been implicated in leukemia<sup>229,230</sup>. Finally, angiopoietin-like 4 (ANGPTL4) expression is induced by hypoxia initiating factor 1 alpha (HIF1 $\alpha$ ) which is known to be critical to LSCs in T-ALL<sup>133,231</sup>.

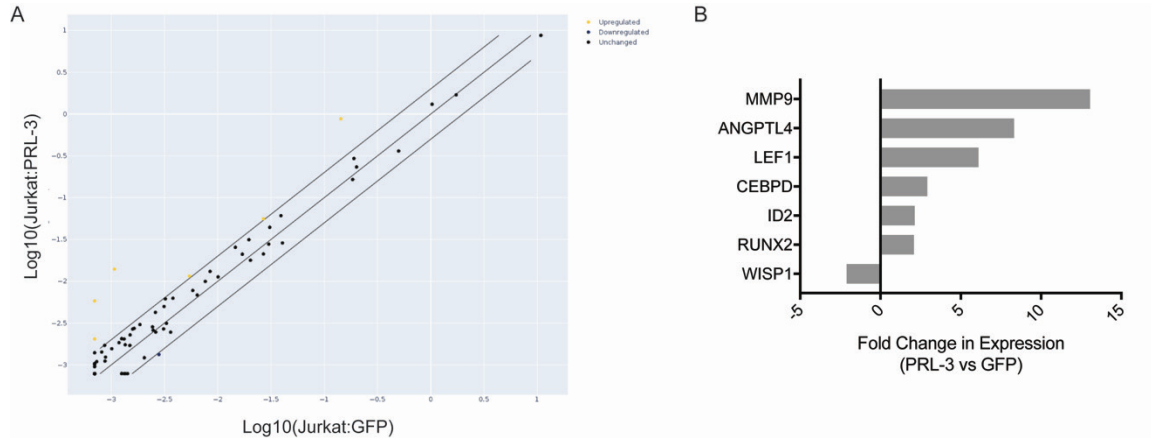


**Figure 4.9 PRL-3 Over-Expression Increases Wnt Target Gene Expression In Vitro**  
 RT-PCR profiler array of Wnt pathway signaling targets on Jurkat-GFP control cells compared to Jurkat-PRL-3 WT cells. (A) Plot showing fold change of PRL-3 WT compared to GFP control of all genes tested. Middle line represents no change, outside lines represent 2 fold change in either direction. Data points above the upper line are upregulated genes and below the lower line are downregulated genes. (B) Fold change in expression of genes that were up- or down-regulated greater than 2 fold.

To determine if PRL-3 was playing a role in modulation of Wnt/ $\beta$ -catenin pathway signaling via direct activation of  $\beta$ -catenin, I treated cells with the PRL-3 inhibitor, JMS-053, and then probed for phosphorylated- $\beta$ -catenin by Western blot. In the absence of Wnt signaling,  $\beta$ -catenin is phosphorylated at serine 33, serine 37, and threonine 41 by GSK3 $\beta$ ,

leading to  $\beta$ -catenin ubiquitination and proteasomal degradation. Inhibition of the proteasome with MG-132 in Jurkat T-ALL cells led to an increase in phospho- $\beta$ -catenin, as it was allowed to accumulate in the cytoplasm of cells without being degraded. Interestingly, treatment with JMS-053, with or without MG-132, resulted in an increase in phospho- $\beta$ -catenin, suggesting that inhibition of PRL-3 may result in an increase in beta-catenin phosphorylation and degradation (**Figure 4.10**).

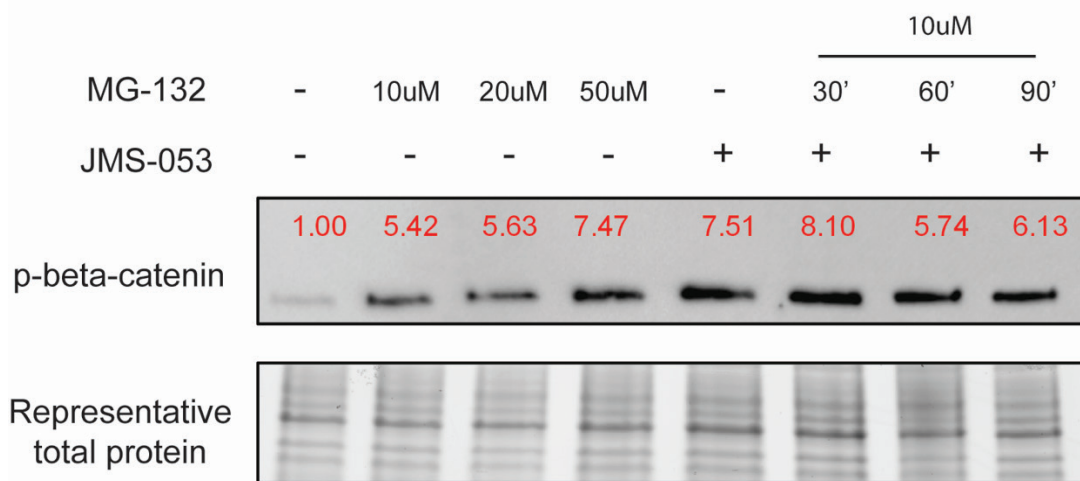


**Figure 4.10 Inhibition of PRL-3 Modulates Beta-Catenin Phosphorylation**

Western blot of Jurkat leukemia cells treated with proteasome inhibitor (MG-132) at increasing doses from 10  $\mu$ M to 50  $\mu$ M and at 10  $\mu$ M for a time course ranging from 30 to 90 minutes. Cells were also treated with a PRL-3 inhibitor JMS-053 (10  $\mu$ M). Western blot was probed with anti-phospho-beta-catenin (Ser33/37/Thr41, Cell Signaling Technology). Fold change in expression is quantified in red compared to untreated Jurkat cells.

### 4.2.3 PRL-3 Modulates Beta-Catenin Signaling *in Vivo*

While a role for PRL-3 in modulation of  $\beta$ -catenin signaling has been established *in vitro*, via TopFlash assays and expression of Wnt pathway target genes, I wanted to confirm that PRL-3 is able to modulate Wnt/ $\beta$ -catenin signaling *in vivo*. A *Tg(6xTCF/LEF:miniP-dGFP)* transgenic wnt pathway reporter zebrafish line was used to

determine the effect of PRL-3 chemical inhibition on  $\beta$ -catenin signaling. In this transgenic zebrafish line, repeats of the TCF/LEF transcription factor binding sites are upstream of a GFP reporter gene with a minimal promoter<sup>232</sup>. When beta-catenin is active, TCF/LEF transcription factor binding leads to expression of GFP. In this model, Wnt signaling is expressed during normal early development in both the head and tail region (**Figure 4.11A**). When fish are treated with XAV939, a Wnt inhibitor, GFP fluorescence in the tail region decreases; treatment with BIO, a Wnt activator, causes an increase in GFP fluorescence (**Figure 4.11D and E**). Chemical inhibition of PRL-3 with PRL3-inhibitor I (Sigma), decreases GFP expression, or Wnt/beta-catenin signaling in a dose-dependent manner, to the level of XAV939, demonstrating that PRL-3 chemical inhibition is capable of modulating beta-catenin signaling *in vivo* (**Figure 4.11C and F**).

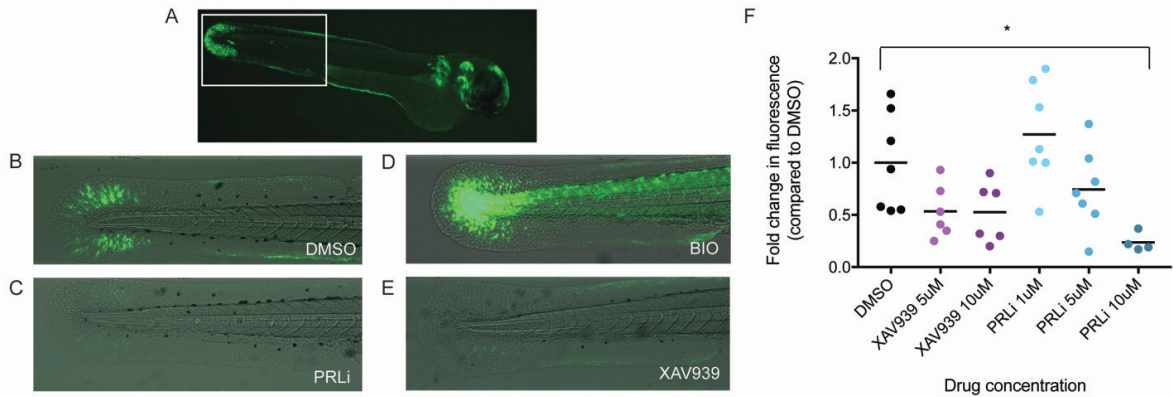


**Figure 4.10 PRL-3 Chemical Inhibition Decreases Beta-catenin Signaling In Vivo** (A) 6xTCF/LEF-miniP:dGFP zebrafish at 48 hpf; GFP fluorescence is an indicator of Wnt signaling during normal development. There is extensive TCF/LEF-driven GFP expression in the head and tail regions. The white box shows the tail area imaged for drug screen in (B-E). (B) DMSO (vehicle) control fish showing normal pattern of GFP expression in the tail. Post-drug treatment tail images were taken at 72 hpf. (C) Chemical inhibition of PRL-3 with PRL3-inhibitor I (PRLi, Sigma) decreases GFP fluorescence. (D) Treatment with the Wnt pathway activator BIO leads to an increase in GFP fluorescence in the tail. (E) Treatment with the Wnt inhibitor XAV939 leads to a decrease or complete loss of GFP fluorescence in the tail. (F) Quantification of fold change in GFP expression compared to DMSO control. \* $p < 0.05$ .

### 4.3 Discussion

Here I found that high PRL-3 expression in both patient samples and our zebrafish T-ALL model correlates with elevated beta-catenin expression. *In vitro*, PRL-3 modulates  $\beta$ -catenin signaling as demonstrated by over-expression, knock-down, and chemical inhibition assays in a TopFlash  $\beta$ -catenin reporter system. Further, PRL-3 chemical inhibition modulates  $\beta$ -catenin signaling *in vivo* in a transgenic  $\beta$ -catenin reporter zebrafish line. In both human T-ALL cell lines and our zebrafish T-ALL I saw elevation of *c-Myc* expression, a down-stream target gene of  $\beta$ -catenin. RNA sequencing comparing PRL-3 over-expressing leukemias to Myc-induced control leukemias demonstrated elevation of CSNK1 $\epsilon$ , another protein involved in Wnt pathway signaling.

Overall, these data suggest that PRL-3 plays a role in modulation of  $\beta$ -catenin signaling both *in vitro* and *in vivo*. This is likely at least in part responsible for the increase in LSC frequency seen in PRL-3 over-expressing zebrafish T-ALL.  $\beta$ -catenin involvement in CSCs in general, and more specifically in T-ALL LSCs, has been well documented. A role for PRL-3 in modulation of  $\beta$ -catenin signaling further strengthens evidence that PRL-3 is serving as a driver of self-renewal in LSCs in T-ALL *in vivo*. Small molecule inhibition of PRL-3 may be able to modulate Wnt pathway signaling without directly targeting Wnt pathway components. As PRL-3 is not ubiquitously expressed, targeting of PRL-3 is not expected to have the widespread side effects that come with direct inhibition of Wnt pathway signaling. Therapeutic targeting of PRL-3 in T-ALL LSCs may therefore be a novel strategy for LSC inhibition.

#### **4.3.1 Future Directions**

Further studies are required for determining the mechanism by which PRL-3 is modulating Wnt pathway signaling. Further analysis and validation of RNA sequencing results from additional tumor samples is ongoing. Additionally, investigation of Wnt pathway protein expression in zebrafish leukemia samples is underway and will help to reveal the mechanism by which PRL-3 is activating down-stream  $\beta$ -catenin targets and instigating an increase in LSC self-renewal.

### **4.4 Methods**

#### **4.4.1 Gene Set Enrichment Analysis (GSEA)**

GSEA was done using GSEA 4.0.0. The data set GSE13159 was downloaded and phenotype labeling was done using PRL-3 expression levels from Affymetrix probes

209695\_at and 206574\_at. Enrichment was calculated using MsigDB collection C6 (oncogenic gene sets). Gene set enrichment was considered significant if it had a nominal p-value <0.05.

#### **4.4.2 RNAseq**

Total RNA was isolated from leukemia cells using Zymo Research Quick-RNA kit (R1054, Irvine, CA, USA). RNA concentration was quantified using a NanoDrop spectrophotometer. RNA quality and RNA library preparation were performed by Genewiz, Inc. (South Plainfield, NJ). RNA sequencing was done with 2 biological replicates in the Myc control group and three biological replicates in the PRL-3 over-expression group. RNA sequencing was done by Genewiz using an Illumina HiSeq and sequenced reads were mapped to the reference genome. Differential expression analysis and data quality control were also performed by Genewiz. The list of differentially expressed genes was then compared with those that resulted from earlier RNA sequencing performed in the same manner by the University of Louisville sequencing facility that were analyzed using Basepair online software. This prior experiment was done using three biological replicates for the Myc control group and three for the PRL-3 WT group. Any genes that were differentially regulated by both RNA sequencing experiments were reported.

#### **4.4.3 RT-PCR**

To assess gene expression, RNA was isolated from leukemia cells using Zymo Research Quick-RNA kit (R1054, Irvine, CA, USA). Total RNA was reverse transcribed (BioRad iSCRIPT, 1708891) and real time PCR performed using iTaq Universal SYBR

Green Supermix (Biorad, 1725120) with primer sequences available in (Table 4.1). Data were normalized to efla expression and fold change was calculated using the  $2^{-\Delta\Delta Cq}$  method.

**TABLE 4.1 REALTIME RT-PCR PRIMER SEQUENCES**

Gene	Forward Primer	Reverse Primer
<i>z-myca</i>	TATGCTGCAAGTGACCGGAG	TCACCGGCATTTTGACACTTG
<i>h-prl-3</i>	AAAGGCCCCCAAGGTAGTTA	GCACAAGAGTTCCGTAGCTG
<i>h-c-Myc</i>	AGAAGTACGGGGCTACCACT	TCAAACGGCCAGTCCACAAC
<i>h-GAPDH</i>	CGACAGTCAGCCGCATCTT	CCCCATGGTGTCTGAGCG
<i>z-eef1a1</i>	ATGGCACGGTGACAACATGCT	CCACATTACCACGACGGATG

#### 4.4.4 Western Blot

To assess protein expression, western blot analysis was performed using Bio-Rad stain-free gels, allowing for the use of total protein as the loading control for normalization purposes<sup>233</sup>. Gels were transferred using the Bio-Rad Trans-Blot Turbo system according to the manufacturer's instructions. Blots were blocked in 5% milk in 1% TBST. Anti-PTP4A3 (PRL-3) antibody (Genetex, GTX89930) was used at a 1:1000 dilution in 5% milk in 1% TBST. Anti-beta-catenin antibody (Abcam, 16051) was used at a 1:1000 dilution in 5% milk in 1% TBST.

#### 4.4.5 Cell Culture

Cells were cultured at 37°C in a humidified atmosphere with 5% CO<sub>2</sub>. Cell lines were authenticated by short tandem repeat (STR) DNA profiling and tested for mycoplasma contamination prior to experimentation. T-cell acute lymphoblastic leukemia

(Jurkat) cells were grown in RPMI 1640 (ThermoFisher 11875119) supplemented with 10% heat-inactivated fetal bovine serum (FBS) (Atlanta Biologicals, S11150H, Lot M17161, Flowery Branch, GA, USA).

#### **4.4.6 TopFlash Assay**

Stable TopFlash expressing cells and Wnt3A producing cells were a generous gift from Dr. Tianyan Gao (University of Kentucky). Wnt3A conditioned media was made by collecting media from Wnt3A producing cells at 90% confluency and again two days later. Wnt3A conditioned media was assayed for Wnt activity with each experiment. TopFlash cells stably express the TopFlash reporter plasmid and a Renilla luciferase control plasmid<sup>224,225</sup>. For over-expression experiments, these cells were transfected with pMax-GFP control plasmid, CMV-PRL-3 WT, CMV-PRL-3 C170S or CMV-PRL-3 C104S plasmids. For knock-down experiments transfections were done with scrambled (SCR) control shRNA or shRNA O, P, or R against PRL-3. All transfections were done using Lipofectamine 3000 (Life Technologies, L3000015) according to the manufacturers protocol. For drug treatment experiments, cells were treated with DMSO control or JMS-053 at doses ranging from 1-10  $\mu$ M. Two days after transfection or drug treatment, cells were lysed and assayed for firefly and Renilla luciferase activity using Promega Dual-Glo luciferase assay system (Promega, E2940). Firefly luciferase expression was normalized to Renilla luciferase expression before calculating fold change compared to the control samples for each experiment.

#### **4.4.7 TCF/LEF Zebrafish Experiments**

Sheer Tg(6xTCF/LEF-miniP:dGFP) zebrafish were a generous gift from Dr. Dave Langenau (Harvard). Drug screen was performed as previously described (Haney et al 2021, in press, STAR Protocols). Briefly, 6xTCF/LEF-GFP embryos were screened for GFP fluorescence at 24 hours post fertilization (hpf), manually dechorionated, and placed in individual wells of a 96-well plate containing DMSO or PRL-3 Inhibitor I (Sigma-Aldrich). After 48 hours of drug treatment, zebrafish were imaged using the vertebrate automated screening technology (VAST) BioImager (Union Biometrica) for GFP fluorescence<sup>234–236</sup>. GFP fluorescence was quantified using FIJI ImageJ by multiplying the area of fluorescence by the mean fluorescence intensity. Images were normalized to DMSO GFP fluorescence and fold change in GFP expression was calculated for each image compared to DMSO control.

#### **4.4.8 Statistical Analysis**

Results are shown as mean  $\pm$  standard deviation. Statistical analyses were performed using GraphPad Prism 7 (San Diego, CA, USA), combining data from all samples across all replicates. Two-tailed t-tests were performed to compare two groups with similar distribution, and Analysis of Variance with Tukey's multiple comparisons was used to compare more than two groups. Statistical analysis for GSEA was done using GSEA 4.0.0 and enrichment was considered significant if it had a nominal p-value  $<0.05$ . RNA sequencing analysis was done by Genewiz and Basepair.

PART 3. NOVEL TECHNOLOGY/TECHNIQUES TO DETECT AND PREVENT T-ALL PATIENT  
RELAPSE AND IMPROVE OUTCOMES

CHAPTER 5. DEVELOPMENT OF A FLUORESCENTLY TAGGED LEUKEMIA STEM CELL  
MODEL IN ZEBRAFISH

## 5.1 Introduction

The limited techniques available for studying leukemia stem cells has posed a major limitation in the advancement of the field. Limiting dilution transplantation assays and lineage tracing assays make up most experiments available for studying LSC biology and function in animal models. The ability to examine LSC biology *in vitro* is limited because, as has been demonstrated in hematopoietic stem cells (HSCs), the stem cell niche plays an critical role in stem cell biology. Technology for studying LSCs *in vivo* and their interaction with the environment have posed a major challenge.

Zebrafish are a useful and inexpensive model for *in vivo* studies of cellular function. Transgenic lines are relatively easy to create to mark specific cell types and lineages with fluorescent reporters. The interaction of HSCs with their environment and the interplay between HSCs and the vascular system has been extensively characterized using zebrafish models<sup>237</sup>. Optically clear mutant zebrafish lines are available, making high-resolution *in vivo* imaging a unique advantage of zebrafish models. Although these stem cell-niche interactions have been studied extensively in HSCs during development, LSCs in T-ALL and other acute leukemias lack LSC-specific cell surface markers or reporters that can be used to create LSC-tagged zebrafish lines. Having a LSC reporter line in zebrafish would allow for in depth study of leukemia stem cell biology *in vivo* and interaction of LSCs with their niche in T-ALL in a manner that is currently not possible. Additionally, such a line would be useful for large-scale drug screens, in which compounds can be examined for ability to target fluorescently tagged LSCs without the need for extensive limiting dilution transplantation.

### 5.1.1 Hypothesis

As described above, in T-ALL, Wnt-active cells make up a very small minority of bulk leukemia cells. Wnt-active leukemia cells were shown to be highly enriched for LSCs in a mouse T-ALL model. In this study, transfection of mouse leukemia cells with a 6xTCF/LEF reporter plasmid and sorting for cells with active  $\beta$ -catenin signaling demonstrated that T-ALL mouse LSCs could be sorted for and  $\beta$ -catenin negative leukemia cells contained virtually no LSCs<sup>133</sup>. Since LSCs are enriched in  $\beta$ -catenin signaling in T-ALL, *I hypothesized that I could create a transgenic TCF/LEF reporter zebrafish T-ALL model in which Wnt-expressing LSCs were tagged in vivo*. This line could then be used both for visualization of T-ALL LSCs *in vivo* and for higher-throughput screening of LSC response to drug treatment *in vivo*.

## 5.2 Results

Sheer Tg(6xTCF/LEF:miniP-GFP) zebrafish embryos were microinjected with *rag2:mMyc + rag2:mCherry* to make a mCherry-fluorescent T-ALL with a GFP  $\beta$ -catenin reporter. In this model,  $\beta$ -catenin expressing cells are GFP-fluorescent, leukemia cells are mCherry-fluorescent, and leukemia cells that also express  $\beta$ -catenin are fluorescent in both GFP and mCherry (**Figure 5.1**). Tg(6xTCF/LEF:miniP-GFP) injected embryos screened for GFP fluorescence at 48 hpf and any negative embryos were discarded. At 21 dpf, injected larvae were screened for mCherry-fluorescence in the thymus and then followed as the leukemia progressed. In some of the zebrafish,  $\beta$ -catenin expressing leukemia cells could be seen residing in the thymus, which is the site of leukemia initiation (**Figure 5.2A**). Confocal imaging revealed a small sub-population of  $\beta$ -catenin cells that could be

visualized in the leukemic thymus (**Figure 5.2B and C**). This provides preliminary evidence that transgenic zebrafish can be used as a reporter line to visualize LSCs *in vivo*.

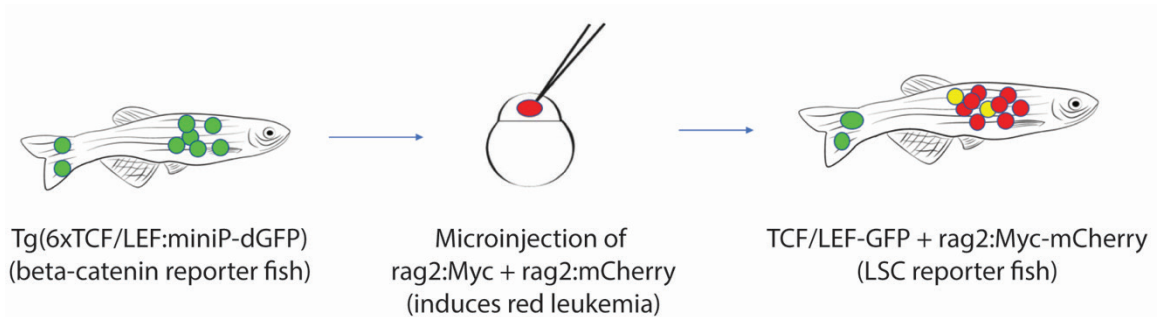


**Figure 5.1 Schematic of LSC Reporter Model Generation**

Tg(6xTCF/LEF:miniP-dGFP) sheer zebrafish embryos were injected with *rag2:Myc + rag2:mCherry* inducing a mCherry fluorescent leukemia. The resulting LSC reporter fish is TCF/LEF-GFP and *rag2:Myc-mCherry*. In this model,  $\beta$ -catenin expressing cells are GFP-fluorescent, leukemia cells are mCherry-fluorescent, and leukemia cells that also express beta-catenin are fluorescent in both GFP and mCherry.

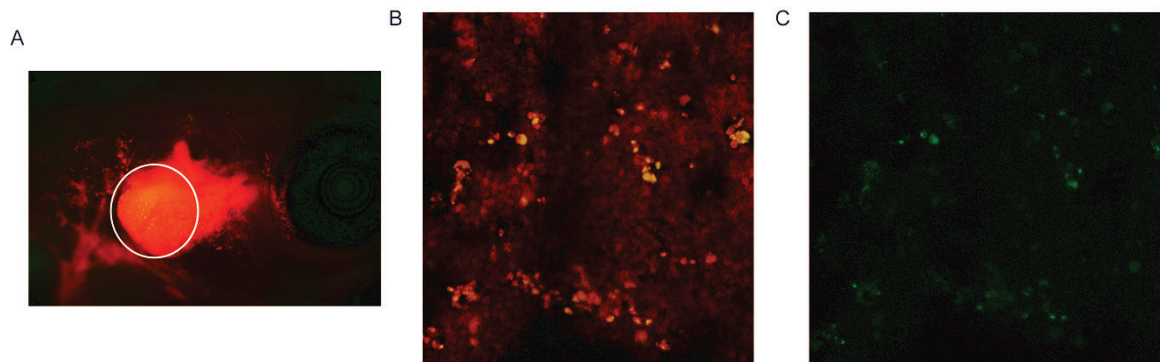


**Figure 5.2 Beta-catenin Expressing Leukemia Cells Located in Thymus**

Imaging of *TCF/LEF-GFP rag2:Myc-mCherry* zebrafish. (A) Leukemic mCherry thymus. Circle indicates an area where GFP-positive cells can be seen. (B) Confocal imaging of circled area from panel (A) depicting mCherry-fluorescent leukemic cells and double-positive (yellow) cells that are beta-catenin expressing leukemic cells, or potential LSCs. (C) Confocal imaging in GFP channel alone depicting a small subset of beta-catenin expressing cells present in the leukemic thymus.

In addition to imaging of zebrafish LSCs, I wanted to try to isolate potential LSCs from leukemic zebrafish. Although this sheer Tg(6xTCF/LEF:miniP-GFP) zebrafish line is not a syngeneic zebrafish line and transplantation studies cannot be performed, I hoped to show that it was possible to isolate these potential LSCs for transplantation and functional studies in the future. *6xTCF/LEF:miniPGFP;rag2:Myc-mCherry* leukemic zebrafish were monitored until their leukemia burden became about 70% of the animal's body and the animals were sacrificed. Tumors were harvested, and flow cytometry was performed to quantify the percentage of mCherry-positive and double positive (mCherry and GFP) leukemic cells. This showed that the percent of beta-catenin expressing leukemic cells made up 0.1% to 1.78% of total cells (**Figure 5.3**).

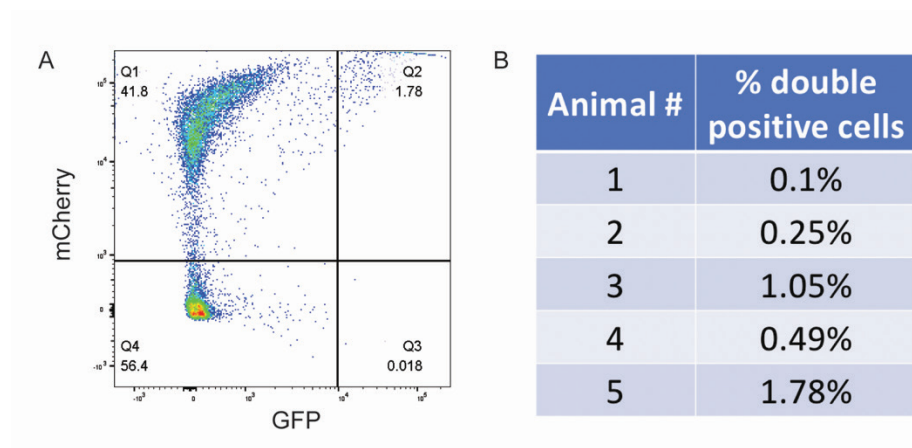


**Figure 5.3 Beta-catenin Expressing LSCs Can Be Sorted By Flow Cytometry**  
 (A) Flow cytometry of leukemic *TCF/LEF-GFP rag2:Myc-mCherry* leukemia.  
 (B) Table showing percentage of mCherry and GFP positive (double positive) cells.

### 5.3 Discussion

Here, I created a new zebrafish model to label Wnt/beta-catenin positive leukemia cells, which are potential leukemia stem cells, utilizing a 6xTCF/LEF-GFP transgenic zebrafish line to make mCherry fluorescent leukemias. I demonstrated that a small

proportion of leukemia cells are enriched for  $\beta$ -catenin signaling and that these cells tend to reside in the thymus during leukemia initiation. This model may allow for *in vivo* studying of  $\beta$ -catenin positive leukemia cells, their niche, and their interaction with their surrounding environment, as well as for high-throughput *in vivo* drug screening.

### 5.3.1 Future Directions

In order to confirm these  $\beta$ -catenin positive leukemia cells are actually enriched for leukemia stem cells, transplantation studies need to be done to demonstrate that the  $\beta$ -catenin positive leukemia cell population is enriched for self-renewal and able to form new leukemias in recipient zebrafish. This would demonstrate that this model can actually serve as a marker of LSCs *in vivo*. The above model was created in a genetically diverse and immunologically competent zebrafish line in which cells cannot be transplanted from one fish to another. I created a syngeneic Tg(6xTCF/LEF:miniP-dGFP) zebrafish line in a CG1 background that can be used for transplantation studies. T-ALL will be generated in these zebrafish with microinjection of *rag2:mMyc* and *rag2:mCherry*, the leukemia harvested, sorted into  $\beta$ -catenin expressing and non- $\beta$ -catenin expressing leukemic cell populations, and then transplanted into recipient zebrafish. With these studies, I would expect to see engraftment upon transplantation of the  $\beta$ -catenin positive leukemia cells and a lack of engraftment in the non- $\beta$ -catenin expressing cells, confirming that our model is labeling LSCs *in vivo* and could be used to study LSC *in vivo* biology, environment, and function at a level that has not been possible before.

## 5.4 Methods

### 5.4.1 Generation of Model in Sheer TCF/LEF Zebrafish

Microinjections of 60 ng/ $\mu$ L *rag2:Myc* + 60 ng/ $\mu$ L *rag2:mCherry* were used to generate zebrafish T-ALL in sheer Tg(6xTCF/LEF:miniP-dGFP) zebrafish as previously described<sup>128,196,207</sup>. Zebrafish were screened for GFP fluorescence at 48 hpf and then monitored for leukemia onset and progression starting at 21 days post-fertilization (dpf) and every 3 days onwards by analyzing percent of the body expressing mCherry-positive leukemia cells using a Nikon fluorescence-equipped SMZ25 microscope. Animals were monitored until they had to be sacrificed due to leukemia burden at approximately 70% leukemic burden.

### 5.4.2 Generation of TCF/LEF CG1 Transgenic Line

Microinjections of 60 ng/ $\mu$ L of a tol2:6xTCF/LEF-GFP reporter plasmid were used to generate a transgenic TCF/LEF-GFP reporter zebrafish line in CG1 syngeneic zebrafish. Zebrafish were screened for GFP fluorescence at 48 hpf using a Nikon fluorescence-equipped SMZ25 microscope and grown on the nursery for two months until they were capable of breeding. This F<sub>0</sub> generation was then outcrossed to CG1 zebrafish and embryos were again screened for GFP fluorescence at 48 hpf to make the F<sub>1</sub> generation. This F<sub>1</sub> generation was then incrossed and screened for GFP fluorescence to make the F<sub>2</sub> generation. The line was then maintained by incross of the F<sub>2</sub> generation or later before use for further studies.

For the LSC reporter model in CG1 Tg(6xTCF/LEF:miniP-GFP) zebrafish microinjections of 30 ng/ $\mu$ L *rag2:Myc* + 30 ng/ $\mu$ L *rag2:mCherry* were used to generate zebrafish T-ALL in CG1 Tg(6xTCF/LEF:miniP-dGFP) zebrafish as previously described<sup>128,196,207</sup>. Zebrafish were screened for GFP fluorescence at 48 hpf and then monitored for leukemia onset and progression starting at 21 days post-fertilization (dpf) and every 3 days onwards by analyzing percent of the body expressing mCherry-positive leukemia cells using a Nikon fluorescence-equipped SMZ25 microscope. Animals were monitored until they had to be sacrificed due to leukemia burden at approximately 70% leukemic burden.

### **5.4.3 Flow Cytometry**

Flow cytometry experiments were performed using a iCyt-Sony Cell Sorter System. Cells were stained for viability using DAPI at a final concentration of 1 mg/mL. Gating was drawn to include live cells and exclude doublets. Fluorescence thresholds were set with single positive controls in each channel.

### **5.4.4 Microscopy**

Confocal microscopy of the zebrafish thymus was done with the help of Dr. Jakub Famulski. Zebrafish were anesthetized with Tricaine-S prior to imaging on a Nikon C2 confocal microscope.

## CHAPTER 6. ZEBRAFISH AS A XENOGRAFT MODEL

*Taken from: Drug Screening of Primary Patient Derived Tumor Xenografts in Zebrafish. Meghan Haney, Henry Moore, and Jessica Blackburn. JoVE, 2020; and Suitability of Zebrafish as a Recipient of Mammalian Xenografts in Translational Cancer Research. Meghan Haney et al. In submission to Cancers, 2021.*

## 6.1 Introduction

Xenografting of human cell lines and primary tumor cells into model organisms has become a widespread practice, particularly for validating response of tumor cells to novel drug therapies<sup>238,239</sup>. Historically, immune compromised mice have been used as the most common xenograft model; however, using mice is costly and impractical for large scale drug screening. Zebrafish have emerged as an alternative to mouse models. The zebrafish's advantages in xenografts lie primarily in their cost-effectiveness. Zebrafish have a large brood size, quick generation time and low-cost upkeep. These factors have moved the zebrafish forward as an ideal candidate for high-throughput experiments.

Considering all the advantages of the zebrafish model, it is compelling to think that they could provide a platform for a cost-effective approach to personalized medicine where xenografted patient tumors undergo drug susceptibility testing prior to clinical treatment<sup>240,241</sup>. With this model, small amounts of cancerous cells could be taken from patients, injected into a large number of zebrafish larvae, and subjected to large-scale high-throughput drug screening, determining responsiveness of individual patient tumors to a wide variety of drugs within a matter of days to a week<sup>240-243</sup>. This information could then be used for predicting patient response to a variety of treatments, including targeted therapies, stratifying patients into clinical trials, or identifying treatment-resistant cells within a tumor that could be responsible for relapse later on.

Typically, quantification of xenografted cells after drug screening is measured by one of two ways: dissociation of xenografted fish into single cell suspensions and quantification of remaining, fluorescently-labeled tumor cells<sup>244,245</sup> or by semi-automated imaging methods where fixed larval fish are imaged in 96-well plates using an inverted

fluorescent microscope before realignment of composite images and quantification of tumor cell foci <sup>246</sup>. Our lab and others have previously published on the use of the Vertebrate Automated Screening Technology (VAST) Bioimager and Large Particle (LP) Sampler <sup>235,236</sup>(Union Biometrica) which has opened the door for an even more high-throughput method of drug screening of zebrafish <sup>247</sup>.

Despite the advantages and opportunities with zebrafish xenograft models, there are several considerations that may be limiting their wide-spread use. First, xenografting tumor cells into larval zebrafish is technically challenging, with different labs adopting their own approaches for this technique. This lack of consensus leads to inconsistencies from one group to the next in how the models are created. Another challenge to consider is that zebrafish are normally housed at 28°C, much cooler than the 37°C body temperature of humans and other mammalian model organisms. As a compromise between the two, xenografted fish are typically kept at 34°C to try to maintain both zebrafish and human cell survival; however, there is a lack of knowledge on how this temperature change affects normal fish and cancer cell physiology. Finally, using larval zebrafish for xenografts is merely a short-term model that does not permit the study of long-term drug response, tumor recurrence, or late stage tumor-host interactions, since the fish start to develop an immune system around 7dpf<sup>248</sup>.

To begin to address these issues, I have reconciled some of the variation in xenograft methodology used between research groups. I also address the lack of consensus between the best site for injection of xenografted human cells into larval zebrafish and compared the metabolism of different injection sites in the fish and how these changes could affect downstream assays. I developed a streamlined workflow for xenografting

primary patient leukemia cells into zebrafish and performing high-throughput drug screens with automated imaging and quantification, which can be applied to any other primary patient tumor cells or cancer cell line. Our studies in this chapter address the concerns over suitability of zebrafish as a xenograft model.

## **6.2 Results**

### **6.2.1 Optimization of Xenograft Injection Site and Cell Number**

A major inconsistency between published xenograft studies is the site of mammalian cell injection and number of cells injected per animal to achieve optimized and reliable engraftment while still maintaining high survival rates. In order to determine if there is an optimal engraftment location and cell density I stained cells with DiI and injected into dechorionated zebrafish larvae at 48 hpf at 7 different injection sites: yolk, pericardium, brain, caudal vein, duct of Cuvier, periorbital space, and perivitelline space (**Figure 6.1A-H**). Survival rates of each site were reported, showing that there was no major difference in survival between injection sites at 1 day post-transplant (dpt) (**Figure 6.1I**). However, there was a difference in engraftment rates at different sites and in the loss of engrafted fish from 1 to 5 dpt (**Figure 6.1J**). I found that the pericardium, duct of Cuvier, and yolk injection sites provided the most reliable results with the highest percentage of engrafted fish still alive at 5 dpt.

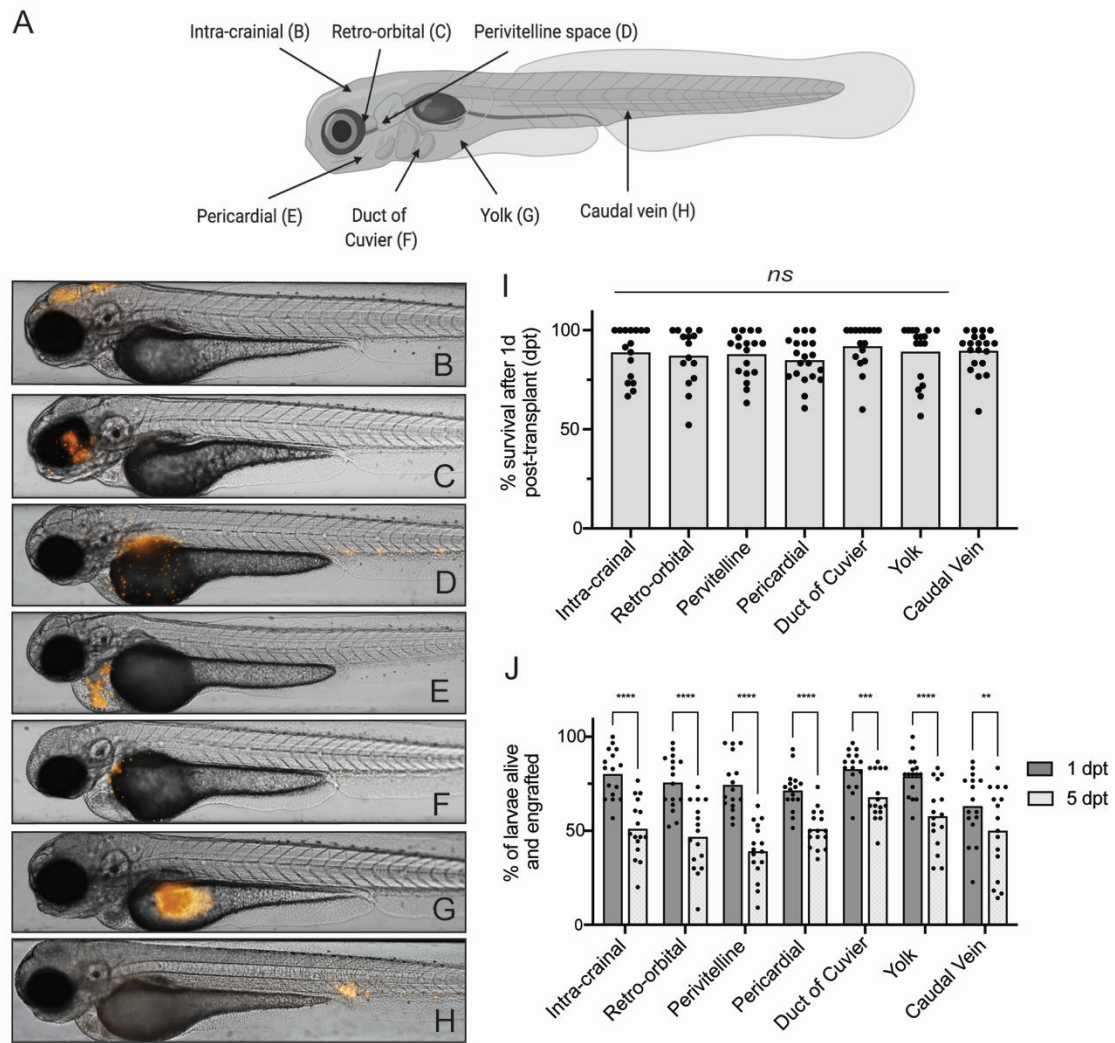


**Figure 6.1 Recipient Survival Post-Xenograft Varies by Injection Site**

(A) Depiction of seven injection sites tested in 48 hpf zebrafish larvae. Representative images of zebrafish larvae at 24 hours post injection (hpi) injected with DiI stained cells at 48 hpf at each of seven injection sites, brain (B), peri-orbital space (C), perivitelline space (D), pericardium (E), duct of Cuvier (F), yolk (G) and caudal vein (H). Images were taken with the VAST BioImager. Scale bar represents 250  $\mu$ m. (I) Percent survival of injected fish after 1 day post-transplant (dpt). Mammalian cancer cell lines were injected at the 7 injection sites listed above in groups of 30, with a minimum of 3 replicates per group. NS = not significant. (J) Comparison of percent of larvae alive and engrafted at 1 and 5 dpt. \*\*\*\* p-value <0.0001, \*\*\* p-value <0.001, \*\* p-value <0.01.

Another important consideration is ease of injection which played a major role in efficiency of being able to practically use zebrafish as a xenograft model for drug screening, with caudal vein and retro-orbital injections taking approximately twice as long as other injection sites (data not shown). Cells can be seen circulating when injected into the caudal vein, duct of Cuvier, peri-orbital space, pericardium, or perivitelline space. Since there was no major difference in survival and the yolk and pericardium were the fastest and most consistent injection sites to have cells in the correct anatomic location, these sites were chosen going forward for further studies.

In collaboration with Dr. Ramon Sun's lab, we decided to characterize the metabolic changes that occur in zebrafish xenograft models. Zebrafish larvae are yolk-dependent organisms and feed off of their yolk for about 5-7 dpf without any external food source. Contrary to the rest of the embryo, the yolk is devoid of cells and made up mostly of stored lipids and proteins<sup>249</sup>. This nutrient-rich area is also the most common injection site for xenograft models in zebrafish. Since yolk composition differs compared to the soma it may have different metabolic activity that can impact how xenografted cells behave and respond to drug treatment. We were interested in the metabolites present in the zebrafish yolk to predict the effect this would have on cells xenografted into this location compared to the body of larval zebrafish. Zebrafish were manually de-yolked at 6 dpf and the metabolites were analyzed by mass spectrometry in the fish that still had an intact yolk compared to de-yolked zebrafish (**Figure 6.2A**). PCA analysis showed that whole fish clustered independently from de-yolked fish based on relative metabolite abundance (**Figure 6.2B**). Additionally, many metabolites were enriched in the body alone, compared to the body plus yolk (**Figure 6.2C**).

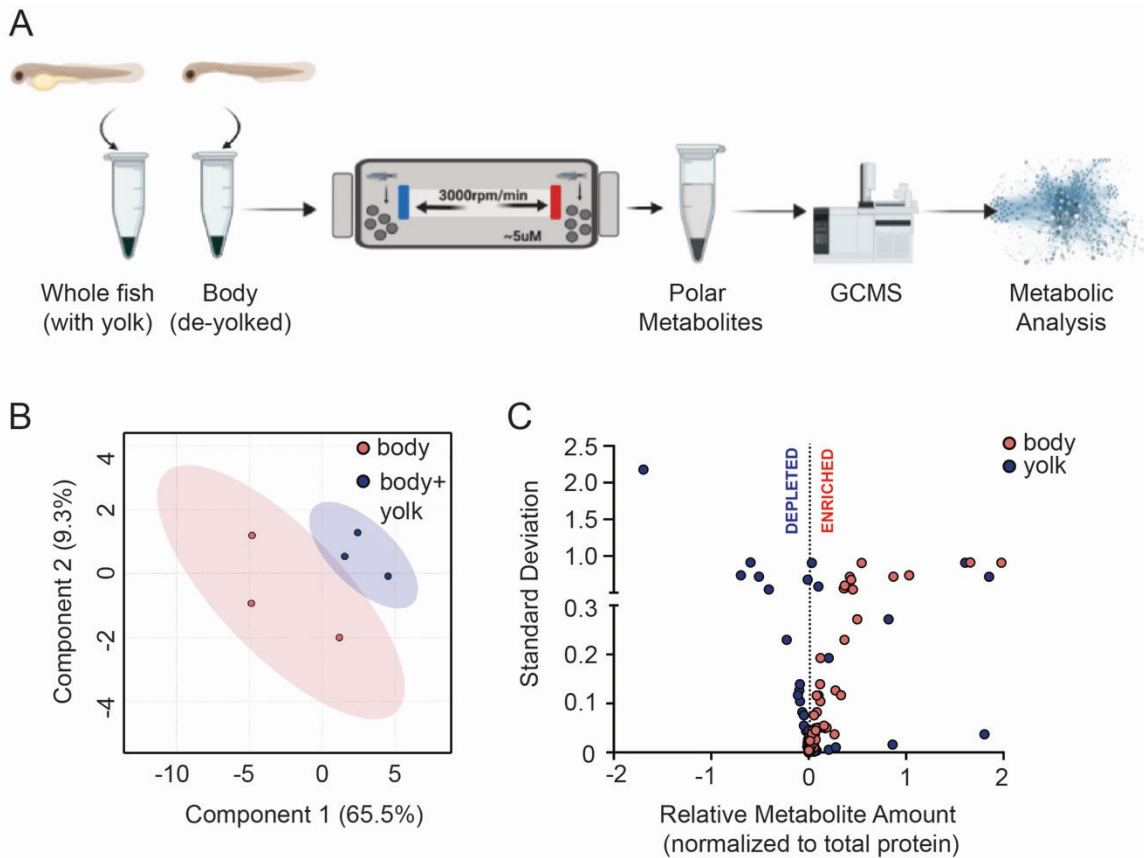


**Figure 6.2 Zebrafish Metabolites Vary Between Body and Yolk Injection Sites**  
 (A) Schematic of workflow for GC-MS metabolic analysis of whole zebrafish larvae and de-yolked zebrafish larvae. (B) PCA showing that whole (body + yolk) zebrafish larvae (blue) cluster independently from de-yolked (body) zebrafish larvae (orange) based on metabolites present. (C) Volcano plot of enriched and depleted metabolites from whole (body + yolk, orange) and de-yolked (body, blue) zebrafish larvae.

I also compared injection cell density of 100, 250, 500, and 1,000 cells per zebrafish larvae both in the yolk and in the body of the fish. I was able to see consistent engraftment of the cells at 1 dpi in the yolk above 100 cells injected, but in the pericardium I was unable to reliably visualize and quantify engrafted cells when less than 500 cells were injected (**Figure 6.3A**). When I examined the survival between the groups, I found that there was a higher survival in the 500 cell group than in the 1,000 cell group and this difference was

significant in the yolk injected fish, with a p-value of 0.0396 (**Figure 6.3B**). I chose to continue forward using 500 cells injected per zebrafish as this had the highest survival and allowed for consistent engraftment and quantification of engrafted cells for drug-screening applications.

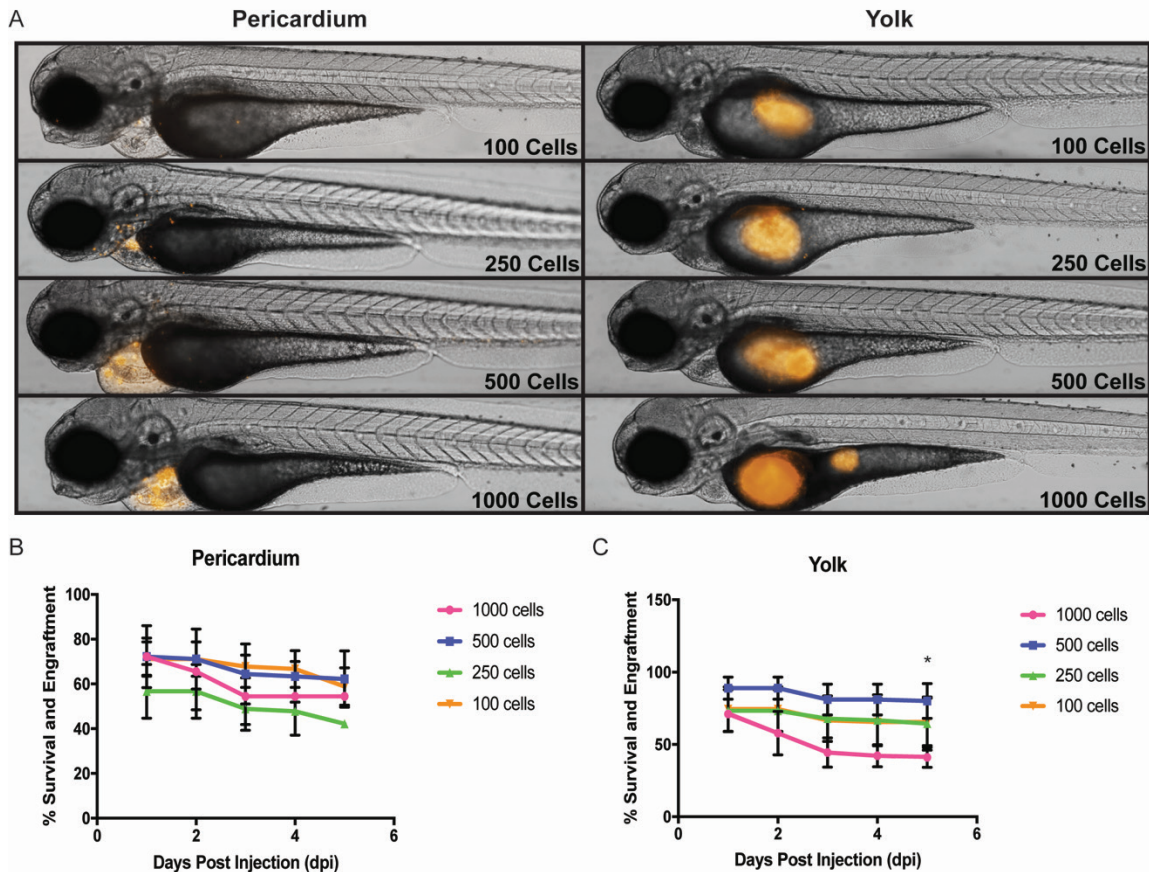


**Figure 6.3 Optimization of Cell Number for Injection**

DiI stained cells were injected into the pericardium or yolk of dechorionated zebrafish larvae at 48hpf at concentrations of 100, 250, 500, or 1,000 cells per injection. (A) Images were taken at 1 dpi with VAST Bioimager. (B) Injected fish were screened at days 1, 3, and 5 post-injection for the number of fish that remained alive and engrafted with DiI stained cells. Three independent experiments with n=30 zebrafish per experiment were done for each site and cell number. Plots show mean with error bars representing standard deviation. \* =  $p < 0.05$  between the percent survival and engraftment of the 500 and 1,000 cell groups at 5 dpi in the yolk.

## 6.2.2 Temperature Affects Zebrafish Survival and Metabolism

Another challenge that has arisen with zebrafish as a model for cancer cell xenografts is the difference in optimal growth temperature between zebrafish and human cancer cells. Zebrafish are normally housed at 28°C, while normal human body temperature is 37°C. Different groups have reported using a range of temperatures between 28°C and 37°C for generation and maintenance of zebrafish xenografts<sup>250,251</sup>. Temperature has a significant impact on zebrafish early growth and development and the effect this change has on xenograft survival and biology has not been addressed<sup>252,253</sup>. To assess increased housing temperature on larval survival I first tracked the translucent Casper zebrafish larvae over three different temperatures and found that although the survival was highest at 28°C with 95% survival, the survival rate after 5 days at 34°C and 37°C was still 80% and 67% respectively (**Figure 6.4A**). Gross morphologic changes were noted in the zebrafish when the temperature increased from 28°C to 34°C and 37°C, with the size of the yolk sac decreasing with increasing temperature and the fish looking smaller in size and less active at higher temperatures (**Figure 6.4B**).

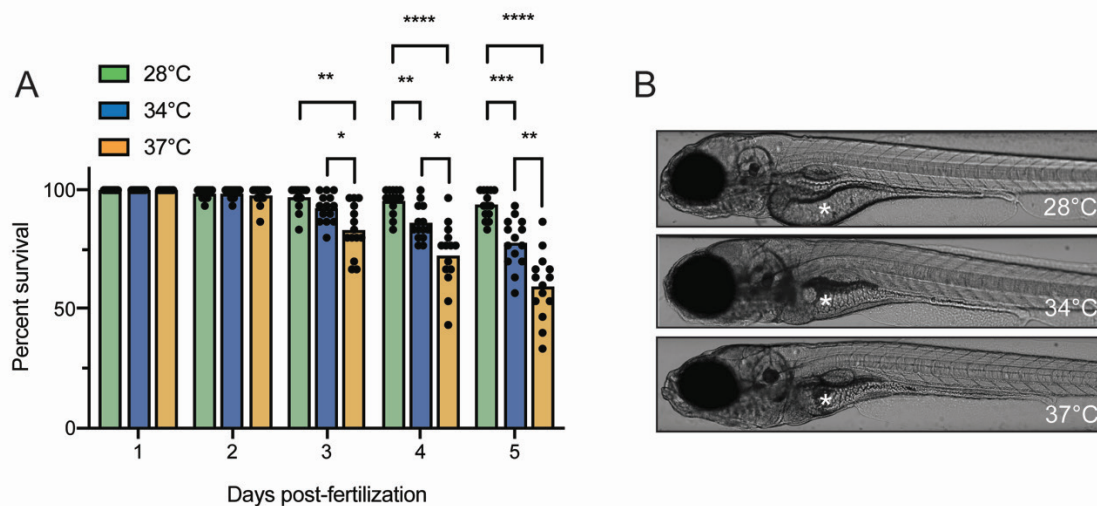


**Figure 6.4 Optimization of Temperature for Xenograft Maintenance**  
Survival of zebrafish larvae at 28°C, 34°C, and 37°C. Fish were dechorionated at 48 hpf and incubated at the designated temperature for 5 days. P-values comparing temperatures at each time point shown above the graph. (B) Representative images of zebrafish larvae grown at 28°C, 34°C, or 37°C for 5 days. Images taken on VAST Bioimager at 7 dpf. \* indicates yolk size, which decreases with increasing temperature. \*\*\*\* p-value <0.0001, \*\*\* p-value <0.001, \*\* p-value <0.01, \* p-value <0.05.

While both cell lines and zebrafish are able to survive at 34°C, it is known that temperature plays a role in metabolism, so I was interested in the metabolic changes that occur with changes in temperature. Zebrafish at 2 days post fertilization (dpf) were housed at 28°C, 34°C, or 37°C for 48 hours and then collected in triplicate for carbohydrate metabolism analysis by mass spectrometry. In general, almost every carbohydrate metabolite analyzed increased when the temperature was increased from 28°C to 34°C and PLS-DA plotting showed zebrafish larvae grown at 28°C, 34°C or 37°C cluster independently (**Figure 6.5**). This demonstrates that zebrafish maintained at non-physiologic temperatures for xenograft experiments experience metabolic changes. As a whole, it is important to keep in mind that variations in temperature can change the

metabolism of the entire organism, which in turn can affect the nutrient availability and microenvironment of xenografted cells, and that should be taken into consideration when utilizing zebrafish as a xenograft model.

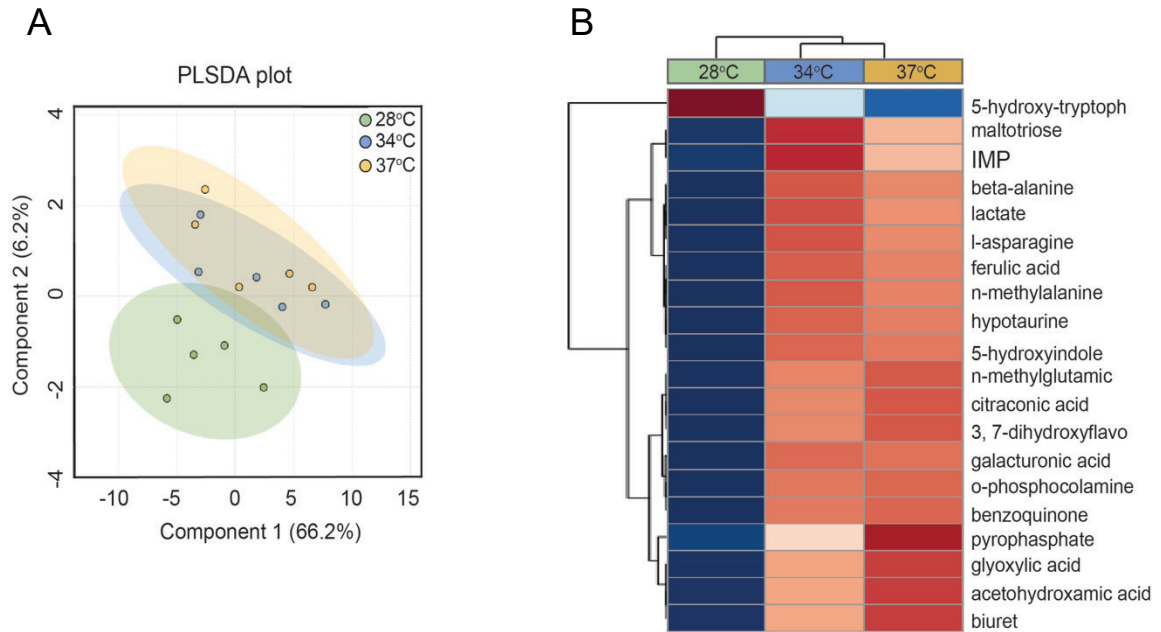


**Figure 6.5 Temperature Affects Zebrafish Metabolism**

PLS-DA plot showing zebrafish larvae grown at 28°C, 34°C or 37°C cluster independently. (B) Heat map showing main differences contributing to PLS-DA clustering of 28°C, 34°C and 37°C groups.

### 6.2.3 Temperature Affects Xenografted Cell Survival and Metabolism

I next studied the effect of temperature on cancer cell growth *in vitro*. I first tracked the growth of Jurkat, HSB2, or HBP-ALL cells over 5 days at 34°C or 37°C. Cells were counted every other day and I found that cells grew at both 34 and 37°C, with a faster rate of growth at 37°C (**Figure 6.6A**). Cells did not grow at 28°C so this temperature was eliminated from further experiments. I next used EdU uptake as a marker of cell cycle in Jurkat cells grown at both 34 and 37°C, finding that significantly more cells were in G0/G1 stage of the cell cycle and significantly less in S phase, or actively replicating, in cells

maintained at 34°C compared to 37°C (**Figure 6.6B**). Staining of human leukemia cell lines grown at 34 and 37°C with Annexin V to quantify the amount of apoptosis in cells grown at each temperature revealed that Jurkat and HBP-ALL leukemia cell lines had significantly increased apoptosis at 34°C compared to 37°C (**Figure 6.6C**). Combining this data with the zebrafish survival data from Figure 6.4, I found 34°C to be the optimal compromise to attain the highest survival of both zebrafish larvae and mammalian cancer cells.

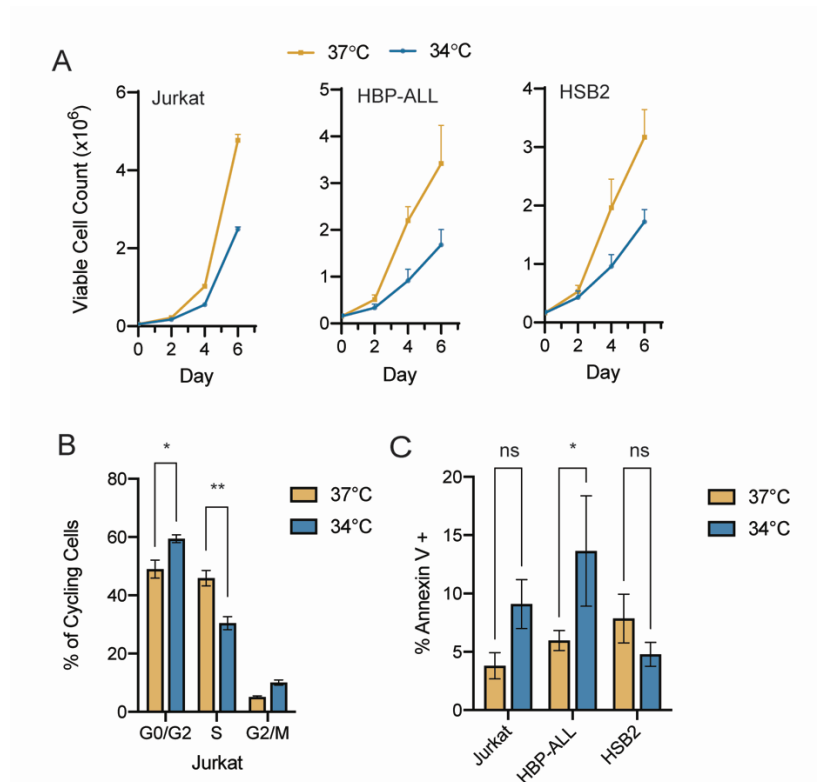


**Figure 6.6 Effect of Temperature on Cancer Cell Lines**

Growth curves of three human leukemia cell lines (Jurkat, HBP-ALL and HSB2) at 34 (blue) and 37°C (yellow). Data represents an average of 3 biological replicates with at least n=3 technical replicates per experiment. (B) Percent of Jurkat cells in each phase of the cell cycle determined by EdU uptake at 34°C and 37°C. (C) Percent apoptosis in three human leukemia cell lines determined by Annexin V staining at 34°C and 37°C. Data for EdU and Annexin staining represents an average of n=3 replicates done per temperature and \*\* p-value <0.01, \* p-value <0.05.

Finally, I evaluated how metabolic activity changed in leukemia cell lines grown in sub-optimal temperatures. Jurkat cells cultured at 34 and 37°C were prepped and analyzed in triplicate for metabolites via mass spectrometry. This data showed minor changes in metabolites in the glycolysis pathway with variation in temperature (**Figure 6.7B**). Interestingly, cells maintained at 34 and 37°C clustered independently by principal component analysis (PCA) based on relative abundance of metabolites (**Figure 6.7C**). I also used the Agilent Seahorse Xfe96 to further compare metabolism changes in Jurkat and HSB2 cells maintained at 34 and 37°C. Cells were plated in Cell-Tak coated plates and assayed for mitochondrial stress and glycolytic rate. This data showed that at 34°C there is a significant increase in ATP production rate and coupling efficiency in both cell lines compared to 37°C (**Figure 6.7D and E**). Again, these metabolic changes in mammalian cells maintained at non-physiologic temperatures may have an impact on results of drug screening or cancer cell engraftment or behavior in zebrafish xenograft models.

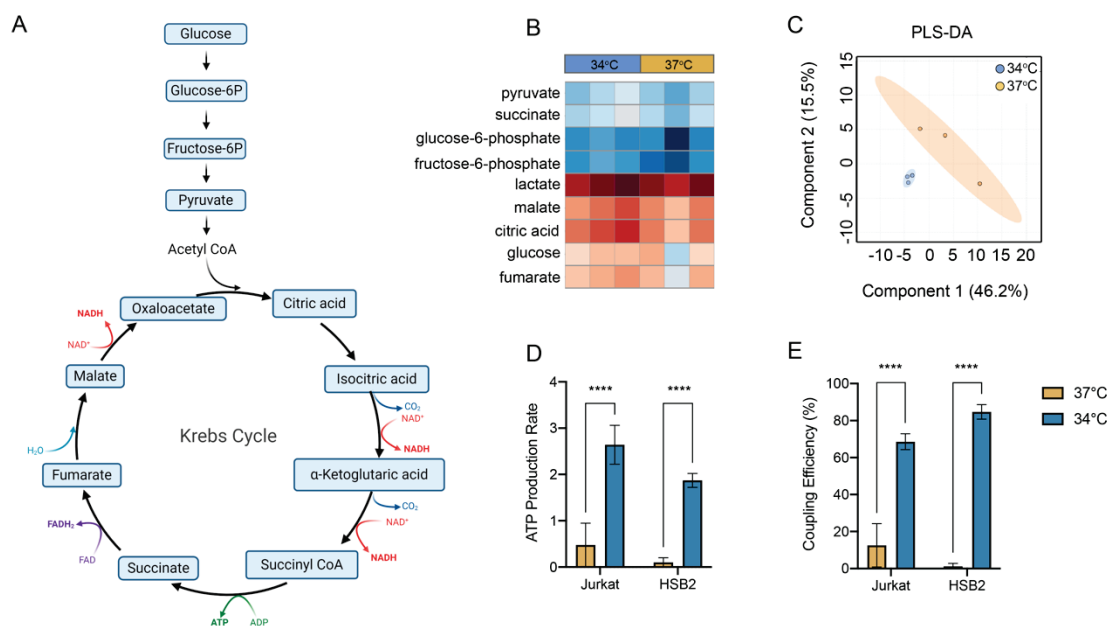


**Figure 6.7 Temperature Affects Mammalian Cell Metabolism**  
 (A) Schematic of Krebs cycle. (B) Heat map of relative abundance of Krebs cycle metabolites present in Jurkat cells grown at 34 or 37°C quantified by GC-MS. n=3 independent replicates were done for each temperature. Data was normalized to L-norvaline standard and adjusted to protein input. (C) PLS-DA showing Jurkat cells grown at 34°C cluster independently from those grown at 37°C based on metabolites present. Seahorse analysis performed on Jurkat and HSB2 cells shows an increase in ATP production rate (D) and coupling efficiency (E) at 34°C compared to 37°C. Data represents average of >10 replicates per group with error bars representing standard deviation and \*\*\*\* p-value <0.0001.

## 6.2.4 Primary Patient Samples Can Be Xenografted into Larval Zebrafish

After optimization of injection site, temperature, and cell number, I optimized a workflow for xenografting of patient samples for performing high-throughput drug screening with automated imaging. Zebrafish were xenografted in the yolk and pericardium with primary patient peripheral blood mononuclear cells (PBMCs) that were originally isolated from a T-cell Acute Lymphoblastic Leukemia (T-ALL) patient at diagnosis and banked as a viable, frozen sample. At 48 hpi, xenografted fish were screened for

fluorescently labeled tumor cells (**Figure 6.8**) and treated with chemotherapy (dexamethasone or vincristine) or DMSO. Fish were imaged at 7 dpi, after 3 days on drug treatment using a fluorescence microscope equipped imaging unit and automated sampler unit (**Figure 6.9**).

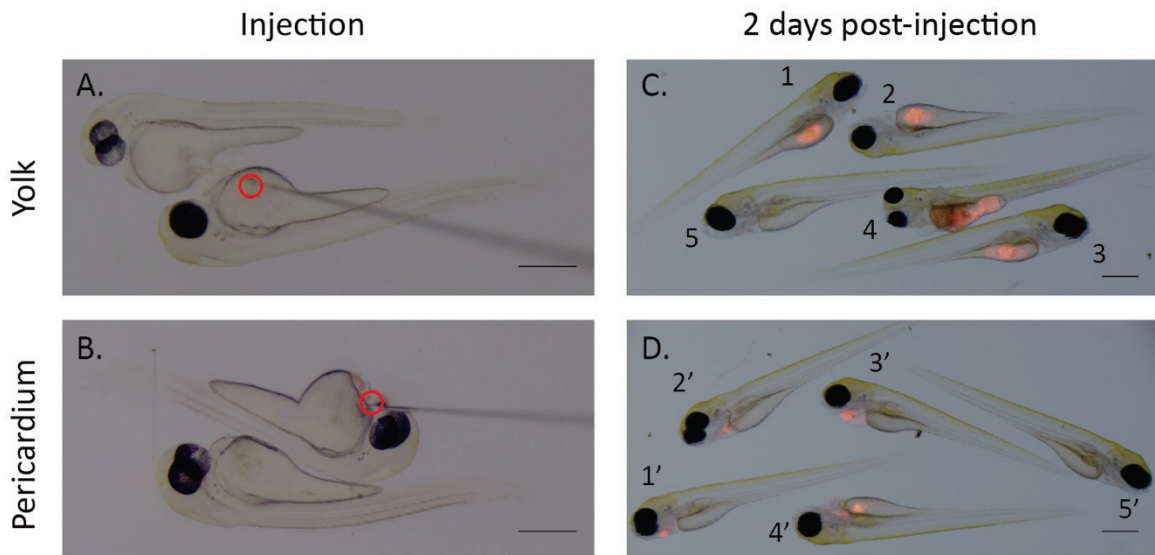


**Figure 6.8 Injection Site and Representative Images of Screening Xenografted Fish**  
Images of microinjector needle at time of injection into either the yolk (A) or pericardium (B) of 2 dpf zebrafish larvae. Representative images of screening at 2 dpi depict selection of zebrafish for drug screen (C and D). Zebrafish with similar engraftment (1-3 and 1'-3') should be selected, un-engrafted zebrafish (5 and 5') should be removed. For yolk injected fish, remove fish where borders of the yolk cannot be seen around engrafted cell mass (4) as it makes quantification difficult. For pericardium injected fish, remove fish where injected cell mass encroaches into yolk sac (4'). Scale bars represent 0.5 mm.

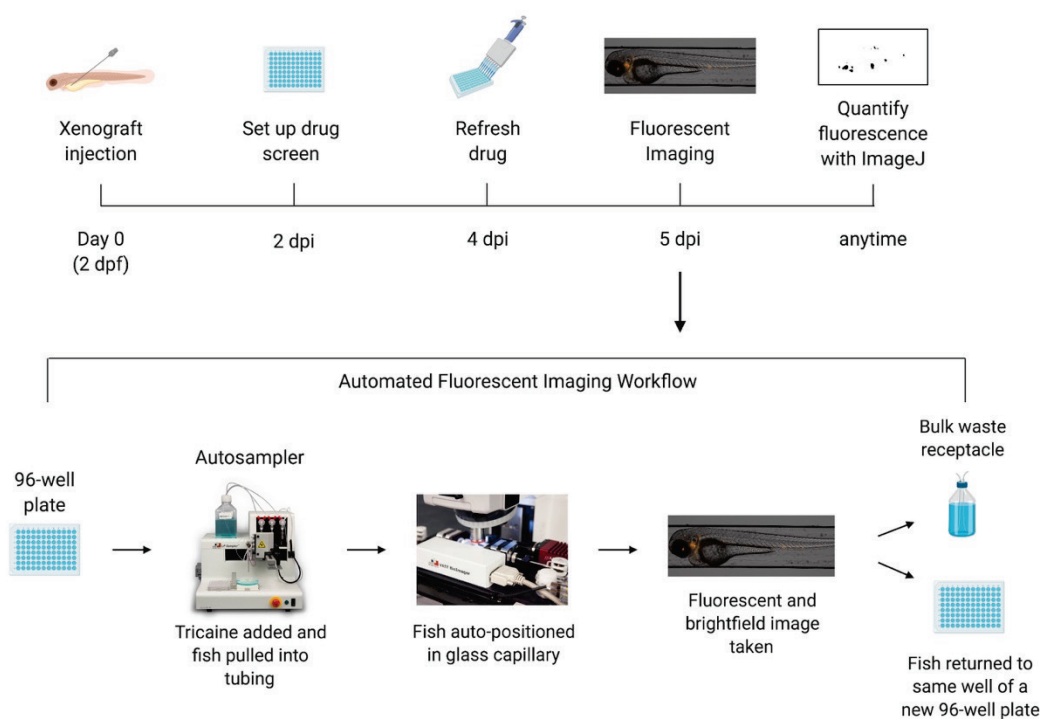


**Figure 6.9 Xenograft Drug Screen and Imaging Workflow**

Schematic of workflow of xenografting zebrafish larvae and performing drug screen, including imaging on a fluorescence microscope equipped imaging unit and automated sampler unit.

The fluorescent area/tumor burden was measured for each fish imaged using ImageJ and compared between the different drug treatment groups and DMSO (**Figure 6.10A**). Overall, xenografted fish treated with vincristine showed the largest and most consistent decrease in xenografted cell mass compared to DMSO treated fish. Dexamethasone treated fish showed about half the reduction in tumor area compared to vincristine, but still showed a reduction in tumor area compared to DMSO (**Figure 6.10B**). This mimicked what was seen in the patient, as their leukemia rapidly responded to therapy with a combination of dexamethasone and vincristine. These results demonstrate the ability of zebrafish xenograft models to be amenable to drug screening and automated imaging

and quantification, providing a platform for testing various patient samples or cell lines with different drugs or drug combinations.

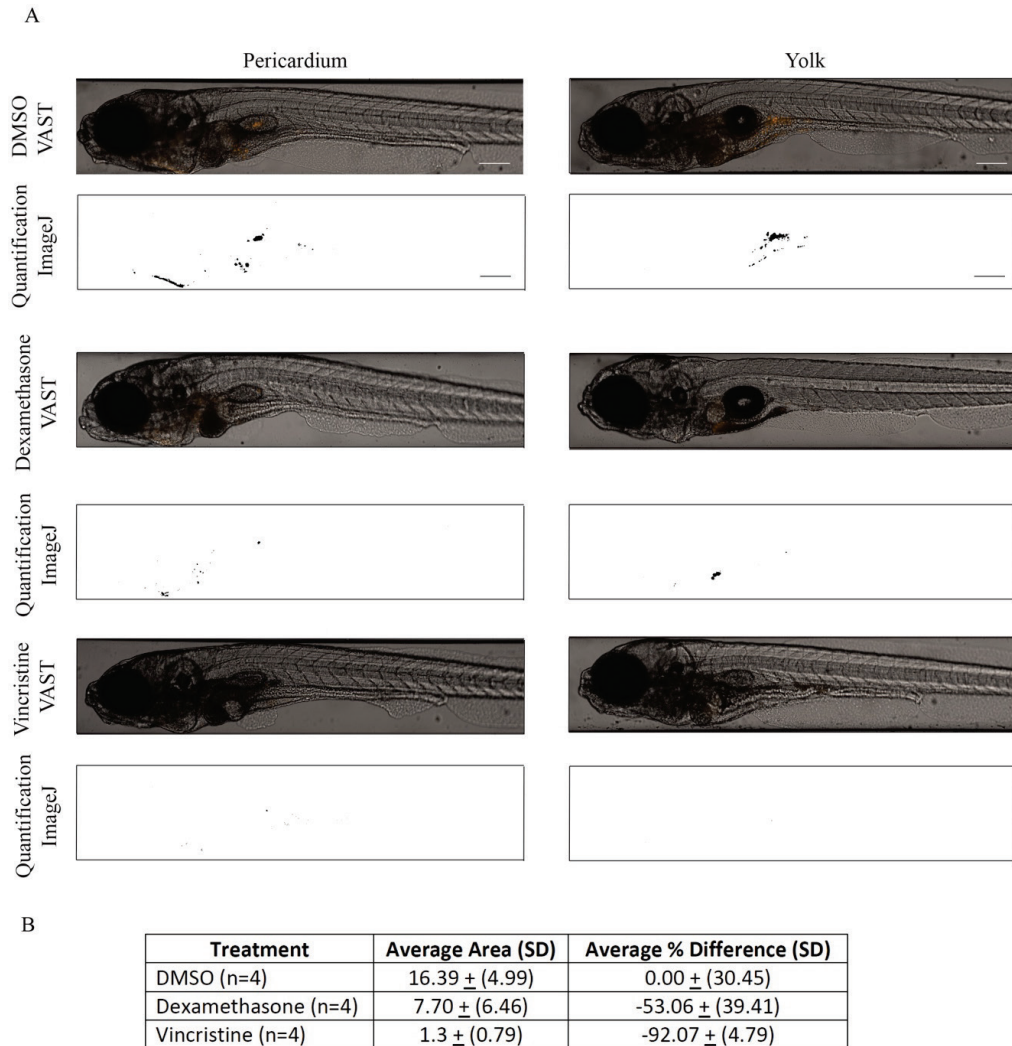


**Figure 6.10 Drug Treatment Can Reduce Xenografted Tumor Area In Vivo**  
 Representative images of zebrafish injected in the pericardium or yolk after 3 days of treatment with DMSO or drugs, either vincristine or dexamethasone. Area of engrafted tumor mass was quantified by setting a fluorescence threshold using ImageJ, selecting all pixels above the set threshold, and measuring the area and mean fluorescence of the selected regions. Pixels above the selected threshold appear in black, while pixels below the threshold appear in white. Pixels were measured in both the yolk and pericardium injected zebrafish images (A). Treatment with vincristine led to a decrease in engrafted tumor area compared to DMSO control with n=4 fish treated per group (B). SD = standard deviation. Scale bar represents 250  $\mu$ m.

### **6.2.5 Zebrafish Xenograft Model Shows Inconsistencies in Drug Screening of Cell Lines**

In order to perform high-throughput, large scale drug screens on patient samples, cells are stained with membrane-labeling dyes so their response to drug can be visualized after engraftment. I followed a staining protocol used by many other zebrafish labs<sup>244</sup> utilizing Vybrant DiI Cell-Labeling Solution to stain human leukemia cell lines before xenografting. However, I noticed these cell lines were not consistently responding to a range of drug treatments as expected and cell masses were not disappearing despite treatment with high-dose chemotherapy that they should have been responding to. I performed Annexin and EdU staining of cells immediately after DiI staining, before injection into the zebrafish, and found that the cells were still actively proliferating and not undergoing apoptosis at an abnormally high rate (data not shown). I performed BrdU staining on DiI stained cells engrafted into zebrafish and we imaged with confocal microscopy to quantify cell proliferation, finding that DiI stained cells were not actively proliferating at all in the yolk. There was inconsistent and infrequent proliferation occurring in cells xenografted into the pericardium at 37°C and almost no proliferation seen in the pericardium at 34°C (**Figure 6.11**). Furthermore, there was a large amount of DiI labeled debris present and many fish did not have discernable nuclei present in engrafted cells, despite appearing as if cells were engrafted normally by DiI fluorescence.

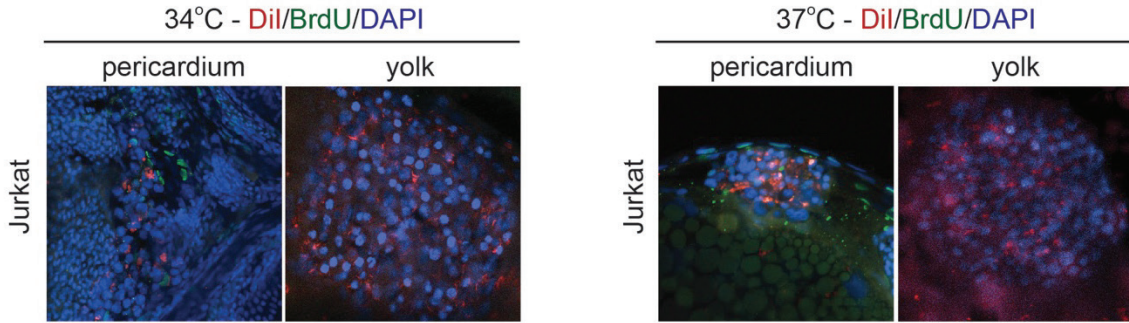


**Figure 6.11 BrdU Staining of DiI Stained Cell Lines**

BrdU staining for proliferation of DiI stained Jurkat leukemia cells xenografted into the pericardium or yolk of larval zebrafish and kept at 34 or 37°C.

Due to the unexpected appearance and behavior of DiI stained cells, I injected zebrafish with GFP-labeled human leukemia cell lines (Jurkat or HSB2) and performed BrdU and TUNEL staining to quantify proliferation and apoptosis, respectively, of engrafted cells. I found that in some cell lines (HSB2) xenografted into the pericardium there is more proliferation occurring at 37°C than there is at 34°C, while in other cell lines (Jurkat) there is a decrease in proliferation at 37°C compared to 34°C (**Figure 6.12**). Similar to the DiI stained cells, I saw virtually no proliferation occurring in cell lines xenografted into the yolk at either temperature. There was also significantly less apoptosis in Jurkat cells engrafted into the pericardium at 37°C compared to 34°C but no significant change in apoptosis of HSB2 cells xenografted into the pericardium between the two temperatures. Finally, there was also a lack of apoptosis seen in cells xenografted into the yolk at either temperature, meaning these cells are not actively dividing or undergoing apoptosis (**Figure 6.12**). This demonstrates that cells do not grow and thrive equally when they are maintained at 34°C compared to their physiologic temperatures, which is required to increase survival and decrease stress on zebrafish larvae.



(light bar) at 34°C (blue) or 37°C (yellow) showing a significant decrease in apoptosis when xenografted fish were kept at 37°C compared to 34°C and a lack of apoptosis occurring in yolk engrafted cells. \*\* p-value <0.01.

Another major consideration with xenograft models in zebrafish is the difference in effectiveness of drug at different temperatures. Since drugs are designed to work on human cells, they are developed and tested at 37°C and their effectiveness at non-physiologic temperatures is not normally studied. To determine if cellular response to drug treatment changes at different temperatures I treated Jurkat and HSB2 cells with four different chemotherapies (Cytarabine, Dexamethasone, Methotrexate or Vincristine) for 72 hours at 34 and 37°C and quantified cell viability by Cell Titer Glo. Here, I found that Jurkat cells were more resistant to Methotrexate at 34°C compared to 37°C and the opposite pattern was seen for Dexamethasone, with increased resistance at 37°C compared to 34°C. While the dose response curves for some drugs were drastically different between temperatures in Jurkat cells, temperature showed little effect on the effectiveness of other drugs: Cytarabine and Vincristine (**Figure 6.13A**). Furthermore, in another human leukemia cell line, HSB2, there was very little difference in dose response curves of any of the chemotherapies tested between temperatures (**Figure 6.13B**). This highlights the possibility that drugs may have varying effectiveness in different cell lines at temperatures outside physiologic temperatures at which they were designed to work at.

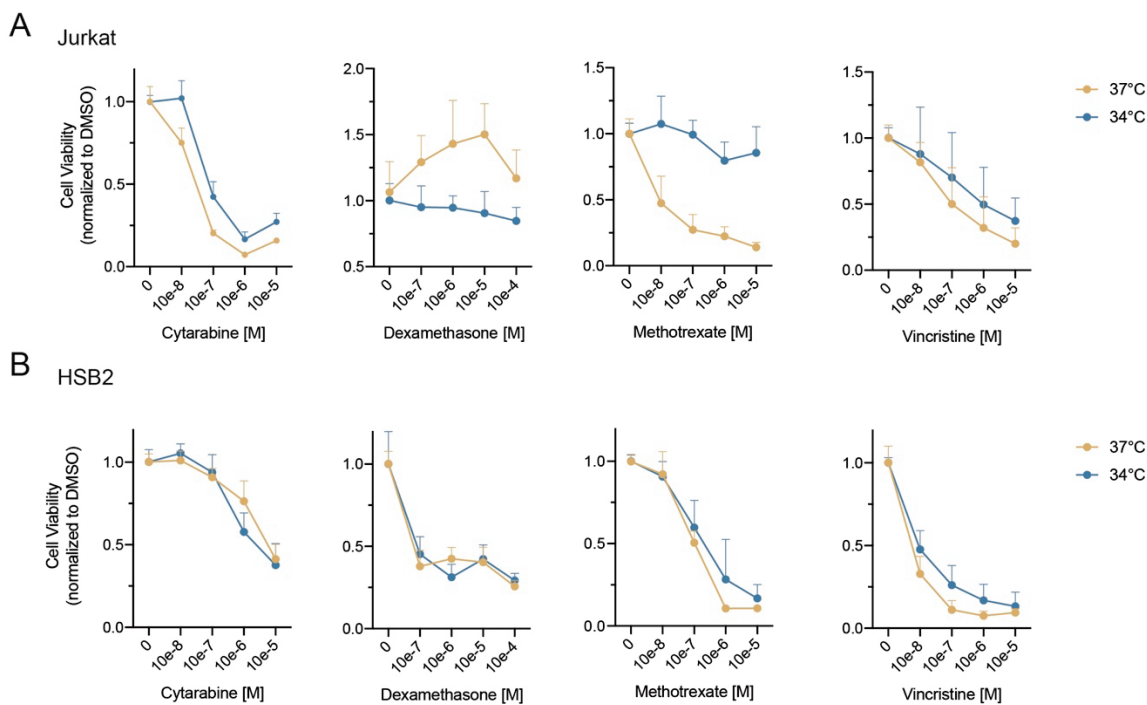


**Figure 6.13 Temperature Affects Response of Mammalian Cell Lines to Drug Treatment** Jurkat (A) and HSB2 (C) human leukemia cell lines were cultured at 34 (blue) or 37°C (yellow) and treated with increasing concentrations of the following drugs: Cytarabine, Dexamethasone, Methotrexate, or Vincristine. Cell viability was measured by CellTiter-Glo after 72 hours of drug treatment and normalized to DMSO vehicle control. Experiments were performed in triplicate with n=3 replicates per experiment. Error bars represent standard deviation.

Zebrafish are a widely accepted model for performing large scale drug toxicity and efficacy screens<sup>240,241,243</sup>. However, the pharmacokinetics of drug uptake into zebrafish larvae has not been well characterized. With this being said, it is not well known how engraftment of mammalian cell lines into different anatomical locations in zebrafish larvae will affect consistency of drug screen results. I xenografted GFP-expressing Jurkat cells into the pericardium and yolk of zebrafish larvae at 2 dpf and then subjected them to drug treatment with Dexamethasone or Vincristine for 48 hours starting at 1 dpt at 34 or 37°C. After drug treatment, larvae were fixed and TUNEL staining was done to quantify the

amount of apoptosis induced by drug treatment as a readout of drug response. I found that in the pericardium xenografted cells, TUNEL + staining was not observed in the DMSO or Dexamethasone treated cells at either temperature. However, Dexamethasone did induce apoptosis in yolk xenografted cells in one larval zebrafish at 34°C and two at 37°C. Vincristine induced some apoptosis in pericardium xenografted cells at 34°C and even more at 37°C, however failed to induce any apoptosis in yolk xenografted cells at 34°C and only induced apoptosis in cells from two yolk xenografted zebrafish larvae at 37°C (**Figure 6.14**). These inconsistencies seen in response of xenografted cells to drug treatment with variations in injection site or temperature the larval fish are maintained for the duration of the drug screen pose major challenges for implementation of zebrafish as a reliable model for mammalian cell xenografting and large scale drug screening.

Jurkat PGK:GFP

TUNEL

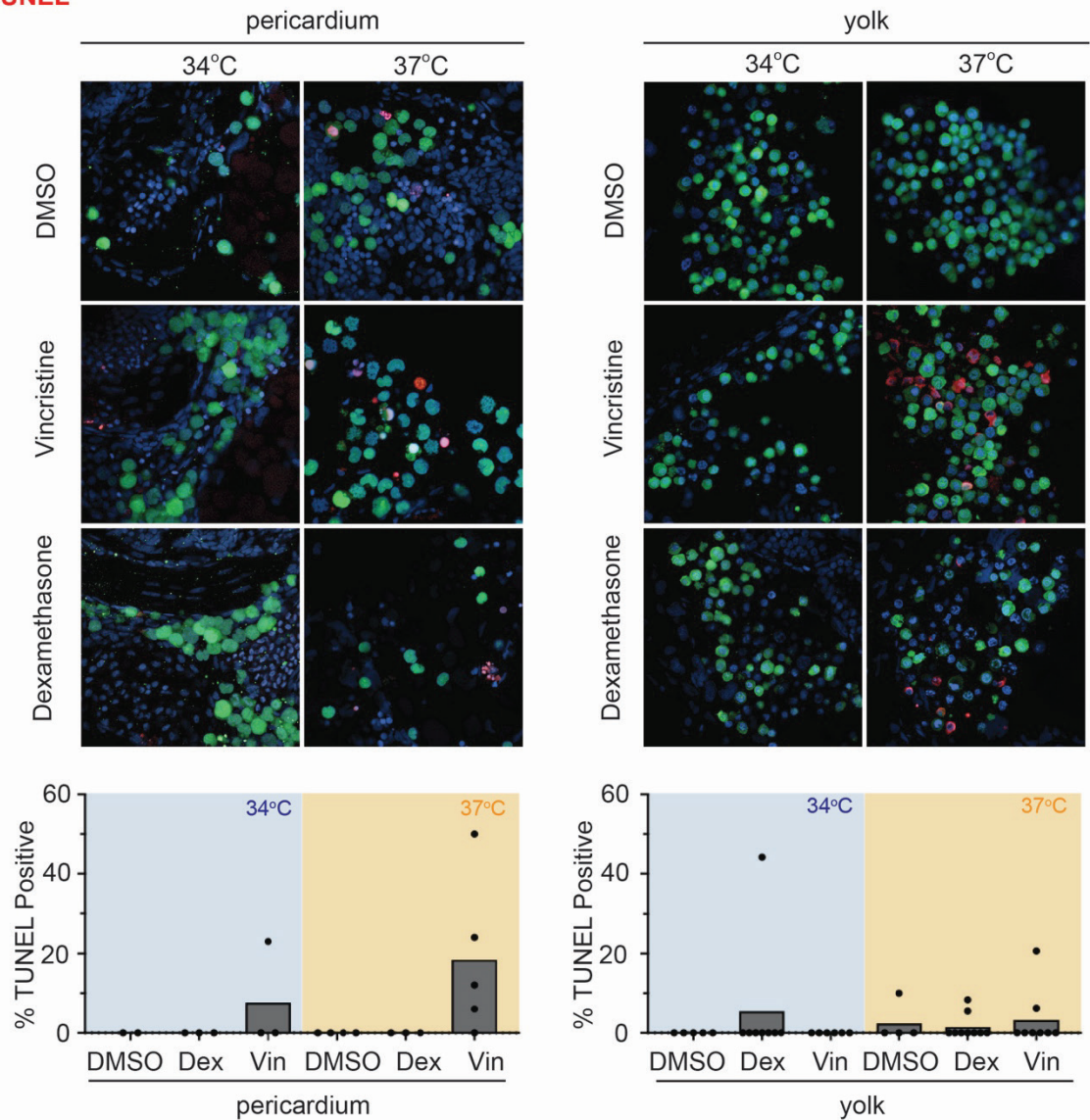


**Figure 6.14 Drug Treatment Produces Inconsistent Results with Variations in Xenograft Site or Temperature**

GFP expressing Jurkat cells were xenografted into the pericardium or yolk of zebrafish larvae and subjected to drug treatment with 10 $\mu$ M Dexamethasone, Vincristine, or DMSO vehicle control for 2 days post-injection (dpi) at 34 or 37°C. Drug-treated larvae were then fixed and stained with TUNEL for apoptosis. Percent TUNEL positive xenografted cells were quantified for each group, showing inconsistent responses of xenografted cells to drug treatment with changes in injection site or temperature.

### 6.3 Discussion

Although zebrafish are a robust model, their application for xenografts is relatively new. As with all novel applications, certain challenges and barriers must be addressed and overcome before that technology can move from seldom to widespread use. I set out to resolve some of the irregularities and incongruities currently in place for this model such as; lack of agreement for optimal injections sites and holding temperatures and shortage of data on metabolic and physiologic behavior of both host and xenografted cells post-transplant.

I first optimized injection sites and conditions, finding that the yolk and pericardium produced the most consistent engraftment and survival of engrafted zebrafish larvae while still being time efficient and practical for large scale applications. I also demonstrated a standardized method for thawing and injection of primary patient leukemia cells into zebrafish as a xenograft model and established a protocol for high-throughput drug screening of xenografted zebrafish using a fluorescence microscope equipped imaging unit and automated sampler unit. Although this approach is more automated and efficient than previously reported workflows, this is still a labor-intensive and technically challenging protocol for anyone without prior experience in microinjecting zebrafish.

The variation in response of xenografted mammalian cells to drug with changes in injection site or housing temperature is a major barrier to widespread acceptability of the use of zebrafish as a xenograft model. FDA-approved drugs have undergone all of their *in vitro*, pre-clinical, and clinical testing at mammalian body temperature of 37°C. It is possible that these drugs do not have optimal stability or do not perform optimally at 34°C as well and this should be taken into consideration when preparing for drug screening.

Additionally, although I found both fish and mammalian cells can be maintained at 34°C without much effect on their survival, I did find that metabolic effects of growing both zebrafish and cancer cells at non-physiologic temperatures are not insignificant.

Despite the above caveats, zebrafish xenografts can be a useful bridge between *in vitro* cell culture and mouse xenograft models. They allow researchers to assess whole animal response to small molecules of interest, while still being more cost-efficient than mice for larger scale *in vivo* drug screens. Additionally, zebrafish xenografts require far fewer cells for injection than mouse models, so a small amount of patient sample can be spread amongst hundreds to thousands of zebrafish, allowing for drug screens with large sample numbers. With fluorescent labeling, tumor cells can be monitored from the moment they are xenografted into the larval zebrafish, providing some standardization between the animals used in drug screens.

Overall, I developed a pipeline for xenografting primary patient leukemia samples into larval xenografts and performing automated drug screening and analysis. While there were challenges that arose with drug screening of leukemia cell lines, in primary patient samples I saw results that were more consistent with what was seen in the patient tumor, with resistance to one drug and sensitivity to another. This opens the doors for being able to take primary cancer cells, xenograft them into zebrafish larvae, and study response to treatment, identifying cell populations that may be resistant to certain types of chemotherapy or targeted therapies with potential for relapse in patients.

## **6.4 Methods**

### **6.4.1 IRB/Collection of Patient Samples**

Patient samples were collected under University of Kentucky's Institutional Review Board (protocol 44672). Patient Bone Marrow Aspirate (BMA) and peripheral blood samples were collected and diluted with an equal volume of room temperature 2% FBS in PBS. The sample was slowly added to a 50mL Sepmate tube (cat. # 85450), containing 15mL of Ficol Density gradient, centrifuged at 1,200xg for 10 mins and the top layer was quickly poured into a new 50mL tube. The volume was brought up to 50mL with RPMI and spun for 15 mins at 1,400 rpm at 4°C. Cells were counted and then washed in 50mL of RPMI and centrifuged for 10 mins at 1,400 rpm at 4°C. The supernatant was removed, and cells were resuspended in 1mL of RPMI + 10% FBS + 10% DMSO per 10<sup>7</sup> cells and added to a cryovial for storage at -80°C.

### **6.4.2 Cell Line Experiments**

All cells were cultured at 37°C in a humidified atmosphere with 5% CO<sub>2</sub>. Cell lines were authenticated by short tandem repeat (STR) DNA profiling and tested for mycoplasma contamination prior to experimentation. T-cell acute lymphoblastic leukemia (Jurkat) cells were grown in RPMI 1640 (ThermoFisher 11875119) supplemented with 10% heat-inactivated fetal bovine serum (FBS) (Atlanta Biologicals, S11150H, Lot M17161, Flowery Branch, GA, USA).

For temperature experiments, cells at 60% confluency were incubated at either 28°C, 34°C, or 37°C in a humidified atmosphere with 5% CO<sub>2</sub> for 24 hours before samples were prepared for mass spectrometry analysis.

For cell growth assay, cells were counted on a Vi-Cell XR cell viability analyzer (Beckman Coulter) and 50,000 cells were plated per well of a 12 well plate in triplicate wells. Cells were incubated at either 28°C, 34°C, or 37°C in a humidified atmosphere with 5% CO<sub>2</sub> for 72 hours. Viable cells were counted on the Vi-Cell XR cell viability analyzer at days 1, 3 and 5 after plating.

To determine IC<sub>50</sub> of the drugs for T-ALL cells at 37°C and 34°C, 50 µL of HBPALL/HSB2 (2×10<sup>5</sup> cells/ml) or Jurkat (1×10<sup>5</sup> cells) were seeded in triplicate wells and then 50 µL of 2X drug solution diluted in cell culture medium or DMSO control was added to corresponding well. Then the cells were cultured at 37°C or 34°C in a humidified atmosphere with 5% CO<sub>2</sub> for 72 hours. CellTiter-Glo Luminescent Cell Viability Assay (Promega, G7570) was used to measure cell survival according to the manufacturer's instructions. A Synergy LX BioTek multi-mode plate reader was used to read luminescent signal.

To compare apoptosis of T-ALL cells at 37°C and 34°C, 500 µL of HBPALL/HSB2 (1×10<sup>5</sup> cells/ml) or Jurkat (5×10<sup>4</sup> cells) cells were seeded in the 24-well cell culture plate and then cultured at 37°C or 34°C in a humidified atmosphere with 5% CO<sub>2</sub> for 72 hours. The cells were harvested and apoptosis was quantified by staining cells with Annexin V APC (ThermoFisher 88-8007-74) according to the manufacturers protocol in the presence of DAPI (0.05µg/ml).

### **6.4.3 Xenograft Experiments**

Prior to cell staining, cells were counted using a Countess® Automated Cell Counter (Invitrogen # C10227). Cells were stained immediately prior to injection using

Vybrant DiI Cell-Labeling Solution (Invitrogen #V22885). DiI was diluted to a final concentration of 4 $\mu$ g/mL in 5mL room-temperature, 1X phosphate-buffered saline (PBS, Caisson Labs #PBL06-6X500ML). Cells were centrifuged at 1200 rpm for 5minutes, resuspended in the 5mL DiI + 1X PBS solution, incubated at 37°C for 10 minutes in the dark, then washed 3x using 5mL of a RPMI + 10% FBS solution that was pre-warmed to 37°C, with centrifugation at 1200 rpm for 5 minutes for each wash. Finally, the stained cells were resuspended in the pre-warmed RPMI + 10% FBS solution to a concentration that would deliver 500 cells in a 2nL injection volume. For cell number studies, cells were resuspended at varying concentrations to deliver 100, 250, 500or 1,000 cells per 2nL injection volume.

Zebrafish larvae were manually dechorionated with forceps at 48 hours post-fertilization (hpf) prior to injection. Injections for all cancer cell types were performed using non-filament borosilicate glass capillaries (Sutter Instrument Company #B100-50-10). Capillaries were heated and pulled into needlepoints using a Flaming/Brown micropipette puller (Sutter Instrument #P-87). Needlepoints were cut to a bevel using a sterile razor. Droplet size was measured to 2nL (~.15mm diameter) using a micrometer and kept at a constant volume throughout injection. Xenograft injections were performed using an air-pressure driven system as previously described in Haney et al, 2020 <sup>247</sup>. Post-injection, embryos were kept in 1X E3 media and incubated at 28°C for a 1-hour recovery time then moved to either 34°C or 37°C. Fish were anesthetized prior to microinjection using 4mg/mL Tricaine-S (Pentair Aquatic #NC0342409). If clumping of cells in the needle occurred, stained cells were pushed through a sterile 40 $\mu$ m cell strainer and needles were chilled on ice prior to loading with cells.

Embryos were screened at 1, 3, and 5 days post injection (dpi) for survival studies. Initial screening for cancer cell engraftment was performed using a Nikon SMZ18 fluorescence microscope. Dead embryos and embryos without engrafted cancer cells were removed.

#### **6.4.4 Zebrafish Immunofluorescence and Imaging Experiments**

For TUNEL staining, embryos were fixed in 4% PFA overnight followed by graded MeOH fixation. Fixed embryos were rehydrated back to PBS and permeabilized in 0.1% Sodium Citrate, 0.1% TritonX, 20ug/ml ProteinaseK for 30 min at room temperature then washed extensively in PBS. TUNEL solution was mixed as per manufacturer's interactions using either the TMR or Fluorescein kit (SIGMA cat# 11684795910 and 12156792910) and added to embryos for 1hr in the dark followed by five PBS washes and staining with 1:1000 Hoechst 33342 (Thermo #H3570).

For BrdU staining, embryos were treated with 10mM BrdU for 24hrs post xenograft followed by fixation in 4% PFA and gradual dehydration to 100% Methanol. After rehydrating back to PBS tissues were permeabilized in 20ug/ml Proteinase K solution for 1hr and denatured in 2N HCl for 1hr. Blocking was done in 2% BSA. Anti-BrdU (BD cat#A11001) at 1:200 with a mixture of 1:1000 Hoechst stain.

All imaging was carried out on the A1 inverted confocal using NIS elements software. Embryos were mounted and cover slipped on glass slides in 3% Methylcellulose. All exposure settings were first adjusted to negative controls.

#### **6.4.5 Thawing of Patient Samples**

Primary patient samples were gradually warmed to 37°C in a 37°C water bath until a small ice pellet remained. Thaw media (25% FBS in IMDM) pre-warmed to 37°C was added drop-wise and the volume brought to 10 mL in a 15 mL conical tube (approximately 2–3 seconds per ml). Cells were centrifuged at 1,000 rpm for 10 minutes and media was aspirated. Addition of thaw media, centrifugation and aspiration was repeated again to remove residual DMSO. Cells were washed once in PBS and counted.

#### **6.4.6 Drug Screening**

For drug screen with panel of different chemotherapies, xenografted larvae that were injected with either Jurkat or HSB2 cells were screened for consistent cell engraftment then treated with DMSO (Sigma-Aldrich, D8418-50ML) control or the following drugs all at a 10uM concentration in E3 media: Cytarabine (Selleck Chemicals, S1648), Cyclophosphamide (Sigma-Aldrich, PHR1404-1G), Dexamethasone (VWR, 89157-624), Doxorubicin (Selleck Chemicals, S1208), Methotrexate (Sigma-Aldrich, A6770-10MG), and Vincristine (Selleck Chemicals, S1241). This drug screen was setup as described in Haney et al<sup>247</sup> with the only differences being that, in this experiment, drug treatment began at 24 hours post injection (hpi) with the total treatment lasting 48 hours.

For maximum tolerated dose experiments, zebrafish larvae were injected with either Jurkat or HSB2 cells at 2dpf and were screened for consistent cell engraftment at 24 hpi before treatment. Larvae were treated with either Dexamethasone or Vincristine at 24 hpi at 0uM (DMSO control), 10uM, 25uM, 50uM, and 100uM concentrations in E3 media. Larvae were treated for 48 hours before imaging. All DMSO and drug-treated fish were

imaged at 72hpi, after 48 hours of drug treatment using the VAST BioImager (Union Biometrica)<sup>234,235</sup>.

#### **6.4.7 Metabolism Experiments**

For temperature studies, zebrafish were manually dechorionated at 2 dpf and placed at either 28°C, 34°C, or 37°C with 30 embryos per 10 cm<sup>2</sup> dish in E3 media for 24 hours. After 24 hours, zebrafish were sacrificed by putting on ice, collected, and processed for MS analysis as described below. For drug metabolism studies, zebrafish larvae at 4 dpf were treated with either 25 µM vincristine or 10 µM dexamethasone in E3 media in 10 cm<sup>2</sup> dishes with 30 embryos per dish for 48 hours at 34°C. A total of about 100 mg of tissue was needed for metabolomic analysis which required about 120 zebrafish larvae per sample, with each sample done in triplicate. After 48 hours, zebrafish were sacrificed by putting on ice, collected, and processed for MS analysis as described below.

Zebrafish larvae were collected into 1.5 mL tubes, the E3 media was removed, and fish were washed with 1 mL of ice-cold PBS+4%BSA to wash. To de-yolk zebrafish, fish were pipetted up and down with a P200 pipette tip approximately 20 times in 200 µL of ice-cold PBS+4%BSA until yolks were removed and supernatant was cloudy. The supernatant was then removed and fish were washed 2 more times with 1 mL of ice-cold PBS+4%BSA. A quick spin was done to pellet larvae, all supernatant was removed using a Kim wipe or q-tip to dry the inside of the tube and samples were flash frozen in liquid nitrogen.

Fish pellets were removed from cryostorage and transferred to a microvial set (6757) for a Freezer/Mill Cryogenic Grinder (SPEX SamplePrep model 6875D). Fish were

pulverized to pulverized to 5  $\mu\text{m}$  particles. Metabolites were extracted directly from the microvial by the addition of 1ml of 50% methanol containing 20 $\mu\text{M}$  L-norvaline (procedural, internal control) and separated into polar (aqueous layer) and insoluble pellet (protein/DNA/RNA/glycogen) by centrifugation at 4°C, 15,000rpm for 10 minutes. The pellet was subsequently washed four times with 50% methanol and once with 100% methanol to remove polar contaminants. The polar fraction was dried at 10-3 mBar using a SpeedVac (Thermo) followed by derivatization. The insoluble pellet was hydrolyzed similar to the technique described in Andres et al., 2020<sup>254</sup>.

Dried polar and insoluble samples were derivatized by the addition of 20mg/ml methoxyamine hydrochloride in pyridine and incubated for 1.5hrs at 30°C. Sequential addition of N-methyl-trimethylsilyl-trifluoroacetamide (MSTFA) followed with an incubation time of 30 minutes at 37°C with thorough mixing between addition of solvents. The mixture was then transferred to a v-shaped amber glass chromatography vial and analyzed by GCMS.

An Agilent 7800B gas-chromatography coupled to a 5977B mass spectrometry (GCMS) detector was used for this study. GCMS protocols were similar to those described previously<sup>255,256</sup> except a modified temperature gradient was used for GC: Initial temperature was 130°C, held for 4 minutes, rising at 6°C/minutes to 243°C, rising at 60°C/minutes to 280°C, held for 2 minutes. The electron ionization (EI) energy was set to 70 eV. Scan (m/z:50-800) and full scan mode were used for metabolomics analysis. Mass spectra were translated to relative metabolite abundance using the Automated Mass Spectral Deconvolution and Identification System (AMDIS) software matched to the FiehnLib metabolomics library (available through Agilent) for retention time and

fragmentation pattern matching<sup>256,257</sup>. Quantitation was performed using the software Data Extraction for Stable Isotope-labelled metabolites (DExSI)<sup>258</sup>. Relative abundance was corrected for recovery using the L-norvaline standard and adjusted to protein input.

#### **6.4.8 Seahorse Experiments**

Cells were cultured overnight at 34°C or 37°C in a humidified atmosphere with 5% CO<sub>2</sub>. Seahorse Xfe96 PDL Miniplate was coated fresh with Cell-Tak Cell and Tissue Adhesive (Corning, Cat # 354240) at a dilution factor of 79.5 in 0.1M sodium bicarbonate and washed twice with distilled water. This coating and wash process was repeated a second time. Cells were then plated at a cell density of 70,000 cells/well for Jurkat cells or 100,000 cells/well for HSB2 cells in RPMI 1640 supplemented with 10% heat-inactivated FBS, allowed to incubate for 5 minutes at room temperature, and spun down at 200xg for 1 minute with zero brake. The plate was then incubated at 34°C or 37°C for 30 mins before media was replaced with assay media (below).

All OCR and ECAR analyses were performed with a minimum of 6–8 technical replicates for each treatment or assay. All cells were incubated for 60 min in a non-CO<sub>2</sub> incubator before plate calibration was performed and mitochondria and glycolytic rate test experiments were initiated at corresponding temperature conditions.

The Seahorse XFe96 (Agilent Technologies) was used to measure oxygen consumption rates (OCR) or extracellular acidification rates (ECAR) of cells. One hour prior to assay, growth media was replaced with XF RPMI assay media supplemented with 2mM L-glutamine, 1mM pyruvate, and 10mM glucose (assay media and all supplements from Agilent Technologies). Cells were then placed in the non-CO<sub>2</sub>, 34°C or 37°C Bioteck

Cytation 1 for degassing and brightfield image scanning. The Seahorse XFe96 sensor cartridge was calibrated and the degassed microplate was then placed in the Seahorse XFe96. For mitochondrial stress assays baseline OCR and ECAR measurements were followed by acute injections of oligomycin (1 $\mu$ M), FCCP (0.6 $\mu$ M), and a combination of antimycin A (1 $\mu$ M) and rotenone (1 $\mu$ M). For glycolytic rate assays baseline PER measurements were followed by acute injections of a combination of antimycin A (1 $\mu$ M) and rotenone (1 $\mu$ M) followed by 50mM 2DG. The Seahorse data was viewed with Wave 2.6.0.

#### **6.4.9 Statistical Analysis**

Statistical analyses were carried out using GraphPad Prism. One-way ANOVA with Tukey's test for comparison of means was used for comparison of day 5 values of % survival and cell growth studies. All metabolic numerical data are presented as mean  $\pm$  SE. A P-value less than 0.05 using a student t-test was considered statistically significant. Clustering heatmap and partial least squares discriminant analysis (PLS-DA) were performed using the MetaboAnalyst package for R (available through MetaboAnalyst, <https://www.metaboanalyst.ca/>)<sup>257,259</sup>. For PLS-DA and heatmap analysis log-transformed metabolomics data were used, and unit variance scaling was employed for row numbers and SVD with imputation for PLS-DA clustering. Correlation and tightest cluster first options were used for heatmap visualization<sup>257,259</sup>. All available metabolomics data points were used for multivariate analysis.

CHAPTER 7. CIRCULATING TUMOR DNA AS A BIOMARKER IN ACUTE LYMPHOBLASTIC  
LEUKEMIA

*Partially taken from: Cell free DNA as a Biomarker to Identify Clonal IGH  
Rearrangements in Acute Lymphoblastic Leukemia using Nanopore Sequencing. Shilpa  
Sampathi, Yelena Chernyavskaya, Meghan Haney, et al. In submission to Journal of  
Clinical Oncology.*

## 7.1 Introduction

A major clinical concern when dealing with relapse is predicting which patients are more likely to relapse than others. As described above, relapse is due to leukemia stem cells that undergo self-renewal and differentiation and form a new leukemia in patients. We do not currently have good markers for determining the proportion of LSCs present in a patient's tumor to study as a potential biomarker for relapse. While determining exact LSC frequency of patient tumors is not feasible, research is ongoing to identify better predictors to stratify patients risk status and potential for relapse. Utilizing cell-free circulating tumor DNA as a biomarker in ALL has the potential to risk stratify patients and predict patient relapse better than current methods.

Despite cure rates approaching 90%, relapsed ALL remains the second leading cause of cancer related death in the pediatric population. Response to therapy as measured by the detection of minimal residual disease of  $>0.01\%$  at the end of reduction remains the most powerful prognostic indicator of outcome<sup>9</sup>. A vast majority of patients are cleared of blasts in their bone marrow and CNS during initial treatment. A subset of patients will have a positive MRD and are upstaged and receive more intensive chemotherapy and more frequent monitoring of disease progression. Patients are monitored for relapse by regular CBC and evaluation of the CSF for the presence of lymphoblasts. These methods do not detect low levels of disease and relapse in the bone marrow and CNS disease often occurs in children who are clinically cleared of blasts, measured by FACS of bone marrow and CSF, collected by biopsy and lumbar puncture, respectively. It is possible that leukemic cells remain at levels too low to be detected by standard clinical diagnostic procedures. Accurate, non-invasive methods for continuously monitoring for the presence of low level

disease may allow for interventions directed against a single chemo resistant clone. A more sensitive, less invasive assay, like quantification of ctDNA from routine blood draw, could predict the emergence of relapse and help clinicians better classify patients into a high-risk status. As the use of adoptive immunotherapy strategies expands, early identification of low levels of leukemia cells resistant to cytotoxic chemotherapy will likely become increasingly important in the search for resistant clone-specific targets.

The infrequent collection of samples to assess disease status also makes it difficult to gauge the extent of ALL response to treatment throughout therapy. While collection of bone marrow samples before and after treatment is sufficient for current care of ALL patients, this presents challenges in the development of new, more targeted therapies for ALL, which could decrease adverse side-effects seen with the current cytotoxic chemotherapy regimen. When 95% of blasts are normally cleared from the bone marrow by the end of consolidation, it is difficult to determine if a new therapy has had any effect on ALL response rate. Having a method to track disease response more frequently using ctDNA in the peripheral blood would allow detection of differences in treatment response at early stages, which may aid in the development of less toxic drugs for ALL patients.

Furthermore, chimeric antigen receptor T-cell (CAR-T) therapy is becoming increasingly popular in the field of pediatric oncology, but requires a >30 day lead time for patient specific CAR-T production. Early experiences with CAR-T therapy indicate that a higher disease burden at the time of treatment is associated with increased incidence of cytokine release syndrome and neurotoxic events<sup>260</sup>; identifying patients that need CAR-T as early as possible may reduce immunotherapy related toxicity. This outlines a critical

need for improvements in technologies that can be used to develop more sensitive and less invasive assays to assess ALL response to therapy and relapse.

### **7.1.1 Cell Free DNA Serves as a Biomarker in Cancer**

Circulating cell-free DNA (cfDNA) molecules were first identified over 50 years ago in patients' blood and have been found to be present at higher levels in patients with cancer <sup>261-263</sup>. cfDNA is currently used clinically to detect fetal diseases in pregnant mothers. Cancer cells release cell-free DNA that circulates in the blood of patients. This circulating tumor DNA (ctDNA) can be detected and quantified by digital droplet PCR (ddPCR), which is currently the most sensitive PCR system available <sup>264</sup>. ctDNA quantification is emerging as an important and sensitive biomarker of solid tumor progression and metastasis in pre-clinical testing but has not been looked at extensively in hematologic malignancies <sup>265,266</sup>.

In order to assess ctDNA, a marker must be identified that is present in the cancer cells, but not in normal cells, which has proven challenging in ALL, one of the cancers with the lowest number of mutations. All T and B cells undergo VDJ recombination to generate functional B and T cell receptors, and the specific sequence of the rearrangement in the receptor is unique to an individual B or T cell. ALL results from the abnormal expansion of typically 1-5 T or B cell clones, which can be identified based on a major expansion of that particular B and T cell receptor sequence <sup>267,268</sup>. Recent studies have shown that detection of clonal rearrangements of T- and B-cell receptors in ctDNA of a leukemia will persist in the peripheral blood longer than circulating blasts, making it a useful test for following response to treatment and determining MRD status <sup>269-271</sup>.

Importantly, in hematologic malignancies, ctDNA assays diagnosed relapse 30 days earlier than the clinical, FACS based diagnosis <sup>271</sup>.

Utilizing Next Generation Sequencing (NGS) of T- and B-cell rearrangements to monitor clonality for MRD has shown success in B-ALL <sup>272</sup>, however repeated deep sequencing via Illumina sequencing looking for reappearance of leukemic clones is time consuming and costly. The development of the MinION sequencer (Nanopore Oxford Technologies), which is a portable, real-time benchtop sequencer that is more user friendly and cost-effective than Illumina sequencing has made clonality tracking in leukemia samples more practical <sup>273</sup>. Large scale, rapid sequencing can be performed within the lab in a matter of hours, base-called, and analyzed easily via a web-based Nanopipe server <sup>274</sup>. This opens the door for clonality tracking utilizing ctDNA, which provides a more sensitive and less invasive way to closely monitor leukemia patients for response to therapy and development of relapse.

### **7.1.2 Cancer-Specific Methylation Signatures are Present in Hematologic Malignancies**

Although detection of leukemia clones from ctDNA based on T- and B-cell receptor rearrangements may prove useful in predicting relapse status, and provide the diagnostic lead time required for manufacturing CAR-T cell therapy, this workflow is fairly labor-intensive, time-consuming, and requires a significant amount of knowledge for data interpretation. For this reason, it would be advantageous to design a more universal assay for identifying ALL ctDNA that does not depend on patient specific clonal rearrangements. Solid tumors typically utilize PCR primers specific to a panel of common mutations to detect ctDNA by droplet digital PCR (ddPCR), yet there aren't enough common mutations

in pediatric ALL to develop a similar universal primer set for ctDNA in ALL <sup>275-277</sup>. Methylation status has been studied as a possible biomarker in AML and lymphoma previously. Hypermethylation of a cell-cycle regulator and cyclin dependent kinase inhibitor, CDKN2B, has been correlated with decreased survival rate in Acute Myeloid Leukemia (AML) <sup>278</sup>. In a study on Non-Hodgkin's Lymphoma (NHL), methylation changes were frequently identified in 3 different promoter regions and more recent data shows that one of these promoter regions, Spartin (SPG20), is completely or highly methylated in all NHL cell lines tested, and is able to distinguish normal B lymphocytes from lymphoma cells <sup>279</sup>. Development of primer sets that can be used across many patient samples will be more practical for routine clinical use.

### **7.1.3 Hypothesis**

ctDNA has been used in combination with next generation sequencing to successfully detect MRD in B-ALL based on B-cell receptor rearrangements unique to the leukemia, and has been used in combination with ddPCR to detect clonal response to therapy in CLL. I predict that disease progression and response of specific clones to treatment in ALL can be studied using a Nanopore MinION sequencer and yield results that are cheaper, less invasive, and as accurate at tracking leukemia clonality as current methods. Additionally, I am hopeful that sequencing a significant number of primary patient ALL samples will identify methylation changes that are present across ALL samples that are not present in normal lymphocytes, and could be used to detect ctDNA in place of using patient specific T and B cell clonal rearrangements for identifying leukemic clones. I predict that hyper- or hypo- methylation profiles can be detected in ALL, and used to develop a universal ddPCR assay to quantify ctDNA.

## 7.2 Results

### 7.2.1 Clonality Tracking in cfDNA using MinION Sequencing

I developed a novel workflow for identifying VDJ rearrangements in leukemia cells and tracking their presence in cfDNA. I collected bone marrow and peripheral blood samples from newly diagnosed ALL patients, and cfDNA was isolated from peripheral blood samples at diagnosis and throughout treatment. Invivoscribe Lymphotrack PCR assays combined with MinION (Oxford Nanopore Technologies) sequencing were used to identify the VDJ sequence of the immunoglobulin (B-ALL) or T-cell receptor (T-ALL) rearrangements of leukemic clones in genomic DNA. These sequences can then be mapped back to the genome for identification of major clones present at the time of diagnosis and throughout treatment (**Figure 7.1**).

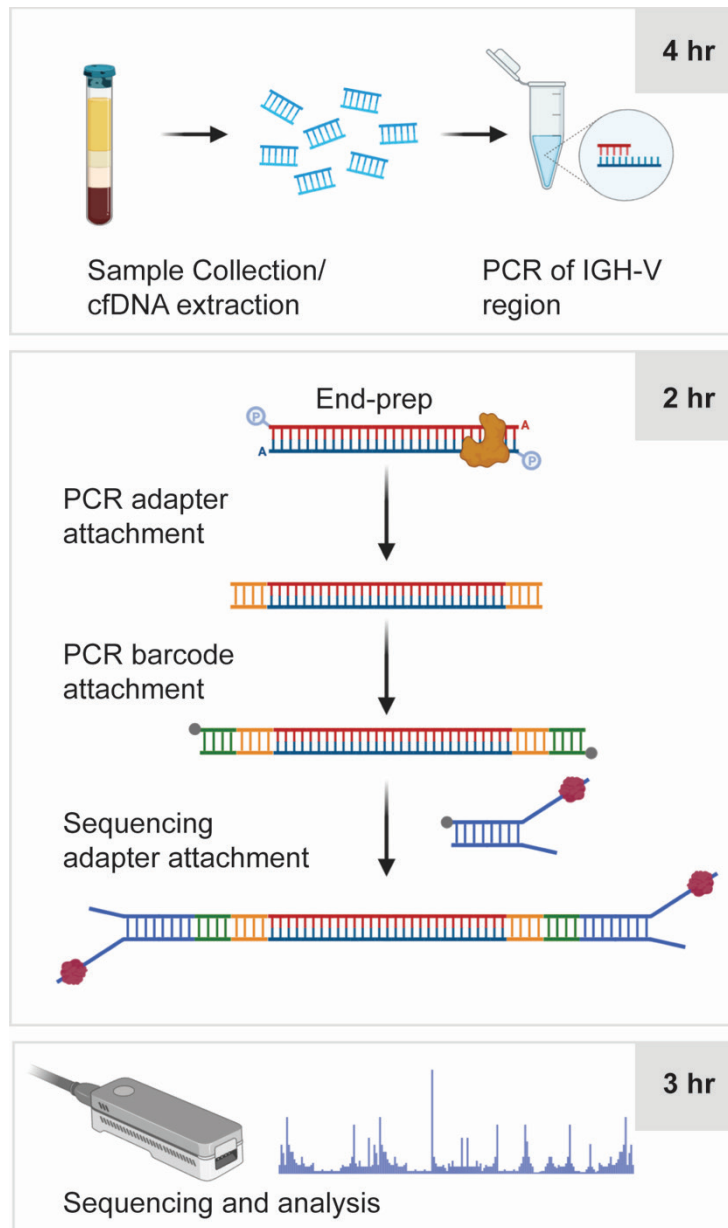


**Figure 7.1 Workflow for MinION Sequencing of IgH Variable Regions**

Schematic of the workflow for sequencing of IgH variable regions on MinION nanopore sequencer. Total pipeline from collection of patient samples to completion of analysis can be performed in a single day.

Traditionally, next generation sequencing, commonly Illumina MiSeq, is used for sequencing of IgH variable regions to study leukemic cell clonality in bone marrow samples. However, performing MiSeq on every patient is time consuming, extremely

expensive, and difficult to perform the data analysis. Our workflow using Nanopore MinION sequencing is relatively quick, significantly less expensive, and provides an easy-to-use analysis pipeline. We are able to get sufficient coverage using the bench-top Nanopore MinION sequencer to sequence patient samples. For preliminary studies, I performed IgH PCR and sequenced genomic DNA (gDNA) from bone marrow biopsy samples from two patients at diagnosis. I also did PCR and sequencing on the cell-free DNA samples isolated at diagnosis and six months to a year into treatment. Each sample was given a unique barcode prior to running on the MinION sequencer. Total reads for each sample were reported and more than 70 percent of reads mapped to chromosome 14, where the IgH variable region is located (**Figure 7.2**).

Sample Name	Barcode	Total Reads	% Mapping to Ch14
ALL-004-gDNA	1	165,557	69.9%
ALL-004-Cfp1-Dx	2	72,363	93.0%
ALL-004-Cfp13	3	38,681	94.5%
ALL-010-gDNA	4	32,231	73.8%
ALL-010-Cfp1-Dx	5	101,800	86.9%
ALL-010-Cfp13	6	4,625	98.5%

**Figure 7.2 MinION Library Run Statistics**

Library run statistics from Nanopore MinION. IgH variable regions from two patient samples (004 and 010) were amplified by PCR and sequenced using the MinION sequencer. gDNA and cell-free DNA isolated from the plasma (cfp) at diagnosis (Dx) and 6 months to a year after treatment (Cfp13). The total reads and percentage of reads that mapped to chromosome 14, where the IgH variable region is located are reported.

The PCRs from the IgH variable region were run on a gel to see amplification of this region. Products were in a range of sizes as many different variable regions were amplified (**Figure 7.3A**). After successful PCR was confirmed, individual clones were identified from the MinION sequencing data. The most prominent clones from each sample at diagnosis were tracked over time in each patient. In both subject 004 and 010, major clones present at diagnosis decreased in abundance or were completely undetectable after treatment. Additionally, the major clones present in the cell-free DNA at diagnosis matched the major clones present in the gDNA isolated from bone marrow biopsy at the time of diagnosis (**Figure 7.3B and C**). This provided preliminary data that major clones from patient leukemia samples can be tracked from either bone marrow biopsies or cell-free DNA samples over time using the MinION sequencer and seem to correlate with what is being seen clinically.

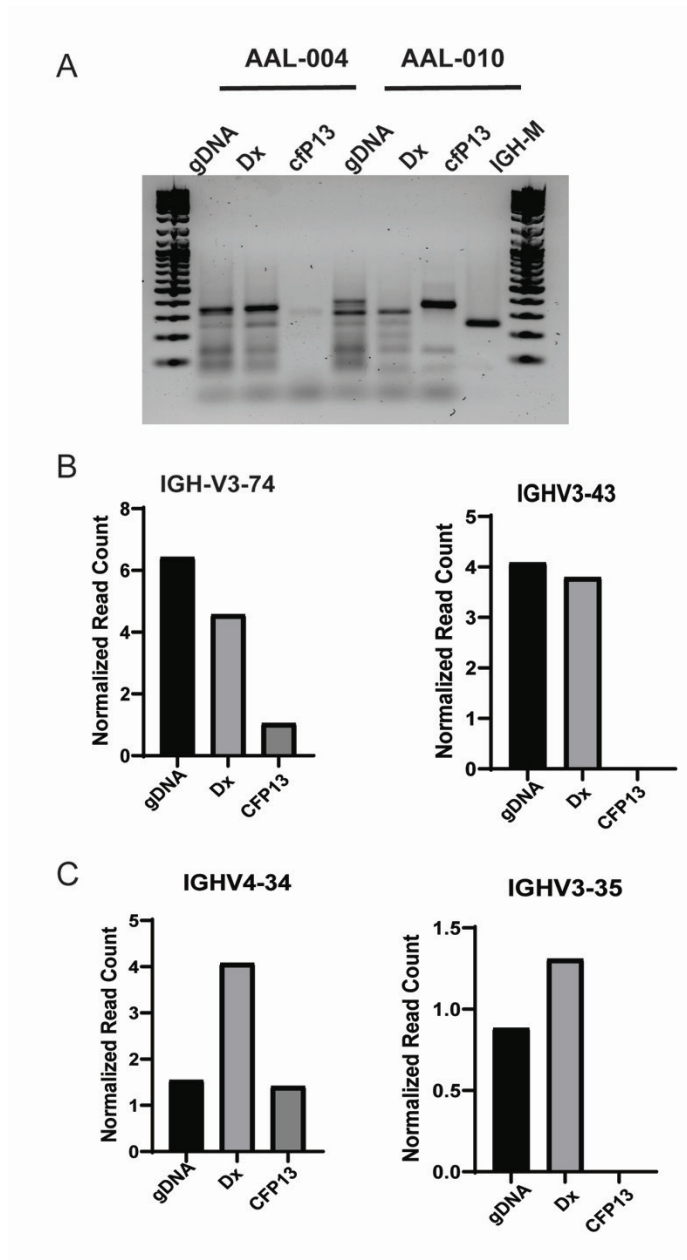


**Figure 7.3 MinION Clonality Tracking**

(A) Gel of Invivoscribe PCRs. Clonality tracking by IgH variable region of patient AAL-004 (B) and AAL-010 (C) shows abundance of cell-free DNA or genomic DNA (gDNA) derived from two different leukemic clones in each sample at diagnosis and post-treatment (CFP13).

## 7.2.2 ctDNA Methylation as a Biomarker in ALL

As described above, we know that tracking patient clonality is a great way to study disease progression, specific leukemia cell populations, and how different clones respond to chemotherapy, hinting at resistance mechanisms. However, using clonality as a biomarker for disease progression and relapse is somewhat complicated and coming up with more universal biomarkers that do not require sequencing and analysis would be advantageous. We performed methylation sequencing on seven patient ALL samples and three healthy PBMC samples to identify sites that are differentially methylated in ALL compared to healthy controls. This sequencing data revealed that the ALL samples clustered independently from the healthy PBMC samples based on their methylation profile (Figure 7.4).

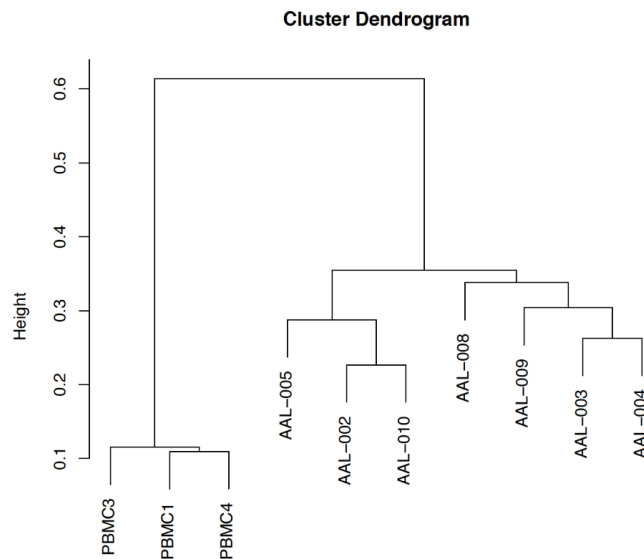


**Figure 7.4 Leukemia Samples Cluster Independently From Healthy Based on Methylation Profile**

Methylation sequencing of seven ALL samples and 3 healthy PBMC controls revealed that the leukemia samples clustered independently from the healthy controls based on their methylation profiles.

From this data, we were able to identify a large number of sites and regions that were consistently hyper- or hypomethylated compared to healthy PBMCs (**Figure 7.5A**). There was approximately the same percentage of regions that were hypermethylated as there were hypomethylated regions (**Figure 7.5B**). Additionally, this methylation is spread throughout the chromosomes with both hyper- and hypomethylation observed on each chromosome (**Figure 7.5C**). These differentially methylated regions were mapped to which genomic regions they were located and the vast majority were located in intronic regions, followed by exons, then promoters, then finally intergenic regions (**Figure 7.6**). Finally, these differentially methylated sites and regions were compared with publicly available datasets of methylation-based arrays identifying differentially methylated sites or regions in pediatric leukemias. This analysis included 865 ALL and 79 healthy samples and yielded 55 regions and 19 specific methylation sites that were uniquely present in ALL samples from our own methylation sequencing and prior methylation datasets and not in healthy controls. After validation of these sites and regions, I will have designed a panel of uniquely methylated sites and regions in ALL that have the potential to be used as biomarkers of disease progression and relapse in patients.

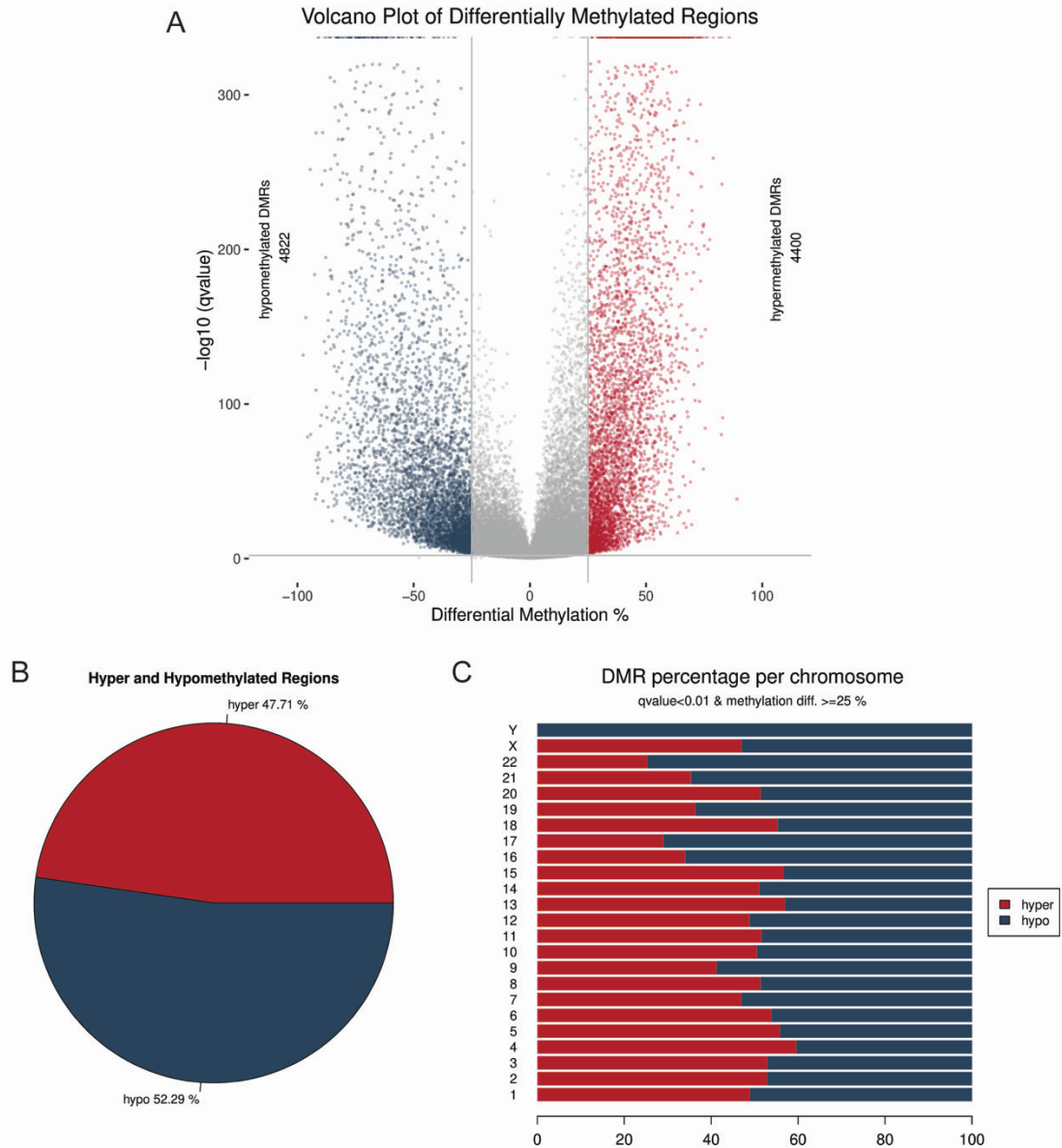


**Figure 7.5 Methylation Sequencing Results**  
 Methylation sequencing of 7 ALL patients and 3 healthy PBMCs revealed differentially methylated regions. (A) Volcano plot showing the percent of differential methylation of hyper (red) and hypo (blue) methylated regions. (B) Percent of differentially methylated regions that were hypermethylated versus hypomethylated. (C) Percentage of hyper- and hypomethylated regions located on each chromosome.

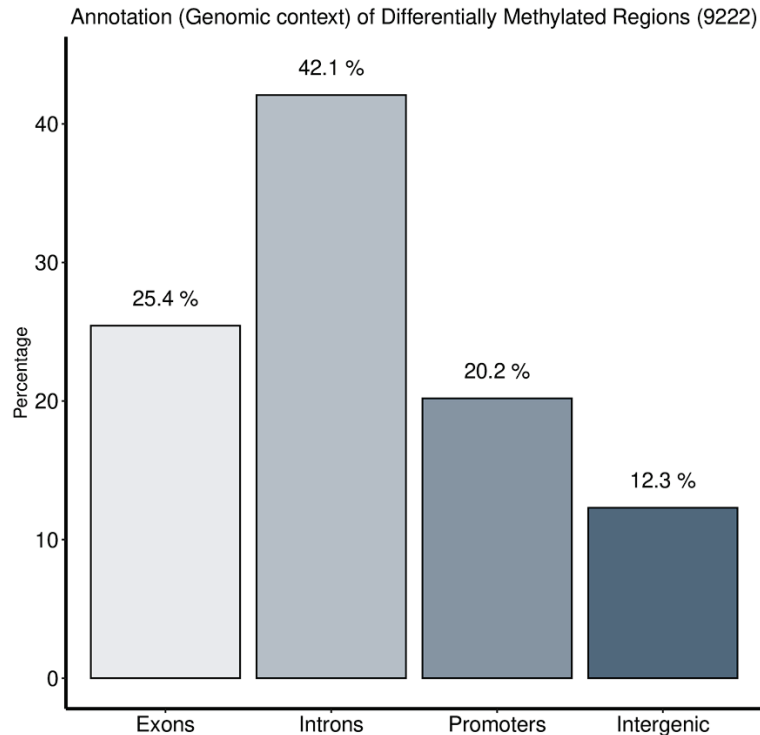


**Figure 7.6 Genomic Location of Differentially Methylated Regions**  
 Percentage of differentially methylated regions that were located in introns, exons, promoters, and intergenic regions from methylation sequencing data.

### 7.3 Discussion

Overall, I developed a novel workflow for identifying VDJ rearrangements in leukemia cells and tracking their presence in cfDNA. I collected bone marrow, blood, and CSF samples from newly diagnosed patients, and cfDNA was isolated from blood and CSF samples throughout treatment. Invivoscribe Lymphotrack PCR assays combined with MinION (Oxford Nanopore Technologies) sequencing were used to identify the VDJ sequence of the immunoglobulin rearrangements of leukemic clones in genomic DNA. The MinION workflow was used to follow leukemic cfDNA throughout the course of treatment, and performed equivalent or better at detecting leukemic clones compared to MiSeq and droplet digital polymerase chain reaction (ddPCR), and is faster and less

expensive than traditional Illumina sequencing. This is important because it provides more frequent and less invasive clinical monitoring of patient disease progression than current methods. This information can then be used to increase lead time required for manufacturing CAR-T cells or switching patients that show early resistance to chemotherapy over to more targeted therapies.

One downside of tracking disease progression and relapse potential by leukemia cell clonality is that it relies on patient-specific sequencing. To evade this issue, I am also in the process of developing a universal assay that utilizes recurrent methylation changes in ALL to identify leukemic cfDNA in patient samples. Methylation sequencing of our patient samples compared to publicly available datasets identified 55 regions and 19 specific methylation sites that were uniquely present in ALL samples. I am validating these sites by ddPCR to establish a panel of biomarkers to track ALL over time via cfDNA.

In total, I have provided proof-of-principle studies, setting up the framework for tracking disease progression and predicting patient relapse. The end goal of this study is to provide a more sensitive and less invasive method for tracking MRD, the best predictor of patient relapse currently, than current approaches. Results will ultimately be correlated with patient response to therapy, the presence of relapse or CNS disease, and overall outcomes determined by standard clinical diagnostic procedures.

### **7.3.1 Future Directions**

While I have begun the preliminary studies for working out a pipeline for MRD prediction using both clonality and methylation as biomarkers, there is still work to be done before these assays can be utilized. For the clonality experiments, we have run Illumina

MiSeq and designed ddPCR primers for the prominent clones, to compare our assays to. So far, our MinION pipeline performs equivalent to MiSeq and better than ddPCR at detecting clones present in patient samples, yet this still needs to be validated on more patient samples. Additionally, I am running our workflow on patient genomic and cell-free DNA samples from diagnosis, mid-induction, end of induction, and end of consolidation timepoints to see how our data compares to clinical determinants of MRD. If we can come up with a less invasive method than bone marrow biopsy for determining MRD, that would save patients from having to go through multiple painful and expensive procedures when the risk stratification from this procedure is not a completely accurate predictor of future relapse anyways.

For methylation assays, I am in the process of validating the differentially methylated regions and sites that were identified by comparing our methylation sequencing data with publicly available databases. These will be verified by RT-PCR and ddPCR. Once I have narrowed down to a few sites that are consistently differentially methylated in leukemic but not healthy samples, I will design a panel of ddPCR primers for these sites and run them on patient gDNA and cfDNA from diagnosis and throughout treatment. This will then be compared with clinical data from the patient to determine if methylation changes can be used as a biomarker of disease progression and relapse in patients in the future.

## **7.4 Methods**

### **7.4.1 Collection of Patient Samples**

Patient samples were collected under University of Kentucky's Institutional Review Board (protocol 44672). Patient Bone Marrow Aspirate (BMA) and peripheral blood samples were collected and diluted with an equal volume of room temperature 2% FBS in PBS. The sample was slowly added to a 50mL Sepmate tube (cat. # 85450), containing 15mL of Ficol Density gradient, centrifuged at 1,200xg for 10 mins and the top layer was quickly poured into a new 50mL tube. The volume was brought up to 50mL with RPMI and spun for 15 mins at 1,400 rpm at 4°C. Cells were counted and then washed in 50mL of RPMI and centrifuged for 10 mins at 1,400 rpm at 4°C. The supernatant was removed, and cells were resuspended in 1mL of RPMI + 10% FBS + 10% DMSO per 10<sup>7</sup> cells and added to a cryovial for storage at -80°C.

### **7.4.2 Isolation of genomic DNA from Patient Samples**

gDNA was isolated from patient bone marrow aspirate collected at the time of diagnosis. Frozen buffy coat layer cells isolated from bone marrow aspirates at time of diagnosis were gradually warmed to 37°C and transferred to a sterile 15 mL conical tube. Dropwise 10 mL of pre-warmed, 25% fetal bovine serum (FBS) in Iscove's Modified Dulbecco's Media (IMDM) was added to the cells at a rate of approximately 2-3 seconds/mL. Cells were centrifuged at 1,000 rpm for 10 minutes and supernatant was gently aspirated. Addition of media, centrifugation and removal of supernatant was repeated again. Cells were then washed once in phosphate buffered saline (PBS) and counted before proceeding to gDNA isolation. gDNA was isolated using the Qiagen

Puregene Blood Core Kit B (catalog #158467), following manufacturer's protocol 'DNA Purification from Buffy Coat Using the Gentra Puregene Blood Kit.

### **7.4.3 Isolation of Cell-Free DNA from Plasma and CSF**

ctDNA was isolated from patient blood and cerebrospinal fluid (CSF). Samples were collected into cell-free DNA collection tubes (Streck, 218962). Upon collection, all samples were centrifuged at room temperature for 10 minutes at 1,600xg.

After initial spin of patient blood samples, the plasma was removed, careful not to disturb the buffy coat layer, and moved to a clean tube. Plasma was centrifuged again for 10 mins at 16,000xg at room temperature and the supernatant was carefully removed, leaving behind a thin layer to not disturb any cell pellet. ctDNA was then isolated using the Qiagen QIAmp MinElute cfDNA Midi Kit (catalog #55284) as per manufacturer's protocol, with the modification of heating the ultra-clean water to 56°C prior to elution.

After initial spin of patient CSF samples, the supernatant was removed, careful not to disturb the any cell pellet, and moved to a clean tube. CSF was centrifuged again for 10 mins at 16,000xg at room temperature and the supernatant was carefully removed again, leaving behind a thin layer to not disturb any cell pellet. Zymo Research Quick-cfDNA Serum and Plasma Kit (catalog #D4076) was used to isolate ctDNA from CSF using the manufacturer protocol 'Purification of cell-free DNA from ≤5mL sample Vacuum Protocol'. The following modifications were made to the manufacturer protocol: after adding proteinase K to the tube the samples were incubated at 55°C for 1hr and the final elution step was carried out in 35ul of 56°C pre-heated nuclease free water. All gDNA and

ctDNA samples were quantified using a Qubit Fluorometer using the high-sensitivity DNA quantification kit according to the manufacturer's instructions and stored at -20°C.

#### **7.4.4 Clonality PCR**

Clonality PCR was performed using Invivoscribe IGHV kit for amplification of the IgH variable region in patient B-ALL samples according to the manufacturer instructions.

#### **7.4.5 Nanopore Library Preparation and Minion Sequencing**

Following the IGHV PCR 50 ng of each sample was used as input for the PCR Barcoding Kit (SQK-PBK004). I adhered to the manufacturer's protocol except for the following. Since amplicon was used as starting material the initial fragmentation step of the protocol was omitted. End-prep was performed by mixing 50ng of PCR product with 3.5ul Ultra II End-prep buffer and 1.5ul of enzyme in a total volume of 30ul. This was followed by Ampure purification and Barcode Adapter (BCA) ligation. Ligated products were again Ampure purified and amplified for 14 cycles in order to attached barcodes (Barcode 1-6). Following a third Ampure purification and Qubit quantification barcoded libraries were pooled together at equal amounts for a total of 10ul. One microliter of RAP was added to the final pooled library and incubated 5 minutes. Although all reactions/washes prior to RAP addition were performed at half volume, I adhered strictly to the concentration of input DNA for each step. The full volume of the library was mixed with 34ul SQB, 25.5ul LB and 4.5ul nuclease-free water and loaded onto the MinION flow cell. Libraries were run until all barcodes had a minimum of 4K reads which averaged about 1-2 hours.

#### **7.4.6 Methylation Sequencing**

gDNA was isolated from bone marrow aspirates from patient diagnosis or from PBMCs of healthy patients purchased from ZenBio using the Zymo gDNA extraction kit. gDNA was then sent to Diagenode for quality control, methylation sequencing, and analysis.

#### **7.4.7 Statistical Analysis**

Samples were run on the MinION sequencer and analyzed via the Nanopipe web-based data analysis pipeline <sup>274</sup>. Consensus sequences from reads mapped to chromosome 14 were then aligned in IMGT, the international ImMunoGeneTics information system <sup>280</sup>. Bam files were loaded into the Integrative Genomics Viewer (IGV, Broad Institute) for identifying total number of reads that mapped to each clone.

Methylation sequencing data analysis was done by Diagenode and those results were compared to public data sets by Daheng He and Chi Wang in the University of Kentucky, Department of Biostatistics.

## CHAPTER 8. FINAL CONCLUSIONS

This research aimed to both characterize the role of PRL-3 in LSC self-renewal and to develop novel tools and methods for studying LSCs and LSC driven-relapse in animal models and in patient samples. In Part 2 of this dissertation, I demonstrated that PRL-3 modulates LSC self-renewal *in vivo* in a zebrafish T-ALL model, and *in vitro* in colony formation assays. This is in part due to the ability of PRL-3 to modulate the Wnt/beta-catenin signaling pathway, known to be crucial to LSCs in T-ALL. Most importantly, inhibition of PRL-3 is able to decrease the function LSC frequency *in vivo*, suggesting that PRL-3 is a potential therapeutic target for LSC-directed therapy.

While this research clearly illustrates that PRL-3 functions as a driver in LSCs and at least in part through Wnt/beta-catenin signaling, it also raises the question of exactly how PRL-3 is modulating Wnt signaling and if PRL-3 is increasing LSC self-renewal via any other signaling pathways. Future studies characterizing potential substrates of PRL-3 in leukemia will further these conclusions of how PRL-3 functions in LSCs. Additionally, xenograft mouse models testing the efficacy of PRL-3 inhibition on modulating LSC frequency would significantly enrich the therapeutic potential of PRL-3 in LSCs.

In addition to leukemia stem cell biology, this dissertation outlined a few different models and techniques for studying LSCs and disease relapse. First, I designed a model for labeling potential LSCs *in vivo* in our zebrafish T-ALL model, allowing for in depth imaging and characterization of LSC biology and function *in vivo*. I also optimized a zebrafish xenograft model for engrafting patient samples and predicting response to chemotherapy, and identified potential pitfalls with this model. Finally, I established a workflow for monitoring patient samples for disease relapse using cell-free DNA to track

leukemia cell clonality and DNA methylation changes over time in a less invasive method than current clinical standard of care.

The research described in this dissertation provided preliminary data for three novel models or methods for studying LSCs and patient relapse and response to therapy; however further studies would significantly enhance the applicability of these models and methods. Limiting dilution transplantation studies confirming the putative LSC population in the Wnt reporter LSC zebrafish model would allow for this model to begin to take the place of limiting dilution studies for characterizing drug efficacy against LSCs. Validation and application of the cell-free DNA workflow for both clonality purposes and methylation would be the next step in this pipeline making its way into clinical practice to complement current methods for predicting patient response to therapy and disease relapse.

Taken together, the work presented in this dissertation has had an impact in both LSC biology and function in T-ALL and in paving the way for new methods and models to study LSCs in ALL. This work has both identified a potential therapeutic target that has not yet been described to have a function in T-ALL LSCs and innovated methods for improving patient risk stratification and relapse prediction. In combination, these studies will further the field in understanding and characterizing LSC biology and function and their prognostic significance in patient samples in ALL.

## REFERENCES

1. Chiaretti, S. & Foà, R. T-cell acute lymphoblastic leukemia. *Haematologica* **94**, 160–2 (2009).
2. Raetz, E. A. & Teachey, D. T. T-cell acute lymphoblastic leukemia. *Hematology. American Society of Hematology. Education Program* **2016**, 580–588 (2016).
3. Teachey, D. T. & Pui, C.-H. Comparative features and outcomes between paediatric T-cell and B-cell acute lymphoblastic leukaemia. *Lancet Oncol* **20**, e142–e154 (2019).
4. Nguyen, K. *et al.* Factors influencing survival after relapse from acute lymphoblastic leukemia: a Children’s Oncology Group study. *Leukemia* **22**, 2142–2150 (2008).
5. Karrman, K. & Johansson, B. Pediatric T-cell acute lymphoblastic leukemia. *Genes, chromosomes & cancer* **56**, 89–116 (2017).
6. Arber, D. A. *et al.* The 2016 revision to the World Health Organization classification of myeloid neoplasms and acute leukemia. *Blood* **127**, 2391–405 (2016).
7. Chiaretti, S., Zini, G. & Bassan, R. Diagnosis and subclassification of acute lymphoblastic leukemia. *Mediterranean journal of hematology and infectious diseases* **6**, e2014073 (2014).
8. Han, X. & Bueso-Ramos, C. E. Precursor T-cell acute lymphoblastic leukemia/lymphoblastic lymphoma and acute biphenotypic leukemias. *American journal of clinical pathology* **127**, 528–44 (2007).
9. Borowitz, M. J. *et al.* Clinical significance of minimal residual disease in childhood acute lymphoblastic leukemia and its relationship to other prognostic factors: a Children’s Oncology Group study. *Blood* **111**, 5477–85 (2008).
10. Coustan-Smith, E. *et al.* Early T-cell precursor leukaemia: a subtype of very high-risk acute lymphoblastic leukaemia. *The Lancet. Oncology* **10**, 147–56 (2009).
11. Lange, B. J. *et al.* Pediatric leukemia/lymphoma with t(8;14)(q24;q11). *Leukemia* **6**, 613–8 (1992).
12. Parolini, M. *et al.* Highly aggressive T-cell acute lymphoblastic leukemia with t(8;14)(q24;q11): extensive genetic characterization and achievement of early molecular remission and long-term survival in an adult patient. *Blood Cancer Journal* **4**, bcj201372 (2014).
13. Lee, S.-Y. Y. *et al.* Mutations of the Notch1 gene in T-cell acute lymphoblastic leukemia: analysis in adults and children. *Leukemia* **19**, 1841–3 (2005).

14. Weng, A. P. *et al.* Activating mutations of NOTCH1 in human T cell acute lymphoblastic leukemia. *Science (New York, N.Y.)* **306**, 269–71 (2004).
15. Longo, D. L., Hunger, S. P. & Mullighan, C. G. Acute Lymphoblastic Leukemia in Children. *New Engl J Medicine* **373**, 1541–1552 (2015).
16. Micale, M. A. Pediatric T-Cell Acute Lymphoblastic Leukemia. *Atlas Genetics Cytogenet Oncol Haematol* (2018) doi:10.4267/2042/68970.
17. Raimondi, S. C. T-lineage acute lymphoblastic leukemia (T-ALL). *Atlas Genet Cytogenet Oncol Haematol.* **11**, 328–339 (2007).
18. Zhao, X. *et al.* The clinical significance of monitoring the expression of the SIL - TAL1 fusion gene in T ~~cell acute lymphoblastic~~ <sup>cell acute lymphoblastic</sup> hematopoietic stem cell transplantation. *Int J Lab Hematol* **39**, 613–619 (2017).
19. Pui, C.-H. *et al.* Childhood Acute Lymphoblastic Leukemia: Progress Through Collaboration. *J Clin Oncol* **33**, 2938–2948 (2015).
20. Tzoneva, G. *et al.* Activating mutations in the NT5C2 nucleotidase gene drive chemotherapy resistance in relapsed ALL. *Nat Med* **19**, 368–371 (2013).
21. Chu, M. *et al.* TFDP3 confers chemoresistance in minimal residual disease within childhood T-cell acute lymphoblastic leukemia. *Oncotarget* **5**, 1405–1415 (2014).
22. SR, R., AI, N. & AT, M. Therapy-Related Secondary Cancers. in *Holland-Frei Cancer Medicine* (eds. DW, K., RE, P., RR, W. & al., et) (BC Decker, 2003).
23. Waber, D. P. *et al.* Cognitive Sequelae in Children Treated for Acute Lymphoblastic Leukemia With Dexamethasone or Prednisone. *J Pediatric Hematology Oncol* **22**, 206–213 (2000).
24. Plas, E. van der *et al.* Neurocognitive Late Effects of Chemotherapy in Survivors of Acute Lymphoblastic Leukemia: Focus on Methotrexate. *J Can Acad Child Adolesc Psychiatry J De L'académie Can De Psychiatrie De L'enfant Et De L'adolescent* **24**, 25–32 (2015).
25. Pinnix, C. C., Yahalom, J., Specht, L. & Dabaja, B. S. Radiation in Central Nervous System Leukemia: Guidelines from the International Lymphoma Radiation Oncology Group. *Int J Radiat Oncol Biology Phys* **102**, 53–58 (2018).
26. Teachey, D. T. & Diorio, C. A Novel Immunotherapy for T-ALL. *Hematologist* **16**, (2019).

27. Hixon, J. A. *et al.* New anti-IL-7R $\alpha$  monoclonal antibodies show efficacy against T cell acute lymphoblastic leukemia in pre-clinical models. *Leukemia* (2019) doi:10.1038/s41375-019-0531-8.
28. Furth, J., Kahn, M. C. & Breedis, C. The Transmission of Leukemia of Mice with a Single Cell. *American Association for Cancer Research Journals* **31**, 276–282 (1937).
29. Makino, S. FURTHER EVIDENCE FAVORING THE CONCEPT OF THE STEM CELL IN ASCITES TUMORS OF RATS. *Ann Ny Acad Sci* **63**, 818–830 (1956).
30. Hewitt, H. Studies of the Dissemination and Quantitative Transplantation of a Lymphocytic Leukaemia of CBA Mice. *Brit J Cancer* **12**, 378–401 (1958).
31. BRUCE, W. & GAAG, V. H. A Quantitative Assay for the Number of Murine Lymphoma Cells capable of Proliferation in vivo. *Nature* **199**, 79–80 (1963).
32. Clevers, H. The cancer stem cell: premises, promises and challenges. *Nat Med* **17**, 313–319 (2011).
33. Park, C. H., Bergsagel, D. E. & McCulloch, E. A. Mouse myeloma tumor stem cells: a primary cell culture assay. *J Natl Cancer I* **46**, 411–22 (1971).
34. Sabbath, K. D., Ball, E. D., Larcom, P., Davis, R. B. & Griffin, J. D. Heterogeneity of clonogenic cells in acute myeloblastic leukemia. *J Clin Invest* **75**, 746–753 (1985).
35. Griffin, J. D. & Löwenberg, B. Clonogenic cells in acute myeloblastic leukemia. *Blood* **68**, 1185–95 (1986).
36. Lapidot, T. *et al.* A cell initiating human acute myeloid leukaemia after transplantation into SCID mice. *Nature* **367**, 645–648 (1994).
37. Al-Hajj, M., Wicha, M. S., Benito-Hernandez, A., Morrison, S. J. & Clarke, M. F. Prospective identification of tumorigenic breast cancer cells. *Proc National Acad Sci* **100**, 3983–3988 (2003).
38. Singh, S. K. *et al.* Identification of a cancer stem cell in human brain tumors. *Cancer Res* **63**, 5821–8 (2003).
39. Yu, Z., Pestell, T. G., Lisanti, M. P. & Pestell, R. G. Cancer stem cells. *The International Journal of Biochemistry & Cell Biology* **44**, 2144–2151 (2012).
40. Batlle, E. & Clevers, H. Cancer stem cells revisited. *Nature medicine* **23**, 1124–1134 (2017).
41. He, S., Nakada, D. & Morrison, S. J. Mechanisms of Stem Cell Self-Renewal. *Cell Dev Biology* **25**, 377–406 (2009).

42. Zhou, B.-B. S. *et al.* Tumour-initiating cells: challenges and opportunities for anticancer drug discovery. *Nat Rev Drug Discov* **8**, 806–823 (2009).
43. Kreso, A. *et al.* Variable Clonal Repopulation Dynamics Influence Chemotherapy Response in Colorectal Cancer. *Science* **339**, 543–548 (2013).
44. Ginestier, C. *et al.* ALDH1 Is a Marker of Normal and Malignant Human Mammary Stem Cells and a Predictor of Poor Clinical Outcome. *Cell Stem Cell* **1**, 555–567 (2007).
45. Rosen, J. M. & Jordan, C. T. The Increasing Complexity of the Cancer Stem Cell Paradigm. *Science* **324**, 1670–1673 (2009).
46. Chen, X., Liao, R., Li, D. & Sun, J. Induced cancer stem cells generated by radiochemotherapy and their therapeutic implications. *Oncotarget* **5**, 17301–17312 (2015).
47. Dylla, S. J. *et al.* Colorectal Cancer Stem Cells Are Enriched in Xenogeneic Tumors Following Chemotherapy. *Plos One* **3**, e2428 (2008).
48. Abubaker, K. *et al.* Short-term single treatment of chemotherapy results in the enrichment of ovarian cancer stem cell-like cells leading to an increased tumor burden. *Mol Cancer* **12**, 24 (2013).
49. Ayob, A. Z. & Ramasamy, T. S. Cancer stem cells as key drivers of tumour progression. *J Biomed Sci* **25**, 20 (2018).
50. Fialkow, P. J. The Origin and Development of Human Tumors Studied with Cell Markers. *New Engl J Medicine* **291**, 26–35 (1974).
51. Udomsakdi, C. *et al.* Rapid decline of chronic myeloid leukemic cells in long-term culture due to a defect at the leukemic stem cell level. *Proc National Acad Sci* **89**, 6192–6196 (1992).
52. Jan, M. *et al.* Clonal Evolution of Preleukemic Hematopoietic Stem Cells Precedes Human Acute Myeloid Leukemia. *Sci Transl Med* **4**, 149ra118-149ra118 (2012).
53. Lu, C. *et al.* IDH mutation impairs histone demethylation and results in a block to cell differentiation. *Nature* **483**, 474–478 (2012).
54. Shlush, L. I. *et al.* Identification of pre-leukaemic haematopoietic stem cells in acute leukaemia. *Nature* **506**, 328–333 (2014).
55. Corces, M. R. *et al.* Lineage-specific and single-cell chromatin accessibility charts human hematopoiesis and leukemia evolution. *Nat Genet* **48**, 1193–1203 (2016).

56. Yilmaz, M. *et al.* Late relapse in acute myeloid leukemia (AML): clonal evolution or therapy-related leukemia? *Blood Cancer J* **9**, 7 (2019).
57. Ding, L. *et al.* Clonal evolution in relapsed acute myeloid leukaemia revealed by whole-genome sequencing. *Nature* **481**, 506–510 (2012).
58. Shlush, L. I. *et al.* Tracing the origins of relapse in acute myeloid leukaemia to stem cells. *Nature* **547**, 104–108 (2017).
59. Holyoake, T., Jiang, X., Eaves, C. & Eaves, A. Isolation of a Highly Quiescent Subpopulation of Primitive Leukemic Cells in Chronic Myeloid Leukemia. *Blood* **94**, 2056–2064 (1999).
60. Bonnet, D. & Dick, J. E. Human acute myeloid leukemia is organized as a hierarchy that originates from a primitive hematopoietic cell. *Nature medicine* **3**, 730–7 (1997).
61. Ishikawa, F. *et al.* Chemotherapy-resistant human AML stem cells home to and engraft within the bone-marrow endosteal region. *Nat Biotechnol* **25**, 1315–1321 (2007).
62. Eppert, K. *et al.* Stem cell gene expression programs influence clinical outcome in human leukemia. *Nat Med* **17**, 1086–1093 (2011).
63. Goardon, N. *et al.* Coexistence of LMPP-like and GMP-like Leukemia Stem Cells in Acute Myeloid Leukemia. *Cancer Cell* **19**, 138–152 (2011).
64. Quek, L. *et al.* Genetically distinct leukemic stem cells in human CD34<sup>−</sup> acute myeloid leukemia are arrested at a hemopoietic precursor-like stage Human CD34<sup>−</sup> AML stem cells. *J Exp Medicine* **213**, 1513–1535 (2016).
65. Vetrie, D., Helgason, G. V. & Copland, M. The leukaemia stem cell: similarities, differences and clinical prospects in CML and AML. *Nat Rev Cancer* **20**, 158–173 (2020).
66. Saito, Y. *et al.* Induction of cell cycle entry eliminates human leukemia stem cells in a mouse model of AML. *Nat Biotechnol* **28**, 275–280 (2010).
67. Goldman, J. *et al.* Chronic myeloproliferative diseases with and without the Ph chromosome: some unresolved issues. *Leukemia* **23**, 1708–1715 (2009).
68. Prost, S. *et al.* Erosion of the chronic myeloid leukaemia stem cell pool by PPAR $\gamma$  agonists. *Nature* **525**, 380–383 (2015).
69. Baquero, P. *et al.* Targeting quiescent leukemic stem cells using second generation autophagy inhibitors. *Leukemia* **33**, 981–994 (2019).

70. Horne, G. A. & Copland, M. Approaches for targeting self-renewal pathways in cancer stem cells: implications for hematological treatments. *Expert Opin Drug Dis* **12**, 465–474 (2017).
71. Horne, G. A., Jackson, L., Helgason, V. & Holyoake, T. L. Stem Cell Guardians - Old and New Perspectives in LSC Biology. *Current drug targets* **18**, 405–413 (2017).
72. Sands, W. A., Copland, M. & Wheadon, H. Targeting self-renewal pathways in myeloid malignancies. *Cell Commun Signal* **11**, 33 (2013).
73. Bernt, K. M. *et al.* MLL-Rearranged Leukemia Is Dependent on Aberrant H3K79 Methylation by DOT1L. *Cancer Cell* **20**, 66–78 (2011).
74. Ng, S. W. K. *et al.* A 17-gene stemness score for rapid determination of risk in acute leukaemia. *Nature* **540**, 433–437 (2016).
75. Jung, N., Dai, B., Gentles, A. J., Majeti, R. & Feinberg, A. P. An LSC epigenetic signature is largely mutation independent and implicates the HOXA cluster in AML pathogenesis. *Nat Commun* **6**, 8489 (2015).
76. Krivtsov, A. V. *et al.* Cell of origin determines clinically relevant subtypes of MLL-rearranged AML. *Leukemia* **27**, 852–860 (2013).
77. Shih, A. H. *et al.* Mutational Cooperativity Linked to Combinatorial Epigenetic Gain of Function in Acute Myeloid Leukemia. *Cancer Cell* **27**, 502–515 (2015).
78. George, J. *et al.* Leukaemia cell of origin identified by chromatin landscape of bulk tumour cells. *Nat Commun* **7**, 12166 (2016).
79. Lagadinou, E. D. *et al.* BCL-2 Inhibition Targets Oxidative Phosphorylation and Selectively Eradicates Quiescent Human Leukemia Stem Cells. *Cell Stem Cell* **12**, 329–341 (2013).
80. Stevens, B. M., O'Brien, C., Jordan, C. T. & Jones, C. L. Enriching for human acute myeloid leukemia stem cells using reactive oxygen species-based cell sorting. *Star Protoc* **2**, 100248 (2021).
81. Nieborowska-Skorska, M. *et al.* Rac2-MRC-cIII-generated ROS cause genomic instability in chronic myeloid leukemia stem cells and primitive progenitors. *Blood* **119**, 4253–4263 (2012).
82. Bolton-Gillespie, E. *et al.* Genomic instability may originate from imatinib-refractory chronic myeloid leukemia stem cells. *Blood* **121**, 4175–4183 (2013).
83. Pei, S. *et al.* AMPK/FIS1-Mediated Mitophagy Is Required for Self-Renewal of Human AML Stem Cells. *Cell Stem Cell* **23**, 86-100.e6 (2018).

84. Tan, Y., Wu, Q. & Zhou, F. Targeting acute myeloid leukemia stem cells: Current therapies in development and potential strategies with new dimensions. *Crit Rev Oncol Hemat* **152**, 102993 (2020).
85. Hoey, T. *et al.* DLL4 Blockade Inhibits Tumor Growth and Reduces Tumor-Initiating Cell Frequency. *Cell Stem Cell* **5**, 168–177 (2009).
86. Saunders, L. R. *et al.* A DLL3-targeted antibody-drug conjugate eradicates high-grade pulmonary neuroendocrine tumor-initiating cells in vivo. *Sci Transl Med* **7**, 302ra136-302ra136 (2015).
87. Shastri, A. *et al.* Antisense STAT3 inhibitor decreases viability of myelodysplastic and leukemic stem cells. *J Clin Invest* **128**, 5479–5488 (2018).
88. Jin, L. *et al.* Monoclonal Antibody-Mediated Targeting of CD123, IL-3 Receptor  $\alpha$  Chain, Eliminates Human Acute Myeloid Leukemic Stem Cells. *Cell Stem Cell* **5**, 31–42 (2009).
89. Ginestier, C. *et al.* CXCR1 blockade selectively targets human breast cancer stem cells in vitro and in xenografts. *J Clin Invest* **120**, 485–497 (2010).
90. Brandolini, L. *et al.* Targeting CXCR1 on breast cancer stem cells: signaling pathways and clinical application modelling. *Oncotarget* **6**, 43375–43394 (2015).
91. Laszlo, G. S., Estey, E. H. & Walter, R. B. The past and future of CD33 as therapeutic target in acute myeloid leukemia. *Blood Rev* **28**, 143–153 (2014).
92. Tang, X., Mo, C., Wang, Y., Wei, D. & Xiao, H. Anti -tumour strategies aiming to target tumour -associated macrophages. *Immunology* **138**, 93-104 (2013).
93. Loeffler, M., Krüger, J. A., Niethammer, A. G. & Reisfeld, R. A. Targeting tumor-associated fibroblasts improves cancer chemotherapy by increasing intratumoral drug uptake. *J Clin Invest* **116**, 1955–1962 (2006).
94. Miao, L. *et al.* Targeting Tumor-Associated Fibroblasts for Therapeutic Delivery in Desmoplastic Tumors. *Cancer Res* **77**, 719–731 (2017).
95. Tauro, M., McGuire, J. & Lynch, C. C. New approaches to selectively target cancer-associated matrix metalloproteinase activity. *Cancer Metast Rev* **33**, 1043–1057 (2014).
96. Ruffini, F. *et al.* Cilengitide downmodulates invasiveness and vasculogenic mimicry of neuropilin 1 expressing melanoma cells through the inhibition of  $\alpha v \beta 5$  integrin. *Int J Cancer* **136**, E545–E558 (2015).
97. Yata, T. *et al.* Modulation of extracellular matrix in cancer is associated with enhanced tumor cell targeting by bacteriophage vectors. *Mol Cancer* **14**, 110 (2015).

98. Nowak, D., Stewart, D. & Koefler, P. H. Differentiation therapy of leukemia: 3 decades of development. *Blood* **113**, 3655–3665 (2009).
99. Chomienne, C. *et al.* All-trans retinoic acid in acute promyelocytic leukemias. II. In vitro studies: structure-function relationship. *Blood* **76**, 1710–1717 (1990).
100. Elliott, S. *et al.* Proof of differentiative mode of action of all-trans retinoic acid in acute promyelocytic leukemia using X-linked clonal analysis. *Blood* **79**, 1916–9 (1992).
101. Tallman, M. S. *et al.* All-trans-Retinoic Acid in Acute Promyelocytic Leukemia. *New Engl J Medicine* **337**, 1021–1028 (1997).
102. Tallman, M. S. & Altman, J. K. How I treat acute promyelocytic leukemia. *Blood* **114**, 5126–5135 (2009).
103. Fenaux, P. *et al.* A randomized comparison of all transretinoic acid (ATRA) followed by chemotherapy and ATRA plus chemotherapy and the role of maintenance therapy in newly diagnosed acute promyelocytic leukemia. The European APL Group. *Blood* **94**, 1192–200 (1999).
104. Mandelli, F. *et al.* Molecular remission in PML/RAR alpha-positive acute promyelocytic leukemia by combined all-trans retinoic acid and idarubicin (AIDA) therapy. Gruppo Italiano-Malattie Ematologiche Maligne dell'Adulto and Associazione Italiana di Ematologia ed Oncologia Pediatrica Cooperative Groups. *Blood* **90**, 1014–21 (1997).
105. Cobaleda, C. *et al.* A primitive hematopoietic cell is the target for the leukemic transformation in human philadelphia-positive acute lymphoblastic leukemia. *Blood* **95**, 1007–13 (2000).
106. Cox, C. V. *et al.* Characterization of acute lymphoblastic leukemia progenitor cells. *Blood* **104**, 2919–2925 (2004).
107. Cox, C. V., Diamanti, P., Evely, R. S., Kearns, P. R. & Blair, A. Expression of CD133 on leukemia-initiating cells in childhood ALL. *Blood* **113**, 3287–3296 (2009).
108. Kong, Y. *et al.* CD34+CD38+CD19+ as well as CD34+CD38–CD19+ cells are leukemia-initiating cells with self-renewal capacity in human B-precursor ALL. *Leukemia* **22**, 1207–1213 (2008).
109. Viseur, C. le *et al.* In Childhood Acute Lymphoblastic Leukemia, Blasts at Different Stages of Immunophenotypic Maturation Have Stem Cell Properties. *Cancer Cell* **14**, 47–58 (2008).
110. Aoki, Y. *et al.* Identification of CD34+ and CD34– leukemia-initiating cells in MLL-rearranged human acute lymphoblastic leukemia. *Blood* **125**, 967–980 (2015).

111. Castor, A. *et al.* Distinct patterns of hematopoietic stem cell involvement in acute lymphoblastic leukemia. *Nat Med* **11**, 630–637 (2005).
112. Tan, S. H., Bertulfo, F. C. & Sanda, T. Leukemia-Initiating Cells in T-Cell Acute Lymphoblastic Leukemia. *Frontiers Oncol* **7**, 218 (2017).
113. Cox, C. V. *et al.* Characterization of a progenitor cell population in childhood T-cell acute lymphoblastic leukemia. *Blood* **109**, 674–82 (2007).
114. Guo, W. *et al.* Multi-genetic events collaboratively contribute to Pten-null leukaemia stem-cell formation. *Nature* **453**, 529–33 (2008).
115. Gerby, B. *et al.* Expression of CD34 and CD7 on human T-cell acute lymphoblastic leukemia discriminates functionally heterogeneous cell populations. *Leukemia* **25**, 1249–1258 (2011).
116. Gerby, B. *et al.* SCL, LMO1 and Notch1 Reprogram Thymocytes into Self-Renewing Cells. *Plos Genet* **10**, e1004768 (2014).
117. Chiu, P. P., Jiang, H. & Dick, J. E. Leukemia-initiating cells in human T-lymphoblastic leukemia exhibit glucocorticoid resistance. *Blood* **116**, 5268–79 (2010).
118. Tremblay, M. *et al.* Modeling T-cell acute lymphoblastic leukemia induced by the SCL and LMO1 oncogenes. *Genes & development* **24**, 1093–105 (2010).
119. Giambra, V. *et al.* NOTCH1 promotes T cell leukemia-initiating activity by RUNX-mediated regulation of PKC- $\theta$  and reactive oxygen species. *Nature medicine* **18**, 1693–8 (2012).
120. Tatarek, J. *et al.* Notch1 inhibition targets the leukemia-initiating cells in a Tal1/Lmo2 mouse model of T-ALL. *Blood* **118**, 1579–90 (2011).
121. O’Neil, J., Shank, J., Cusson, N., Murre, C. & Kelliher, M. TAL1/SCL induces leukemia by inhibiting the transcriptional activity of E47/HEB. *Cancer Cell* **5**, 587–596 (2004).
122. McCormack, M. P. *et al.* The Lmo2 oncogene initiates leukemia in mice by inducing thymocyte self-renewal. *Science (New York, N.Y.)* **327**, 879–83 (2010).
123. Smith, A. C. *et al.* High-throughput cell transplantation establishes that tumor-initiating cells are abundant in zebrafish T-cell acute lymphoblastic leukemia. *Blood* **115**, 3296–303 (2010).
124. González-García, S. *et al.* IL-7R is essential for leukemia-initiating cell activity of T-cell acute lymphoblastic leukemia. *Blood* **134**, 2171–2182 (2019).

125. García-Peydró, M. *et al.* The NOTCH1/CD44 axis drives pathogenesis in a T cell acute lymphoblastic leukemia model. *J Clin Invest* **128**, 2802–2818 (2018).
126. Passaro, D. *et al.* CXCR4 Is Required for Leukemia-Initiating Cell Activity in T Cell Acute Lymphoblastic Leukemia. *Cancer Cell* **27**, 769–779 (2015).
127. Pitt, L. A. *et al.* CXCL12-Producing Vascular Endothelial Niches Control Acute T Cell Leukemia Maintenance. *Cancer cell* **27**, 755–68 (2015).
128. Blackburn, J. S. *et al.* Clonal evolution enhances leukemia-propagating cell frequency in T cell acute lymphoblastic leukemia through Akt/mTORC1 pathway activation. *Cancer cell* **25**, 366–78 (2014).
129. Martins, V. C. *et al.* Thymus-autonomous T cell development in the absence of progenitor import. *J Exp Medicine* **209**, 1409–1417 (2012).
130. Peaudecerf, L. *et al.* Thymocytes may persist and differentiate without any input from bone marrow progenitors. *J Exp Medicine* **209**, 1401–1408 (2012).
131. Yui, M. A. & Rothenberg, E. V. Developmental gene networks: a triathlon on the course to T cell identity. *Nat Rev Immunol* **14**, 529–545 (2014).
132. Schubbert, S. *et al.* Targeting the MYC and PI3K pathways eliminates leukemia-initiating cells in T-cell acute lymphoblastic leukemia. *Cancer research* **74**, 7048–59 (2014).
133. Giambra, V. *et al.* Leukemia stem cells in T-ALL require active Hif1 $\alpha$  and Wnt signaling. *Blood* **125**, 3917–27 (2015).
134. Tamiro, F., Weng, A. P. & Giambra, V. Targeting leukemia-initiating cells in acute lymphoblastic leukemia (ALL). *Cancer Res canres.2571.2020* (2021) doi:10.1158/0008-5472.can-20-2571.
135. Tanaka, T., Sewell, H., Waters, S., Phillips, S. E. V. & Rabbitts, T. H. Single Domain Intracellular Antibodies from Diverse Libraries EMPHASIZING DUAL FUNCTIONS OF LMO2 PROTEIN INTERACTIONS USING A SINGLE VH DOMAIN\*. *J Biol Chem* **286**, 3707–3716 (2011).
136. Appert, A. *et al.* Targeting LMO2 with a Peptide Aptamer Establishes a Necessary Function in Overt T-Cell Neoplasia. *Cancer Res* **69**, 4784–4790 (2009).
137. Pais, H. *et al.* Surfaceome interrogation using an RNA-seq approach highlights leukemia initiating cell biomarkers in an LMO2 T cell transgenic model. *Sci Rep-uk* **9**, 5760 (2019).

138. Sánchez-Martínez, D. *et al.* Fratricide-resistant CD1a-specific CAR T cells for the treatment of cortical T-cell acute lymphoblastic leukemia. *Blood* **133**, 2291–2304 (2019).
139. Mamonkin, M., Rouce, R. H., Tashiro, H. & Brenner, M. K. A T-cell-directed chimeric antigen receptor for the selective treatment of T-cell malignancies. *Blood* **126**, 983–992 (2015).
140. Gomes-Silva, D. *et al.* CD7-edited T cells expressing a CD7-specific CAR for the therapy of T-cell malignancies. *Blood* **130**, 285–296 (2017).
141. Png, Y. T. *et al.* Blockade of CD7 expression in T cells for effective chimeric antigen receptor targeting of T-cell malignancies. *Blood Adv* **1**, 2348–2360 (2017).
142. Kwiatkowski, N. *et al.* Targeting transcription regulation in cancer with a covalent CDK7 inhibitor. *Nature* **511**, 616–620 (2014).
143. Carroll, W. L., Aifantis, I. & Raetz, E. Beating the Clock in T-cell Acute Lymphoblastic Leukemia. *Clin Cancer Res* **23**, 873–875 (2017).
144. Knoechel, B. *et al.* An epigenetic mechanism of resistance to targeted therapy in T cell acute lymphoblastic leukemia. *Nat Genet* **46**, 364–370 (2014).
145. Giambra, V. *et al.* Epigenetic Restoration of Fetal-like IGF1 Signaling Inhibits Leukemia Stem Cell Activity. *Cell Stem Cell* **23**, 714-726.e7 (2018).
146. Peirs, S. *et al.* Targeting BET proteins improves the therapeutic efficacy of BCL-2 inhibition in T-cell acute lymphoblastic leukemia. *Leukemia* **31**, 2037–2047 (2017).
147. Loosveld, M. *et al.* Therapeutic Targeting of c-Myc in T-Cell Acute Lymphoblastic Leukemia (T-ALL). *Oncotarget* **5**, 3168–3172 (2014).
148. Genta, S., Piroso, M. C. & Stathis, A. BET and EZH2 Inhibitors: Novel Approaches for Targeting Cancer. *Curr Oncol Rep* **21**, 13 (2019).
149. Stahl, M. *et al.* Epigenetics in Cancer: A Hematological Perspective. *Plos Genet* **12**, e1006193 (2016).
150. Nervi, C., Marinis, E. D. & Codacci-Pisanelli, G. Epigenetic treatment of solid tumours: a review of clinical trials. *Clin Epigenetics* **7**, 127 (2015).
151. McGranahan, N. & Swanton, C. Clonal Heterogeneity and Tumor Evolution: Past, Present, and the Future. *Cell* **168**, 613–628 (2017).
152. Wei, M., Haney, M. G., Rivas, D. R. & Blackburn, J. S. Protein tyrosine phosphatase 4A3 (PTP4A3/PRL-3) drives migration and progression of T-cell acute lymphoblastic leukemia in vitro and in vivo. *Oncogenesis* **9**, 6 (2020).

153. Patterson, K., Brummer, T., O'Brien, P. & Journal, D.-R. Dual-specificity phosphatases: critical regulators with diverse cellular targets. *null* (2009).
154. Mohn, K. *et al.* The immediate-early growth response in regenerating liver and insulin-stimulated H-35 cells: comparison with serum-stimulated 3T3 cells and identification of 41 novel immediate-early genes. *Mol Cell Biol* **11**, 381–390 (1991).
155. Zeng, Q., Hong, W. & Tan, Y. H. Mouse PRL-2 and PRL-3, two potentially prenylated protein tyrosine phosphatases homologous to PRL-1. *Biochemical and biophysical research communications* **244**, 421–7 (1998).
156. Stephens, B. J., Han, H., Gokhale, V. & Hoff, D. D. V. PRL phosphatases as potential molecular targets in cancer. *Molecular cancer therapeutics* **4**, 1653–61 (2005).
157. Rios, P., Li, X. & journal, K. M. Molecular mechanisms of the PRL phosphatases. *null* (2013) doi:10.1111/j.1742-4658.2012.08565.x.
158. Wei, M., Korotkov, K. V. & Blackburn, J. S. Targeting phosphatases of regenerating liver (PRLs) in cancer. *Pharmacology & therapeutics* **190**, 128–138 (2018).
159. Kozlov, G. *et al.* Structural insights into molecular function of the metastasis-associated phosphatase PRL-3. *The Journal of biological chemistry* **279**, 11882–9 (2004).
160. Zhang, H. *et al.* PRL3 phosphatase active site is required for binding the putative magnesium transporter CNNM3. *Scientific reports* **7**, 48 (2017).
161. Guo, K. *et al.* Catalytic domain of PRL-3 plays an essential role in tumor metastasis: formation of PRL-3 tumors inside the blood vessels. *Cancer biology & therapy* **3**, 945–51 (2004).
162. Zeng, Q. *et al.* Prenylation-dependent association of protein-tyrosine phosphatases PRL-1, -2, and -3 with the plasma membrane and the early endosome. *The Journal of biological chemistry* **275**, 21444–52 (2000).
163. Fagerli, U.-M. *et al.* Overexpression and involvement in migration by the metastasis-associated phosphatase PRL-3 in human myeloma cells. *Blood* **111**, 806–815 (2008).
164. Al-Aidaros, A. Q. & Zeng, Q. PRL-3 phosphatase and cancer metastasis. *Journal of cellular biochemistry* **111**, 1087–98 (2010).
165. Skinner, A., Vartia, A., Williams, T. & Biochemistry, L.-J. Enzyme activity of phosphatase of regenerating liver is controlled by the redox environment and its C-terminal residues. *null* (2009) doi:10.1021/bi900241k.

166. Bessette, D. C., Qiu, D. & Pallen, C. J. PRL PTPs: mediators and markers of cancer progression. *Cancer Metast Rev* **27**, 231–252 (2008).
167. Sun, J.-P. *et al.* Structure and Biochemical Properties of PRL-1, a Phosphatase Implicated in Cell Growth, Differentiation, and Tumor Invasion † , ‡. *Biochemistry-us* **44**, 12009–12021 (2005).
168. Castiglioni, S. & Maier, J. A. Magnesium and cancer: a dangerous liason. *Magnesium research* **24**, S92-100 (2011).
169. Uetani, N. *et al.* PRL2 links magnesium flux and sex-dependent circadian metabolic rhythms. *JCI insight* **2**, (2017).
170. Yan, H., Kong, D., Ge, X., Gao, X. & research, H.-X. of biomedical. Generation of conditional knockout alleles for PRL-3. *null* (2011).
171. Zimmerman, M. W., Homanics, G. E. & Lazo, J. S. Targeted deletion of the metastasis-associated phosphatase Ptp4a3 (PRL-3) suppresses murine colon cancer. *PLoS one* **8**, e58300 (2013).
172. Zhang, Z.-Y. Y. Drugging the Undruggable: Therapeutic Potential of Targeting Protein Tyrosine Phosphatases. *Accounts of chemical research* **50**, 122–129 (2017).
173. Saha, S. *et al.* A phosphatase associated with metastasis of colorectal cancer. *Science (New York, N.Y.)* **294**, 1343–6 (2001).
174. Kato, H. *et al.* High expression of PRL-3 promotes cancer cell motility and liver metastasis in human colorectal cancer: a predictive molecular marker of metachronous liver and lung metastases. *Clinical cancer research : an official journal of the American Association for Cancer Research* **10**, 7318–28 (2004).
175. Peng, L. *et al.* PRL-3 promotes the motility, invasion, and metastasis of LoVo colon cancer cells through PRL-3-integrin  $\beta$ 1-ERK1/2 and-MMP2 signaling. *Mol Cancer* **8**, 110 (2009).
176. Wang, Z. *et al.* High expression of PRL-3 can promote growth of gastric cancer and exhibits a poor prognostic impact on patients. *Annals of surgical oncology* **16**, 208–19 (2009).
177. Wang, H. *et al.* PRL-3 down-regulates PTEN expression and signals through PI3K to promote epithelial-mesenchymal transition. *Cancer research* **67**, 2922–6 (2007).
178. Bardelli, A. *et al.* PRL-3 expression in metastatic cancers. *Clinical cancer research : an official journal of the American Association for Cancer Research* **9**, 5607–15 (2003).

179. Radke, I. *et al.* Expression and prognostic impact of the protein tyrosine phosphatases PRL-1, PRL-2, and PRL-3 in breast cancer. *British journal of cancer* **95**, 347–54 (2006).
180. Wang, L. *et al.* Overexpression of phosphatase of regenerating liver-3 in breast cancer: association with a poor clinical outcome. *Ann Oncol* **17**, 1517–1522 (2006).
181. Miskad, U. A., Semba, S., Kato, H. & Yokozaki, H. Expression of PRL-3 Phosphatase in Human Gastric Carcinomas: Close Correlation with Invasion and Metastasis. *Pathobiology* **71**, 176–184 (2004).
182. Li, Z. *et al.* Inhibition of PRL-3 gene expression in gastric cancer cell line SGC7901 via microRNA suppressed reduces peritoneal metastasis. *Biochemical and biophysical research communications* **348**, 229–37 (2006).
183. Polato, F. *et al.* PRL-3 phosphatase is implicated in ovarian cancer growth. *Clinical cancer research : an official journal of the American Association for Cancer Research* **11**, 6835–9 (2005).
184. Vandsemb, E. N. *et al.* Phosphatase of regenerating liver 3 (PRL-3) is overexpressed in human prostate cancer tissue and promotes growth and migration. *Journal of translational medicine* **14**, 71 (2016).
185. Ming, J., Liu, N., Gu, Y., Qiu, X. & Wang, E. PRL-3 facilitates angiogenesis and metastasis by increasing ERK phosphorylation and up-regulating the levels and activities of RhoA/C in lung cancer. *Pathology* **41**, 118–126 (2009).
186. Qu, S. *et al.* Independent oncogenic and therapeutic significance of phosphatase PRL-3 in FLT3-ITD-negative acute myeloid leukemia. *Cancer* **120**, 2130–41 (2014).
187. Beekman, R. *et al.* Retroviral integration mutagenesis in mice and comparative analysis in human AML identify reduced PTP4A3 expression as a prognostic indicator. *PloS one* **6**, e26537 (2011).
188. Hjort, M. A. *et al.* Phosphatase of regenerating liver-3 is expressed in acute lymphoblastic leukemia and mediates leukemic cell adhesion, migration and drug resistance. *Oncotarget* **9**, 3549–3561 (2018).
189. Parker, B. S. *et al.* Alterations in Vascular Gene Expression in Invasive Breast Carcinoma. *Cancer Res* **64**, 7857–7866 (2004).
190. Campbell, A. M. & Zhang, Z.-Y. Y. Phosphatase of regenerating liver: a novel target for cancer therapy. *Expert opinion on therapeutic targets* **18**, 555–69 (2014).

191. Daouti, S. *et al.* A Selective Phosphatase of Regenerating Liver Phosphatase Inhibitor Suppresses Tumor Cell Anchorage-Independent Growth by a Novel Mechanism Involving p130Cas Cleavage. *Cancer Res* **68**, 1162–1169 (2008).
192. McQueeney, K. E. *et al.* Targeting ovarian cancer and endothelium with an allosteric PTP4A3 phosphatase inhibitor. *Oncotarget* **9**, 8223–8240 (2018).
193. Thura, M. *et al.* PRL3-zumab as an immunotherapy to inhibit tumors expressing PRL3 oncoprotein. *Nature communications* **10**, 2484 (2019).
194. Kohlmann, A. *et al.* An international standardization programme towards the application of gene expression profiling in routine leukaemia diagnostics: the Microarray Innovations in LEukemia study prephase. *British journal of haematology* **142**, 802–7 (2008).
195. Haferlach, T. *et al.* Clinical utility of microarray-based gene expression profiling in the diagnosis and subclassification of leukemia: report from the International Microarray Innovations in Leukemia Study Group. *Journal of clinical oncology : official journal of the American Society of Clinical Oncology* **28**, 2529–37 (2010).
196. Langenau, D. M. *et al.* Myc-induced T cell leukemia in transgenic zebrafish. *Science (New York, N.Y.)* **299**, 887–90 (2003).
197. Blackburn, J. S., Liu, S. & Langenau, D. M. Quantifying the frequency of tumor-propagating cells using limiting dilution cell transplantation in syngeneic zebrafish. *Journal of visualized experiments : JoVE* e2790 (2011) doi:10.3791/2790.
198. Blackburn, J. S. & Langenau, D. M. Zebrafish as a model to assess cancer heterogeneity, progression and relapse. *Disease models & mechanisms* **7**, 755–62 (2014).
199. Lin, M.-D. D. *et al.* Expression of phosphatase of regenerating liver family genes during embryogenesis: an evolutionary developmental analysis among *Drosophila*, amphioxus, and zebrafish. *BMC developmental biology* **13**, 18 (2013).
200. Kobayashi, M. *et al.* Phosphatase of regenerating liver in hematopoietic stem cells and hematological malignancies. *Cell cycle (Georgetown, Tex.)* **13**, 2827–35 (2014).
201. Kobayashi, M. *et al.* PRL2/PTP4A2 phosphatase is important for hematopoietic stem cell self-renewal. *Stem cells (Dayton, Ohio)* **32**, 1956–67 (2014).
202. Zhang, M. *et al.* Metastatic Phosphatase PRL-3 Induces Ovarian Cancer Stem Cell Sub-population through Phosphatase-Independent Deacetylation Modulations. *Iscience* **23**, 100766 (2020).

203. Hu, Y. & Smyth, G. K. ELDA: Extreme limiting dilution analysis for comparing depleted and enriched populations in stem cell and other assays. *J Immunol Methods* **347**, 70–78 (2009).
204. Ahn, J. H. *et al.* Synthesis and biological evaluation of rhodanine derivatives as PRL-3 inhibitors. *Bioorg Med Chem Lett* **16**, 2996–2999 (2006).
205. Bollu, L. R., Mazumdar, A., Savage, M. I. & Brown, P. H. Molecular Pathways: Targeting Protein Tyrosine Phosphatases in Cancer. *Clinical cancer research : an official journal of the American Association for Cancer Research* **23**, 2136–2142 (2017).
206. Mizgirev, I. V. & Revskoy, S. A new zebrafish model for experimental leukemia therapy. *Cancer biology & therapy* **9**, 895–902 (2010).
207. Blackburn, J. S. *et al.* Notch signaling expands a pre-malignant pool of T-cell acute lymphoblastic leukemia clones without affecting leukemia-propagating cell frequency. *Leukemia* **26**, 2069–78 (2012).
208. Clevers, H. & Nusse, R. Wnt/ $\beta$ -catenin signaling and disease. *Cell* **149**, 1192–205 (2012).
209. Heidel, F. H. *et al.* Genetic and pharmacologic inhibition of  $\beta$ -catenin targets imatinib-resistant leukemia stem cells in CML. *Cell stem cell* **10**, 412–24 (2012).
210. Majeti, R. *et al.* Dysregulated gene expression networks in human acute myelogenous leukemia stem cells. *Proceedings of the National Academy of Sciences of the United States of America* **106**, 3396–401 (2009).
211. Zhao, C. *et al.* Loss of beta-catenin impairs the renewal of normal and CML stem cells in vivo. *Cancer cell* **12**, 528–41 (2007).
212. Guo, Z. *et al.* Beta-catenin stabilization stalls the transition from double-positive to single-positive stage and predisposes thymocytes to malignant transformation. *Blood* **109**, 5463–72 (2007).
213. Gekas, C. *et al.*  $\beta$ -Catenin is required for T-cell leukemia initiation and MYC transcription downstream of Notch1. *Leukemia* **30**, 2002–2010 (2016).
214. Kahn, M. Can we safely target the WNT pathway? *Nature reviews. Drug discovery* **13**, 513–32 (2014).
215. Katoh, M. Canonical and non-canonical WNT signaling in cancer stem cells and their niches: Cellular heterogeneity, omics reprogramming, targeted therapy and tumor plasticity (Review). *Int J Oncol* **51**, 1357–1369 (2017).

216. Chong, P. S. *et al.* LEO1 is regulated by PRL-3 and mediates its oncogenic properties in acute myelogenous leukemia. *Cancer research* **74**, 3043–53 (2014).
217. Chong, P. S. Y. S. *et al.* Non-canonical activation of  $\beta$ -catenin by PRL-3 phosphatase in acute myeloid leukemia. *Oncogene* **38**, 1508–1519 (2019).
218. Zhou, J. *et al.* A loss-of-function genetic screening reveals synergistic targeting of AKT/mTOR and WTN/ $\beta$ -catenin pathways for treatment of AML with high PRL-3 phosphatase. *Journal of hematology & oncology* **11**, 36 (2018).
219. Zhou, J. *et al.* LIN28B Activation by PRL-3 Promotes Leukemogenesis and a Stem Cell-like Transcriptional Program in AML. *Molecular Cancer Research* **15**, 294–303 (2017).
220. Wong, D. J. *et al.* Module Map of Stem Cell Genes Guides Creation of Epithelial Cancer Stem Cells. *Cell Stem Cell* **2**, 333–344 (2008).
221. Tesell, J., Kelliher, M., Hermance, N., Roderick, J. E. & Bradner, J. E. C-Myc Inhibition Targets the Leukemia-Initiating Cells in a Tall/Lmo2 mouse Model of T-ALL. *Blood* **120**, 1880–1880 (2012).
222. Sakanaka, C., Leong, P., Xu, L., Harrison, S. D. & Williams, L. T. Casein kinase I $\epsilon$  in the Wnt pathway: Regulation of  $\beta$ -catenin function. *Proc National Acad Sci* **96**, 12548–12552 (1999).
223. Sakanaka, C. Phosphorylation and Regulation of  $\beta$ -Catenin by Casein Kinase I. *J Biochem* **132**, 697–703 (2002).
224. Veeman, M. T., Slusarski, D. C., Kaykas, A., Louie, S. H. & Moon, R. T. Zebrafish Prickle, a Modulator of Noncanonical Wnt/Fz Signaling, Regulates Gastrulation Movements. *Curr Biol* **13**, 680–685 (2003).
225. Chen, M. *et al.* The Anti-Helminthic Niclosamide Inhibits Wnt/Frizzled1 Signaling. *Biochemistry-us* **48**, 10267–10274 (2009).
226. Feder, K. *et al.* Differences in expression and function of LEF1 isoforms in normal versus leukemic hematopoiesis. *Leukemia* **34**, 1027–1037 (2020).
227. Ghisi, M. *et al.* Id2 and E Proteins Orchestrate the Initiation and Maintenance of MLL-Rearranged Acute Myeloid Leukemia. *Cancer Cell* **30**, 59–74 (2016).
228. Matthijssens, F. *et al.* RUNX2 regulates leukemic cell metabolism and chemotaxis in high-risk T cell acute lymphoblastic leukemia. *J Clin Invest* (2021) doi:10.1172/jci141566.

229. Verma, D. *et al.* Bone marrow niche-derived extracellular matrix-degrading enzymes influence the progression of B-cell acute lymphoblastic leukemia. *Leukemia* **34**, 1540–1552 (2020).
230. Marchwicka, A. & Marcinkowska, E. Regulation of Expression of CEBP Genes by Variably Expressed Vitamin D Receptor and Retinoic Acid Receptor  $\alpha$  in Human Acute Myeloid Leukemia Cell Lines. *Int J Mol Sci* **19**, 1918 (2018).
231. Tan, M., Teo, Z., Sng, M., Zhu, P. & Tan, N. Emerging Roles of Angiopoietin-like 4 in Human Cancer. *Mol Cancer Res* **10**, 677–688 (2012).
232. Shimizu, N., Kawakami, K. & Ishitani, T. Visualization and exploration of Tcf/Lef function using a highly responsive Wnt/ $\beta$ -catenin signaling-reporter transgenic zebrafish. *Developmental biology* **370**, 71–85 (2012).
233. Gürtler, A. *et al.* Stain-Free technology as a normalization tool in Western blot analysis. *Analytical biochemistry* **433**, 105–111 (2013).
234. Pulak, R. Tools for automating the imaging of zebrafish larvae. *Methods (San Diego, Calif.)* **96**, 118–126 (2016).
235. Chang, T.-Y. Y., Pardo-Martin, C., Allalou, A., Wählby, C. & Yanik, M. F. Fully automated cellular-resolution vertebrate screening platform with parallel animal processing. *Lab on a chip* **12**, 711–6 (2012).
236. Pardo-Martin, C. *et al.* High-throughput in vivo vertebrate screening. *Nature methods* **7**, 634–6 (2010).
237. Gore, A. V., Pillay, L. M., Galanternik, M. V. & Weinstein, B. M. The zebrafish: A fantastic model for hematopoietic development and disease. *Wiley interdisciplinary reviews. Developmental biology* **7**, e312 (2018).
238. Brown, H. K., Schiavone, K., Tazzyman, S., Heymann, D. & Chico, T. J. Zebrafish xenograft models of cancer and metastasis for drug discovery. *Expert opinion on drug discovery* **12**, 379–389 (2017).
239. Chen, X., Li, Y., Yao, T. & Jia, R. Benefits of Zebrafish Xenograft Models in Cancer Research. *Frontiers Cell Dev Biology* **9**, 616551 (2021).
240. Fazio, M., Ablain, J., Chuan, Y., Langenau, D. M. & Zon, L. I. Zebrafish patient avatars in cancer biology and precision cancer therapy. *Nat Rev Cancer* **20**, 263–273 (2020).
241. Cornet, C., Dyballa, S., Terriente, J. & Giacomo, V. D. ZeOncoTest: Refining and Automating the Zebrafish Xenograft Model for Drug Discovery in Cancer. *Pharm* **13**, 1 (2019).

242. Neff, E. P. Building avatar armies with fish and flies. *Lab Animal* **49**, 101–104 (2020).
243. Astone, M., Dankert, E. N., Alam, S. K. & Hoepfner, L. H. Fishing for cures: The aLLURE of using zebrafish to develop precision oncology therapies. *NPJ precision oncology* **1**, (2017).
244. Corkery, D. P., Delleire, G. & Berman, J. N. Leukaemia xenotransplantation in zebrafish--chemotherapy response assay in vivo. *British journal of haematology* **153**, 786–9 (2011).
245. Deveau, A. P., Bentley, V. L. & Berman, J. N. Using zebrafish models of leukemia to streamline drug screening and discovery. *Experimental hematology* **45**, 1–9 (2017).
246. Ghotra, V. P. *et al.* Automated whole animal bio-imaging assay for human cancer dissemination. *PloS one* **7**, e31281 (2012).
247. Haney, M. G., Moore, L. H. & Blackburn, J. S. Drug Screening of Primary Patient Derived Tumor Xenografts in Zebrafish. *J Vis Exp* (2020) doi:10.3791/60996.
248. Novoa, B. & Figueras, A. Current Topics in Innate Immunity II. *Adv Exp Med Biol* **946**, 253–275 (2011).
249. Sant, K. E. & Timme-Laragy, A. R. Zebrafish as a Model for Toxicological Perturbation of Yolk and Nutrition in the Early Embryo. *Curr Environ Heal Reports* **5**, 125–133 (2018).
250. Cabezas-Sainz, P. *et al.* Improving zebrafish embryo xenotransplantation conditions by increasing incubation temperature and establishing a proliferation index with ZFtool. *BMC cancer* **18**, 3 (2018).
251. Cabezas-Sáinz, P., Pensado-López, A., Sáinz, B. & Sánchez, L. Modeling Cancer Using Zebrafish Xenografts: Drawbacks for Mimicking the Human Microenvironment. *Cells* **9**, 1978 (2020).
252. Schnurr, M. E., Yin, Y. & Scott, G. R. Temperature during embryonic development has persistent effects on metabolic enzymes in the muscle of zebrafish. *The Journal of experimental biology* **217**, 1370–80 (2014).
253. Pype, C. *et al.* Incubation at 32.5°C and above causes malformations in the zebrafish embryo. *Reproductive toxicology (Elmsford, N.Y.)* **56**, 56–63 (2015).
254. Andres, D. A. *et al.* Improved workflow for mass spectrometry–based metabolomics analysis of the heart. *J Biol Chem* **295**, 2676–2686 (2020).

255. Brewer, M. K. *et al.* Targeting Pathogenic Lafora Bodies in Lafora Disease Using an Antibody-Enzyme Fusion. *Cell Metab* **30**, 689-705.e6 (2019).
256. Sun, R. C. *et al.* Nuclear Glycogenolysis Modulates Histone Acetylation in Human Non-Small Cell Lung Cancers. *Cell Metab* **30**, 903-916.e7 (2019).
257. Xia, J., Psychogios, N., Young, N. & Wishart, D. S. MetaboAnalyst: a web server for metabolomic data analysis and interpretation. *Nucleic Acids Res* **37**, W652–W660 (2009).
258. Dagley, M. J. & McConville, M. J. DExSI: a new tool for the rapid quantitation of <sup>13</sup>C-labelled metabolites detected by GC-MS. *Bioinformatics* **34**, 1957–1958 (2018).
259. Pang, Z., Chong, J., Li, S. & Xia, J. MetaboAnalystR 3.0: Toward an Optimized Workflow for Global Metabolomics. *Metabolites* **10**, 186 (2020).
260. Maude, S. L. *et al.* Chimeric antigen receptor T cells for sustained remissions in leukemia. *The New England journal of medicine* **371**, 1507–17 (2014).
261. Wan, J. C. M. *et al.* Liquid biopsies come of age: towards implementation of circulating tumour DNA. *Nat Rev Cancer* **17**, 223–238 (2017).
262. Volik, S., Alcaide, M., Morin, R. D. & Collins, C. C. Cell-free DNA (cfDNA): clinical significance and utility in cancer shaped by emerging technologies. *Mol Cancer Res* **14**, molcanres.0044.2016 (2016).
263. Heitzer, E., Perakis, S., Geigl, J. B. & Speicher, M. R. The potential of liquid biopsies for the early detection of cancer. *Npj Precis Oncol* **1**, 36 (2017).
264. Ginkel, J. H. van *et al.* Preanalytical blood sample workup for cell-free DNA analysis using Droplet Digital PCR for future molecular cancer diagnostics. *Cancer medicine* **6**, 2297–2307 (2017).
265. Neumann, M. H. D. H., Bender, S., Krahn, T. & Schlange, T. ctDNA and CTCs in Liquid Biopsy - Current Status and Where We Need to Progress. *Computational and structural biotechnology journal* **16**, 190–195 (2018).
266. Ossandon, M. R. *et al.* Circulating Tumor DNA Assays in Clinical Cancer Research. *Journal of the National Cancer Institute* (2018) doi:10.1093/jnci/djy105.
267. Fries, C. *et al.* Acute lymphoblastic leukemia clonal distribution between bone marrow and peripheral blood. *Pediatr Blood Cancer* **67**, e28280 (2020).
268. Mullighan, C. G. *et al.* Genomic Analysis of the Clonal Origins of Relapsed Acute Lymphoblastic Leukemia. *Science* **322**, 1377–1380 (2008).

269. Kubackzova, V., Vrabel, D., Sedlarikova, L., Besse, L. & Sevcikova, S. Cell-free DNA — Minimally invasive marker of hematological malignancies. *Eur J Haematol* **99**, 291–299 (2017).
270. Kwok, M., Wu, S. P., Mo, C., Summers, T. & Roschewski, M. Circulating Tumor DNA to Monitor Therapy for Aggressive B-Cell Lymphomas. *Current treatment options in oncology* **17**, 47 (2016).
271. Nakamura, S. *et al.* Circulating tumor DNA dynamically predicts response and/or relapse in patients with hematological malignancies. *International journal of hematology* (2018) doi:10.1007/s12185-018-2487-2.
272. Shin, S. *et al.* Detection of Immunoglobulin Heavy Chain Gene Clonality by Next-Generation Sequencing for Minimal Residual Disease Monitoring in B-Lymphoblastic Leukemia. *Ann Laboratory Medicine* **37**, 331–335 (2017).
273. Jain, M., Olsen, H. E., Paten, B. & Akeson, M. The Oxford Nanopore MinION: delivery of nanopore sequencing to the genomics community. *Genome Biol* **17**, 239 (2016).
274. Shabardina, V. *et al.* NanoPipe - a web server for nanopore MinION sequencing data analysis. *Gigascience* **8**, giy169- (2019).
275. Bronkhorst, A. J., Ungerer, V. & Holdenrieder, S. The emerging role of cell-free DNA as a molecular marker for cancer management. *Biomol Detect Quantification* **17**, 100087 (2019).
276. Cohen, J. D. *et al.* Detection and localization of surgically resectable cancers with a multi-analyte blood test. *Science* **359**, eaar3247 (2018).
277. Alix-Panabières, C. & Pantel, K. Clinical Applications of Circulating Tumor Cells and Circulating Tumor DNA as Liquid Biopsy. *Cancer Discov* **6**, 479–491 (2016).
278. Dolatabadi, E. K., Dehaghi, M. O., Amirizadeh, N., Parivar, K. & Mahdian, R. CDKN2B Methylation Correlates with Survival in AML Patients. *Iranian journal of pharmaceutical research : IJPR* **16**, 1600–1611 (2017).
279. Frazzi, R. *et al.* Methylation changes of SIRT1, KLF4, DAPK1 and SPG20 in B-lymphocytes derived from follicular and diffuse large B-cell lymphoma. *Leukemia research* **57**, 89–96 (2017).
280. Ruiz, M. *et al.* IMGT, the international ImMunoGeneTics database. *Nucleic Acids Res* **28**, 219–221 (2000).

## VITA

### Meghan (Green) Haney

---

#### I. EDUCATION

- University of Kentucky College of Medicine, Lexington, KY 8/2014-current
- MD/PhD candidate
- Denison University, Granville, OH 8/2011-5/2013
- Bachelor of Science in Biology with a minor in Spanish, May 2013
- State University of New York at Geneseo, Geneseo, NY 8/2009-5/2011

#### II. RESEARCH EXPERIENCE

- PhD Candidate, University of Kentucky, Lexington, KY 8/2017-current  
Department of Molecular and Cellular Biochemistry  
*Mentor: Jessica Blackburn, PhD*
- Aim 1: Study the mechanism by which the protein tyrosine phosphatase 4a3 (PRL-3) regulates Wnt signaling in leukemia stem cells.
  - Aim 2: Identify novel therapeutics to inhibit the Wnt self-renewal pathway in Leukemia stem cells using zebrafish as a model organism.
  - Aim 3: Study the potential use of cell-free DNA as a marker of central nervous system relapse in acute leukemias.
- Research Rotation, University of Kentucky, Lexington, KY 5/2015-8/2015  
Sanders Brown Aging Center  
*Mentor: Steve Estus, PhD*
- Aim: Study the role of TRPM8 ion channel mutations in migraines.
- Research Rotation, University of Kentucky, Lexington, KY 6/2014-8/2014  
Markey Cancer Center  
*Mentor: Kathleen O'Connor, PhD*
- Aim: Study the role of integrin signaling in breast cancer.
- Clinical Trial Coordinator, University of Florida, Gainesville, FL 6/2013-5/2014  
Powell Gene Therapy Center  
*Mentor: Barry Byrne, MD, PhD*
- Aim 1: Coordinated clinical trials for patients with rare genetic disorders, such as Pompe Disease and Duchenne Muscular Dystrophy.
  - Aim 2: Study the retrograde transduction of rAAV vector into motor neurons of Pompe Disease mice.

- Aim 3: Assisted with coordination and establishment of the University of Florida Pediatric Neuromuscular Disorders Clinic.

Undergraduate Researcher, University of Rochester, Rochester, NY 5/2010-8/2010  
 Department of Immunology  
 Mentor: Jacques Robert, PhD

- Aim: Study the innate and adaptive immune responses of *Xenopus laevis* tadpoles to infection with the ranavirus FV3.

### III. AWARDS AND HONORS

#### Graduate:

2019 Best Oral Presentation Award, Midwest Zebrafish Conference  
 2018 Best Poster Presentation Award, American Academy of Physicians/ American Society for Clinical Investigators/American Academy of Physicians  
 2018 Travel Award Recipient, American Physician Scientists Association  
 2015 - 2016 Professional Student Mentored Research Fellowship, Center for Clinical and Translational Science, University of Kentucky

#### Undergraduate:

2013 Dean's List, Denison University  
 2009-2011 Dean's List, State University of New York at Geneseo  
 2009 Academic All-American in swimming

### IV. TEACHING ACTIVITIES

#### Graduate Courses:

- MI707 Contemporary Topics in Immunology; Immunotherapy Spring 2018  
 Taught 2 hour lecture on natural killer cell immunotherapy

#### Undergraduate Courses:

- Teaching Assistant, Developmental Biology and Microbiology 2012-2013  
 Denison University Biology Department, Granville, OH

#### Other Teaching Experience:

- Markey Cancer Center Appalachian Career Training in Oncology Program 2019  
 Taught 2 hour lecture to high school students on careers in science
- Kaplan MCAT Preparation Course Instructor 2013-2016

### VI. LEADERSHIP ROLES

2019-current UK Markey Cancer Center Trainee Advisory Council  
 2018-current Institutional Representative, American Physician Scientist Association  
 2017-current UK MD/PhD Program Internal Advisory Committee  
 2017-current UK MD/PhD Admissions Committee  
 2017-current UK MD/PhD Program Retreat Committee  
 2016-current UK College of Medicine Dean's Student Advisory Council  
 2016-2017 President, American Medical Association, Medical Student Section, UK

2016-2017	Board of Trustees Member, Kentucky Medical Association
2015-2016	Chair of Advocacy and Policy, American Medical Association, Medical Student Section, UK
2014-2016	Executive Committee, American Medical Association, Medical Student Section

## VII. PROFESSIONAL DEVELOPMENT

### Memberships in Professional Societies:

2019-current	Member, Zebrafish Disease Models Society
2017-current	Associate Member, American Association for Cancer Research
2017-current	Member, American Physician Scientists Association
2017-current	Member, Biomedical Graduate Student Organization, University of Kentucky
2014-2017	Member, Lexington Medical Society
2014-2017	Member, Kentucky Medical Association
2014-2017	Member, American Medical Association, Medical Student Section

### Meetings Attended

- Zebrafish Disease Models Society Annual Meeting, 2020 (Virtual)
- American Society for Clinical Oncology Annual Meeting, 2020 (Virtual)
- American Association for Cancer Research Annual Meeting, 2020 (Virtual)
- American Physician Scientists Association Annual Meeting, 2020 (Virtual)
- St. Jude National Graduate Student Symposium, 2020 (Memphis, TN) – Cancelled due to COVID
- Gordon Research Conference, Wnt Signaling, 2019 (Mount Snow, VT)
- Zebrafish Disease Models Society Conference 2019 (Boston, MA)
- UK Markey Cancer Center Research Day 2019 (Lexington, KY)
- Midwest Zebrafish Conference 2019 (Lexington, KY), Session Moderator
- UK Center for Clinical and Translational Sciences Conference 2019 (Lexington, KY)
- American Academy of Physicians/American Society for Clinical Investigators/American Physician Scientists Association 2019 (Chicago, IL)
- American Association for Cancer Research 2019 (Atlanta, GA)
- UK Markey Cancer Center Research Day 2018 (Lexington, KY)
- American Academy of Physicians/American Society for Clinical Investigators/American Physician Scientists Association 2018 (Chicago, IL)
- American Association for Cancer Research 2018 (Chicago, IL)
- UK Center for Clinical and Translational Sciences Conference 2018 (Lexington, KY)
- University of Kentucky AOA Research Day 2014 (Lexington, KY)
- University of Florida, Clinical and Translational Science Institute Research Day 2014 (Gainesville, FL)

### Workshops Attended:

- Pediatrics Physician Scientist Training Program Trainee Panel (Virtual, AAMC, July 31, 2020)
- Essential Leadership Skills for Future Scientists and Health Care Professionals (Virtual, NIH OITE, Jun 11, 2020)
- NCI Big Data Training for Cancer Research (Virtual, Purdue University, June 9-19, 2020)
- American Physician Scientist Association Residency Fair (Virtual, APSA, May 23, 2020)
- NIH Career Symposium (Virtual, NIH OITE, May 8, 2020)

- Precision Medicine Symposium (University of Kentucky, Markey Cancer Center, February 21, 2020)
- Building a Successful Career in Science (University of Kentucky, Markey Cancer Center Career Enhancement Club, Lexington, KY, September 12, 2019)
- Personal & Social Competence: Emotional Intelligence for Success with Michelle Jones (University of Kentucky, Women in Medicine and Science, Lexington, KY, June 10, 2019)
- Grant Writing Workshop for Trainees: Preparing an NIH F-Series Fellowship Application (University of Kentucky, Markey Cancer Center, Lexington, KY, October 22, 2018 - April 8, 2019)
- New England Biolabs RNAseq Workshop 2018 (University of Kentucky, Lexington, KY, June 5 - 6, 2018)
- NCI-Sponsored Training Awards and Opportunities, American Association for Cancer Research Conference, 2018
- Distilling your Message, Alan Alda Center for Communicating Science, (Lexington, KY, June 2015)

## VIII. PRESENTATIONS

### Oral Presentations:

1. **Haney MG**, University of Kentucky, Biochemistry Department Seminar, Lexington, KY, 2020. *The phosphatase PRL-3 enhances leukemia stem cell self-renewal to drive T-ALL relapse.*
2. **Haney MG**, University of Kentucky, Markey Cancer Center Research Day, Lexington, KY, 2019. *A Protein Tyrosine Phosphatase 4A3 (PRL-3)/Wnt signaling axis as a novel therapeutic target in Acute Lymphoblastic Leukemia (ALL) relapse.*
3. **Haney MG**, Zebrafish Disease Models Society, Boston, MA, 2019. *A Protein Tyrosine Phosphatase 4A3 (PRL3)/Wnt Signaling Axis as a Novel Therapeutic Target in Acute Lymphoblastic Leukemia Relapse*
4. **Haney MG**, Midwest Zebrafish Meeting, Lexington, KY 2019. *A Protein Tyrosine Phosphatase 4A3 (PRL3)/Wnt Signaling Axis as a Novel Therapeutic Target in Acute Lymphoblastic Leukemia Relapse*
5. **Haney MG**, University of Kentucky, Biochemistry Department Seminar, Lexington, KY, 2018. *Circulating Tumor DNA as an Early Outcome Predictor in Cancer*
6. **Haney MG**, University of Kentucky, Biochemistry Department Seminar, Lexington, KY, 2018. *Can we really vaccinate against cancer?*

### Poster Presentations:

1. **Haney MG**, Moore LH, Badgett T, Blackburn JS, “Cell-free DNA as a Biomarker for Acute Lymphoblastic Leukemia Relapse in the Central Nervous System.” University of Kentucky, Center for Clinical and Translational Sciences Conference, Lexington, KY, 2020. (Abstract accepted, conference cancelled due to COVID)
2. **Haney MG**, Miller AK, Wei M, Blackburn JS, “Protein Tyrosine Phosphatase 4A3 modulates B-catenin signaling to promote leukemia stem cell self-renewal in T-ALL.” University of Kentucky, Markey Cancer Center Research Day, Lexington, KY, 2020. (Abstract accepted, conference cancelled due to COVID)
3. **Haney MG**, Miller AK, Wei M, Blackburn JS, “A Protein Tyrosine Phosphatase 4A3 (PRL3)/Wnt Signaling Axis as a Novel Therapeutic Target in Acute Lymphoblastic

- Leukemia (ALL) Relapse.” Gordon Research Conference, Wnt Signaling, Mount Snow, VT, 2019.
4. **Haney MG**, Miller AK, Blackburn JS, “A Protein Tyrosine Phosphatase 4A3 (PRL-3)/Wnt Signaling Axis as a Novel Therapeutic Target in Acute Lymphoblastic Leukemia (ALL) Relapse.” Zebrafish Disease Models Society, Boston, MA, 2019.
  5. **Haney MG**, Miller AK, Blackburn JS, “A Protein Tyrosine Phosphatase 4A3 (PRL-3)/Wnt signaling axis as a novel therapeutic target in Acute Lymphoblastic Leukemia (ALL) relapse” University of Kentucky, Markey Cancer Center Research Day, Lexington, KY, 2019.
  6. **Haney MG**, Miller AK, Blackburn JS, “A Protein Tyrosine Phosphatase 4A3 (PRL-3)/Wnt signaling axis as a novel therapeutic target in Acute Lymphoblastic Leukemia (ALL) relapse” Midwest Zebrafish Meeting, Lexington, KY, 2019.
  7. **Haney MG**, Miller AK, Blackburn JS, “A Protein Tyrosine Phosphatase 4A3 (PRL-3)/Wnt signaling axis as a novel therapeutic target in Acute Lymphoblastic Leukemia (ALL) relapse.” University of Kentucky, Center for Clinical and Translational Sciences Conference, Lexington, KY, 2019.
  8. **Haney MG**, Dockins SD, Blackburn JS, “Optimization of human cancer cell xenografts into zebrafish larvae for high-throughput drug screening.” American Academy of Physicians/American Society of Clinical Investigators/American Physician Scientists Association Annual Meeting, Chicago, IL, 2019.
  9. **Haney MG**, Miller AK, Blackburn JS, “A Protein Tyrosine Phosphatase 4A3 (PRL-3)/Wnt signaling axis as a novel therapeutic target in Acute Lymphoblastic Leukemia (ALL) relapse.” American Association for Cancer Research Annual Meeting, Atlanta, GA, 2019.
  10. **Haney MG**, Liu C, Blackburn JS, “Identifying Novel Therapeutics to Inhibit the Wnt Self-Renewal Pathway in Leukemia Stem Cells” University of Kentucky, Markey Cancer Center Research Day, Lexington, KY, 2018.
  11. **Haney MG**, Liu C, Blackburn JS, “Identifying Novel Therapeutics to Inhibit the Wnt Self-Renewal Pathway in Leukemia Stem Cells” American Academy of Physicians/American Society of Clinical Investigators/American Physician Scientists Association Annual Meeting, Chicago, IL, 2018.
  12. **Haney MG**, Liu C, Blackburn JS, “Identifying Novel Therapeutics to Inhibit the Wnt Self-Renewal Pathway in Leukemia Stem Cells.” American Association for Cancer Research Annual Meeting, Chicago, IL, 2018.
  13. **Haney MG**, Liu C, Blackburn JS, “Identifying Novel Therapeutics to Inhibit the Wnt Self-Renewal Pathway in Leukemia Stem Cells.” University of Kentucky, Center for Clinical and Translational Sciences Conference, Lexington, KY, 2018.
  14. Corti M, Elder M, Falk D, Lawson L, Smith B, Nayak S, Conlon T, Clément N, Erger K, Lavassani E, **Green M**, Doerfler P, Herzog R, Byrne B. “B-Cell Depletion is Protective Against Anti-AAV Capsid Immune Response: A Human Subject Case Study.” University of Kentucky AOA/MD/PhD Research Day, Lexington, KY, 2015.
  15. Corti M, Elder M, Falk D, Lawson L, Smith B, Nayak S, Conlon T, Clément N, Erger K, Lavassani E, **Green M**, Doerfler P, Herzog R, Byrne B. “B-Cell Depletion is Protective Against Anti-AAV Capsid Immune Response: A Human Subject Case Study.” University of Florida Clinical and Translational Science Institute Research Day, Gainesville, FL, 2014.

## IX. PUBLICATIONS

### **Publications**

1. **Haney MG**, Wimsett M, Liu C, Blackburn JS. Protocol for rapid assessment of the efficacy of novel Wnt inhibitors using zebrafish models. (2021) *STAR Protocols*.
2. Zhang W, Sviripa VM, Xie Y, Yu T, **Haney MG**, Blackburn JS, Adeniran CA, Zhan CG, Watt DS, Liu C. Epigenetic Regulation of Wnt Signaling by Carboxamide-Substituted Benzhydryl Amines that Function as Histone Demethylase Inhibitors. (2020) *iScience*.
3. **Haney MG**, Moore LH, Blackburn JS. Drug Screening of Primary Patient Derived Tumor Xenografts in Zebrafish. (2020) *J Vis Exp*.
4. Wei M, **Haney MG**, Rivas DR, Blackburn JS. Protein tyrosine phosphatase 4A3 (PTP4A3/PRL-3) drives migration and progression of T-cell acute lymphoblastic leukemia in vitro and in vivo. (2020) *Oncogenesis*.
5. Smith BK, Renno MS, **Green MM**, Sexton TM, Lawson LA, Martin AD, Corti M, Byrne BJ. Respiratory motor function in individuals with centronuclear myopathies. (2016) *Muscle Nerve*.
6. Corti M, Elder M, Falk D, Lawson L, Smith B, Nayak S, Conlon T, Clément N, Erger K, Lavassani E, **Green M**, Doerfler P, Herzog R, Byrne B. B-Cell Depletion is Protective Against Anti-AAV Capsid Immune Response: A Human Subject Case Study. (2014) *Mol Ther Methods Clin Dev*.

### **Acknowledged for Technical Contributions**

1. De Jesus Andino F, Chen G, Li Z, Grayfer L, Robert J. Susceptibility of *Xenopus laevis* tadpoles to infection by the ranavirus Frog-Virus 3 correlates with a reduced and delayed innate immune response in comparison with adult frogs. (2012) *Virology*.

## X. OUTREACH/COMMUNITY INVOLVEMENT

Feb 1, 2020	Kentucky American Water – Fayette County Public Schools District Science Fair judge, Frederick Douglas High School, Lexington, KY.
Nov, 2019	Weird Science Night, Maxwell Elementary School, Lexington, KY.
Oct 15, 2019	American Cancer Society Hope Lodge Dinner Planning and Preparation, Lexington, KY.
June 9, 2019	Midwest Zebrafish Conference 2019 Session Moderator, University of Kentucky, Lexington, KY.
Feb 2, 2019	Kentucky American Water – Fayette County Public Schools District Science Fair judge, Frederick Douglas High School, Lexington, KY.
Nov, 2018	Weird Science Night, Maxwell Elementary School, Lexington, KY, showed students how zebrafish develop over time with both the naked eye and under a microscope.
Apr 27, 2018	Everything is Science “Mapping the Big C”, University of Kentucky, Lexington, KY College of Pharmacy, acted as a co-presenter at Pazzo’s to introduce zebrafish models in basic research to a non-science audience.
Sep 2018	Alex’s Lemonade Stand Foundation’s Million Mile, Participant, our team raised \$1,988.00 and completed 685 miles to raise funds and awareness for pediatric cancer research.
Nov, 2017	Weird Science Night, Maxwell Elementary School, Lexington, KY, showed students how zebrafish develop over time with both the naked eye and under a microscope.